NMR investigation of non-local effects in a temperature sensitive mutant of the 25 kD tryptophan repressor protein
by Robert Charles Tyler

A dissertation submitted in partial fulfillment of the requirements for the degree of Doctor of Science In Chemistry
Montana State University

Abstract:
The three-dimensional solution structure of a temperature-sensitive mutant of the tryptophan repressor protein, with leucine substituted by phenylalanine at position 75, was determined to high-resolution using structural parameters derived from multidimensional NMR spectroscopy. A total of 1578 distance restraints, 62 hydrogen bonds, and 68 dihedral angles were used to solve the 3D structure of the symmetric apo-L75F-TrpR homodimer in solution. Amide chemical shifts that were significantly shifted in the spectrum of apo-L75F-TrpR compared to that of wild-type TrpR were analyzed in terms of possible perturbations resulting from ring current effects caused by the introduction of phenylalanine at residue position 75. Structural comparison with wild-type protein indicated that relevant alterations in backbone conformations have likely taken place within the 1-tryptophan cofactor binding site as well as in helical orientations within the hydrophobic core of the mutant protein. These data confirmed that the mutation propagates long-range effects throughout the protein.

The origin of these non-local effects was further investigated by comparing the amide backbone dynamics of mutant and wild-type proteins using 15N-NMR relaxation experiments. 15N relaxation parameters (T1, T2, 15N-{1H} nOe) were measured for backbone amides on the apo-forms of both mutant and wild-type proteins. Analysis indicated that on the picosecond to nanosecond timescale, both proteins displayed very similar behavior and that the mutation had no significant effect on overall backbone amide motions. However, the mutation appears to have caused small motional perturbations for amides in areas directly flanking the mutation site. From this analysis it was hypothesized that relevant dynamic changes originating from the mutation may manifest on the slower millisecond timescale and/or in side chain dynamics.

NMR INVESTIGATION OF NON-LOCAL EFFECTS IN A TEMPERATURE SENSITIVE MUTANT OF THE 25 Kd TRYPTOPHAN REPRESSOR PROTEIN

by

Robert Charles Tyler

A dissertation submitted in partial fulfillment
of the requirements for the degree

of

Doctor of Science

In

Chemistry

MONTANA STATE UNIVERSITY
Bozeman, Montana

November 2003

APPROVAL

of a dissertation submitted by

Robert Charles Tyler

This dissertation has been read by each member of the dissertation committee and has been found to be satisfactory regarding content, English usage, format, citations, bibliographic style, and consistency, and is ready for submission to the College of Graduate Studies.

Valerié Copié Valérie Copié 11/25/03
(Signature) Date

Approved for the Department of Chemistry and Biochemistry

Paul Grieco 11/25/03
(Signature) Date

Approved for the College of Graduate Studies

Bruce McLeod Bruce R. McLeod 12-8-03
(Signature) Date

STATEMENT OF PERMISSION TO USE

In presenting this dissertation in partial fulfillment of the requirements for a doctoral degree at Montana State University, I agree that the Library shall make it available to borrowers under rules of the Library. I further agree that copying of this dissertation is allowable only for scholarly purposes, consistent with "fair use" as prescribed in the U.S Copyright Law. Requests for extensive copying or reproduction of this dissertation should be referred to Bell & Howell Information and Learning, 300 North Zeeb Road, Ann Arbor, Michigan 48106, to whom I have granted "the exclusive right to reproduce and distribute my thesis in and from microform along with the non-exclusive right to reproduce and distribute my abstract in any format in whole or in part."

Signature 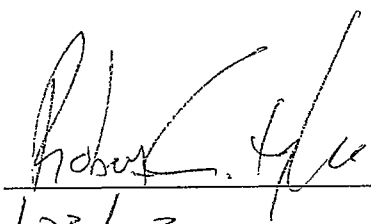

Date 11/23/03

ACKNOWLEDGEMENTS

I would like to thank Jerrod Einerwold, Lara Taubner, and Valerié Copié for their support and friendship.

TABLE OF CONTENTS

TABLE OF CONTENTS – CONTINUED

LIST OF TABLES

LIST OF FIGURES

Abstract

The three-dimensional solution structure of a temperature-sensitive mutant of the tryptophan repressor protein, with leucine substituted by phenylalanine at position 75, was determined to high-resolution using structural parameters derived from multidimensional NMR spectroscopy. A total of 1578 distance restraints, 62 hydrogen bonds, and 68 dihedral angles were used to solve the 3D structure of the symmetric apo-L75F-TrpR homodimer in solution. Amide chemical shifts that were significantly shifted in the spectrum of apo-L75F-TrpR compared to that of wild-type TrpR were analyzed in terms of possible perturbations resulting from ring current effects caused by the introduction of phenylalanine at residue position 75. Structural comparison with wild-type protein indicated that relevant alterations in backbone conformations have likely taken place within the l-tryptophan cofactor binding site as well as in helical orientations within the hydrophobic core of the mutant protein. These data confirmed that the mutation propagates long-range effects throughout the protein.

The origin of these non-local effects was further investigated by comparing the amide backbone dynamics of mutant and wild-type proteins using ^{15}N-NMR relaxation experiments. ^{15}N relaxation parameters (T_1, T_2, ^{15}N-{^{1}H} nOe) were measured for backbone amides on the apo-forms of both mutant and wild-type proteins. Analysis indicated that on the picosecond to nanosecond timescale, both proteins displayed very similar behavior and that the mutation had no significant effect on overall backbone amide motions. However, the mutation appears to have caused small motional perturbations for amides in areas directly flanking the mutation site. From this analysis it was hypothesized that relevant dynamic changes originating from the mutation may manifest on the slower millisecond timescale and/or in side chain dynamics.

Chapter 1

INTRODUCTION

The tryptophan repressor protein (TrpR) of *Escherichia coli* is a DNA binding protein that regulates transcription of genes that control L-tryptophan (L-trp) biosynthesis. The activity of TrpR is modulated by the intracellular concentration of its cofactor L-trp. When the cell contains high levels of L-trp, the inactive, unliganded form of the protein (apo-TrpR) binds two molecules of L-trp, which results in the active form (holo-TrpR). This activated holo-form of the protein then binds to specific operator DNA sequences pertinent to the biosynthesis of L-Trp, thereby preventing transcription. The TrpR is a 25kDa homodimer with each subunit containing 108-residue polypeptide chain (*1*). Structural studies have shown (*2-6*) that each subunit consists of six α-helices labeled as helices A-F. The TrpR is comprised of two structural domains, a hydrophobic core formed by helices A, B, C, and F of both subunits, and a DNA binding domain formed by helices D and E. The two molecules of L-trp bind to the dimer at sites formed between the hydrophobic core and the DNA binding domain.

From the first structural study of TrpR carried out by Schevitz et al (*2*), and later crystallographic comparisons of apo/holo forms (*3*), it was generally thought that binding L-Trp cofactor properly orients helices D and E away from the hydrophobic core for specific interactions within successive major grooves of target DNA. Indeed,

the holo/DNA crystal structure (*7*) confirms that the DNA binding domain of TrpR inserts into successive major grooves of operator DNA. Nuclear magnetic resonance (NMR) solution studies of the different forms of TrpR (*4-6*) have revealed more pronounced effects on the TrpR structure within helices D and E upon binding L-trp and DNA.

Protein structures based on solution NMR techniques rely heavily on the nuclear Overhauser effect (nOe) observed between protons. The nOe is a consequence of the dipolar interaction between nuclei, and is proportional to the inverse sixth power of the distance separating the nuclei. The nOe represents a through-space magnetization transfer from one nuclei to another. More importantly the nOes are sensitive to molecular conformation, and measurement of the nOe allows one to estimate the distance between two nuclei. The nOe, as it pertains to protein NMR, is measured as the cross-peak intensity between two interacting protons, and the greater the intensity of the nOe cross-peak, the shorter the distance separating the two nuclei. The nOe between two nuclei has an interaction range of about 5.5 Å. Once the distance between the two nuclei is estimated, it can be used to define a structural restraint within the protein. Hundreds of nOe structural restraints, along with many other NMR restraint parameters that describe backbone dihedral angles, and hydrogen bonding patterns, are then used to calculate the three dimensional structure of the protein and permits analyses by NMR spectroscopy.

From solution NMR structural investigations, both apo- and holo-TrpR have similar tertiary folds to the ones found in the corresponding crystal structures (2-6).

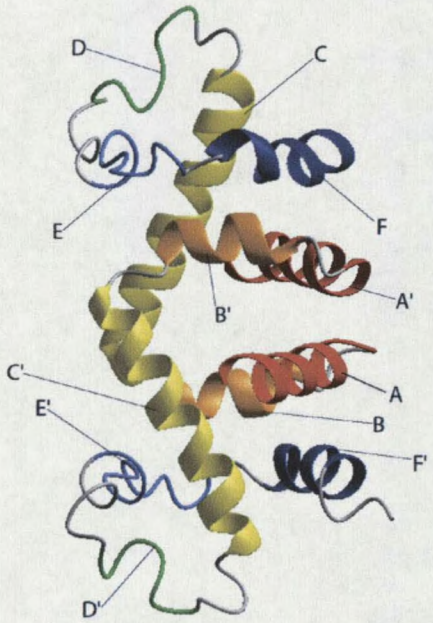

Figure 1: Minimized average structure of apo-WT TrpR based on the work of Zhao et al (5). Helical regions are represented as ribbons with the following boundaries: helix A/A' residues 16-32, helix B/B' residues 37-42, helix C/C' residues 45-63, helix D/D' residues 68-74, helix E residues 81-90, and helix F residues 93-103.

However, analysis of NMR solution structures reveals that the DNA binding domain, i.e. helices D and E, is more flexible and disordered than in the crystal structure (*4;5*). In particular, Zhao et al (*5*) have shown that conformational determinations of helices D and E are difficult to perform for apo-TrpR due to a lack of nOe structural restraints. Figure 1 shows a representation of wild-type apo-TrpR based on the NMR structures of Zhao et al (*5*). The binding of the corepressor L-trp to the protein produces more pronounced nuclear Overhauser effects (nOe) which are characteristic of a better

defined helix E in holo-TrpR. Similarly, more intrahelical nOes are observed in helix D in the holo-TrpR/DNA ternary complex than in DNA-free holo-TrpR and indicate that when holo-TrpR binds to the DNA operator sequence, helix D becomes better defined in solution (*6*).

The lack of order in the DNA-binding region of TrpR, reflected in the paucity of nOes observed in this area, can be further characterized by considering the dynamics of the protein's architecture. Comparison of backbone amide exchange rates revealed pronounced differences between the DNA-binding domain and the hydrophobic core of the protein (*8-11*). The exchange rates observed within the DNA-binding region were orders of magnitude faster then amide groups located within the hydrophobic core. Binding of L-trp caused a slowing of exchange rates in all regions of the protein. Backbone amide groups that exchanged rapidly in apo-TrpR also exchanged fast in holo-TrpR, however the rates were approximately 3 times slower for holo-TrpR (*9*). A more dramatic effect of L-trp binding was observed for the slower exchanging amide groups of the hydrophobic core. The exchange rates observed in this area of holo-TrpR are an order of magnitude slower than corresponding amide groups in apo-TrpR. These results demonstrated that regional differences in dynamics exist within both forms of TrpR, and that binding of L-trp produces global dynamic effects throughout the protein. These experiments provided direct evidence that the DNA-binding domain of TrpR is more flexible, which had been suggested by NMR structural studies (*4;5*).

The backbone dynamics of TrpR were also probed by ^{15}N NMR relaxation analysis by Jardetzky and coworkers (*12*). In this study the relaxation properties (T_1, T_2, and

steady state nOes) of ^{15}N nuclei found within the TrpR backbone were measured. The methodology and theory associated with these types of measurements will be presented in greater detail in Chapter 2 (Materials and Methods). Equations that described NH backbone movement were fitted to ^{15}N relaxation data and provided insight into the motional restrictedness of individual NH bond vectors. This type of analysis allowed a detailed description of NH bond vectors in terms of an amplitude and timescale of motion. To facilitate reliable descriptions of these motional parameters, researchers had to find an accurate model of the rotational diffusion that represents the TrpR protein. This is due to the fact that the theoretical assumptions which allow for the motional characterization of the NH bond vectors within the backbone are dependent upon rotational diffusion of the protein (*13;14*). Rotational diffusion represents the frequency of protein reorientation in solution, which is dependent upon its shape. Conventionally rotational diffusion is described by a 3x3 matrix called a tensor, which when diagonalized produces the principal values of the diffusion coefficients, often written as D_{xx}, D_{yy}, and D_{zz}. These coefficients represent the magnitude of rotation about their respective axis. ^{15}N NMR solution studies approximate these coefficients, the diffusion tensor, by fitting possible diffusion models to experimental ^{15}N T_1/T_2 ratios (*15*). Jardetzky and coworkers found that the rotational diffusion tensor of TrpR was best modeled as an anisotropic axially symmetric prolate ellipsoid (*12*). In this case, the value of D_{xx} is greater than D_{yy} or D_{zz}, and the value of D_{yy} is equal to D_{zz}. For this type of diffusion tensor D_{xx} is referred to as $D_{\parallel}$, with D_{yy} and D_{zz} referred to as $D_{\perp}$. The ^{15}N NMR relaxation data collected on holo-TrpR by Zheng et al were consistent with $D_{\parallel}$

and $D_{\perp}$ values of 1.48 ± 0.06 s^{-1} and 1.15 ± 0.05 s^{-1}, respectively. Prior to this work (1995) many ^{15}N NMR relaxation studies (*16-18*) simply assumed isotropic rotational diffusion, which sets D_{xx}, D_{yy}, and D_{zz} all equal. This assumption models the proteins shape as a sphere. However, this can led to significant errors in dynamic analysis when deviations from spherical shape influence the measured relaxation properties of the protein (*19*). This deviation is measured by the ratio $D_{\parallel}/D_{\perp}$ and is referred to as the anisotropy of the protein. When the protein shape is modeled as a sphere (i.e isotropic rotational diffusion) the ratio $D_{\parallel}/D_{\perp}$ is equal to one. Any $D_{\parallel}/D_{\perp}$ ratio greater than one represents anisotropic axially symmetric rotational diffusion and alters the theoretical equations one must use to probe the internal backbone motions. The $D_{\parallel}/D_{\perp}$ ratio calculated for holo-TrpR was 1.28 and clearly demonstrated that anisotropy should be considered when probing internal backbone motions. Once the diffusion tensor was correctly established, the amplitude and timescale for the internal motion of individual NH bond vectors within TrpR were determined. The work of Jardetzky and coworkers showed that the entire Trp Backbone, excluding the N and C termini, is quite rigid on the nanosecond time scale (*12*). Unlike the amide exchange results, the ^{15}N dynamic study indicated that the DNA-binding domain is as rigid as the hydrophobic core on the nanosecond timescale. This finding demonstrated that there is no independent motion of backbone NH bond vectors within the DNA-binding domain relative to the hydrophobic core, suggesting that as the protein tumbles in solution these two regions move as a unit. The only areas of holo-TrpR that were found to contain large amplitude motions, indicative of flexibility, were the N and C termini.

The contrast between the amide exchange results and the ^{15}N relaxation study made it necessary to distinguishing between "true" flexibility and "apparent" flexibility observed within the TrpR structural domains (*12*). From this perspective, true flexibility is thought to be reflected in both rapid amide exchange and large amplitude motions of NH bond vectors. While on the other hand apparent flexibility was thought to be reflected in the observation of rapid amide exchange rates, but not observed as large amplitude motions of NH bond vectors in ^{15}N relaxation analysis. Taking these two definitions into account it was evident that the terminal domains of holo-TrpR represented true flexibility of the protein structure, while the DNA-binding domain demonstrated only apparent flexibility. It was speculated by Jardetzky and coworkers (*12*) that the apparent flexibility of the DNA binding domain represents a structural instability which manifests only on the longer millisecond timescale of amide exchange experiments. The importance of these findings is that they showed differences in backbone flexibility exist within the TrpR protein. The terminal domains reveal significant flexibility, with the hydrophobic core displaying rigid structural elements. The results of amide exchange and ^{15}N relaxation experiments suggest that the flexibility of the DNA binding domain is in between these two extremes, with amide exchange experiments pointing toward flexibility on the millisecond timescale, and with ^{15}N relaxation experiments indicating that the region is rigid on the nanosecond timescale. This characteristic difference in flexibility of the DNA binding domain could help explain the ill-defined nature of this region of TrpR that had been observed in NMR structural studies.

As mentioned previously, the results from NMR structural calculations revealed the DNA binding domain of apo-TrpR appears disordered, and that the binding of L-trp and DNA produces more nOes consistent with the presence of helical secondary structure. However disorder in this case reflects a lack of nOe structural restraints. The absences of nOes may be due to a high degree of flexibility or due to fast chemical exchange that would prevent the nOes in that region from being observed. Flexibility in this instance should manifest in both rapid amide exchange and in ^{15}N relaxation studies as large amplitude motions. It has been shown that this definition of true flexibility does not apply to the DNA binding domain. Chemical exchange is a process where a nucleus experiences different electronic environments and results in two magnetically distinct sites with different resonance frequencies. The results of a chemical exchange process can led to a broadening of NMR line shape (*20*) and reduce observable nOe interactions between nuclei. The amide exchange rates observed in the DNA binding domain of TrpR supported the notion that chemical exchange processes involving the amide protons are likely the cause of reduced nOes observed in this area (*12*). This does not mean that this area lacks alpha helical structure, but only that observation of nOes is obscured by exchange processes. In fact, chemical shift indexing (CSI) of the alpha protons of TrpR have shown some helical character within the DNA binding region (*5*). The chemical shift of a nucleus is a measure of the unique resonance frequency that it experiences and is sensitive to spatial conformation. When a polypeptide contains helical structure, the alpha protons contained within experience a common change in their chemical shift relative to a random coil value due to systematic

spatial conformations within the helical structure. It is possible to infer elements of helical secondary structure from NMR spectroscopy based on the indexing of these chemical shift differences (*21*).

These findings have led to the view that the DNA binding region in solution is best represented as helical structures (helix D and E) that undergo partial opening (*10*). This partial opening does not represent complete unraveling of the helices, but rather an opening of hydrogen bonds without a departure from an overall helical conformation which is evident from CSI results (*5*). This description best reconciles the findings of both amide exchange and ^{15}N relaxation results observed in the DNA binding domain of TrpR. As this region undergoes partial opening, amide protons are unprotected against rapid solvent exchange, while at the same time an overall helical conformation preserves alpha proton CSI results. This point stresses the importance of time scale as it relates to structure and stability of this region. It should be noted that stability in this case reflects the observation of properties consistent with structural elements, such as protected amide exchange, nOes, and CSI results, which suggest an alpha helical conformation. When considering this region on a millisecond time scale (*9;10*) which is reflected in the amide exchange rates, helices D and E are unstable, but not generally unstable on a nanosecond time scale reflected in ^{15}N relaxation measurements (*12*).

The structural and dynamic investigations of TrpR have led to many important factors that govern the protein's ability to function. Early crystallographic studies of TrpR defined the relationship between structural features of the protein and its cofactor/DNA binding properties. NMR solution studies of TrpR have demonstrated

that dynamics play an equally important role in the ligand and DNA binding processes. Specifically they have shown that a reduction of dynamics occurs upon ligand binding (*8;9*), and results in a stabilization (previously defined) of helix E. A calorimetric binding study of TrpR to its cofactor is consistent with NMR structural data (*22*), and also suggests that conformational change accompanies helix E upon ligand binding. Similar investigations of the holo-TrpR-DNA solution complex have shown a stabilization (previously defined) of helix D is associated with the DNA binding event (*6*).

Significant insights into the workings of TrpR have also been attained via mutational studies. Early on, mutational research was pivotal in supporting the helix-turn-helix model of repressor/DNA recognition (*23*). Through these efforts, it was also discovered that several of the isolated mutants, classified as super-repressors, were able to function at lower intracellular tryptophan concentrations (*23*) relative to wild-type repressor. Four of these super-repressors were the result of a charge change mutation and are denoted here as E13K, E18K, E49K, and D46N. (The convention used is single letter amino acid abbreviation of wild-type protein, followed by codon number, followed by the mutant residue). A fifth super-repressor resulted from a neutral charge change and is represented as A77V. It is interesting to note that each point mutation is located in one of the distinct structural domains of the protein, yet all share a super repressor phenotype. For instance, E13K resides in the unstructured N-terminal arm, while E18K, E49K, and D46N are found in the hydrophobic core of the protein. A77V, on the other hand, is located in the DNA binding domain between helix D and helix E.

In some way each of these mutants is more sensitive to intracellular tryptophan levels *in vivo,* yet a cogent understanding of the relationship between mutation and activity remained illusive.

The inspired work of Barry Hurlburt and Charles Yanofsky (*24*) investigated the relationship between mutation and activity by searching for measurable differences within these five mutant proteins. Specifically, they were looking at *in vitro* variations of ligand and operator binding as a possible explanation for super-repressor activity. Their studies revealed that the charge change mutants bound a synthetic 43 base pair operator-containing DNA fragment with a lower equilibrium dissociation constant (K_d) of ~10^{-11} M, relative to a wild-type value of ~10^{-10} M. Also, the concentration of L-trp needed to activate the charge change mutants (K_{act}) is well below the 10μM threshold required for wild-type repressor. Paradoxically they found that A77V produces identical values of K_d and K_{act} when measurements are compared to wild-type TrpR values *in vitro*, but displays super-repressor phenotype *in vivo*. The work of Hurlburt and Yanofsky concluded that rapid dissociation of repressor from operator targets is critical for TrpR function *in vivo*, and that favorable electrostatic interaction of the charge change mutants decreases this dissociation, which resulted in increased operator affinity (*24*).

Extensive physical characterizations of the A77V mutant were carried out by Ross Reedstrom and Catherine Royer (*25*), and identified many distinct aspects of the mutant protein. Their investigations revealed that A77V exhibits a 10% increase in apparent α-helicity as measured by CD, and 2.1 kcal/mol more stable to chemical denaturation by

urea. This CD data as well as calorimetric data strongly indicated that apo-A77V is more folded then apo-TrpR, and that binding L-trp is no longer coupled to the ordering of the DNA binding domain. It should be stated that calorimetric binding study of apo-A77V to L-trp revealed an identical affinity for cofactor binding when compared to apo-TrpR. While the cofactor binding affinities are identical (measured as Gibbs free energy, ΔG), the contributions from enthalpy (ΔH) and entropy (ΔS) are distinct for A77V. The A77V shows a much reduced unfavorable entropic contribution to ligand binding when compared to TrpR. This reduction in unfavorable entropic contribution, along with other spectroscopic data (*25*), suggested that the DNA binding domain of apo-A77V exists in a pre-folded state that is consistent with holo-TrpR. It was previously shown (*26*) that apo-TrpR dimers will self aggregate into higher order multimers at micro-molar concentrations, and that binding L-trp greatly reduces this self association process. By linking a dansyl label to the N-terminal end of the mutant protein, Reedstrom and Royer demonstrated that apo-A77V had a much lower propensity to form these higher order aggregates, and the addition of L-trp had no effect on protein self association. Once researchers considered all the unique characteristics of the mutant protein, they began to speculate about how conformational differences within apo-A77V could result in a super repressor phenotype. It was clear that the binding of L-trp produced a stabilization (previously defined) within the DNA-binding domain of TrpR, and that the A77V mutation seemed to uncouple these events. They reasoned that since ligand binding affinities of A77V and TrpR are identical due to compensation of enthalpy/entropy terms, this binding event, while important, is not

coupled directly to protein function through ligand binding affinity (*25*). This reasoning led Royer and coworkers to consider additional interactions connecting ligand binding events to operator binding, since the A77V mutation affects function. The measurements of protein aggregation provided the insight into such an interaction. Their hypothesis was that cells expressing apo-A77V would contain lesser amounts of higher order multimer protein as compared to a cells containing wild type apo-TrpR. This would result in lowering the concentration of L-tryptophan required to produce effective levels of holo-A77V capable of binding operator targets.

Numerous studies have revealed many factors that are critical for TrpR function, which include: protein-protein, protein-ligand, and protein-DNA interactions (*22;25-27*). A mutant that substantially alters any one of these events, as measured *in vitro*, can have dramatic effects on the proteins ability to function *in vivo*. TrpR is interesting in the fact that mutations that cause super-repressor activity are not localized to functionally relevant areas of the protein, but rather found throughout the protein structure. Similar biophysical characterizations have been carried out on the charge change mutants and have found analogous differences in alpha helical content, protein stability, protein-protein, and protein-ligand interactions, relative to the wild-type protein (*28*). The flexibility of the DNA binding domain is also important to the function of TrpR. The work of Sigler and coworkers have shown that L-trp binding caused changes in the orientations of helix D and helix E in TrpR crystal structures (*3*). It was then speculated that the translocation event of helices D and E was critical for operator DNA recognition in the TrpR system. Later investigations by Lawson et al

(*29*) revealed that WT-holo-TrpR can adopt two crystal forms, which correspond to two different conformations of the DNA binding domain. This result also indicates that the DNA binding region is quite flexible. NMR has shown that mutations can influence the dynamics of the DNA binding domain which affect function of the protein. The dynamics of the A77V protein have been probed by amide exchange study and revealed backbone exchange rates in the DNA binding domain of A77V are significantly less than rates of holo-WT-TrpR (*30*). DNA binding studies have shown that the A77V mutant cannot recognize the full complement of operator sequences normally accessible to WT-TrpR (*31*). Together these results have indicated that the dynamic features of the TrpR DNA binding domain are a critical source of adaptability and allow the protein to recognize a range of operator sequences, while maintaining the ability to reject closely related DNA targets. This is in contrast to the view implied by crystallographic studies which suggested only the orientations of helices D and E were important for operator binding. It is now understood that control of gene regulation within the TrpR system is accomplished through the coupling of multiple equilibria events. Only by the careful dissection of structure and molecular reactions within the repressor protein, have the factors governing gene control in the TrpR system been made clearer.

Due to the potential of temperature-sensitive mutants, (ts), to yield additional information about the relationship between TrpR structure, stability, and dynamics, a genetic selection for such mutants was performed. The selection process was based on the compound 5-methyltryptophan (5-MT), an analog of L-trp, that binds to apo-TrpR about two times more tightly (*32*), with the resulting 5-MT/TrpR complex binding to

operator DNA about ten times more tightly (*33;34*). Furthermore 5-MT cannot substitute for the amino acid L-tryptophan during protein synthesis. As a result cells which contain functional TrpR will starve for L-trp on minimal media containing 5-MT, while cells lacking a functional TrpR survive because the operon that controls L-trp production is not repressed (*35;36*). However after mutagenesis, transformants that grow in the presence of 5-MT are believed to contain inactivating mutations in TrpR (*35*). Recently Jin et al (*35*) discovered a (ts) mutant of TrpR, which was selected for growth at 42 °C in the presence of 5-methyltryptophan, and screened for altered growth at 37 °C. This mutation was found to contain a single point mutation at position 75 at the C-terminus of the first helix of the helix-turn-helix motif, with leucine 75 replaced by phenylalanine, and was labeled L75F TrpR (*35*). To verify that the ts phenotype was due only to the mutation at position 75, the coding sequence for L75F was subcloned into vectors that produced non-regulated levels of the mutant protein. The resulting plasmids were transformed into cells lacking the TrpR gene and displayed the same ts phenotype, growth at 42 °C with weak growth at 37 °C. The results indicated that the L75F mutant has a temperature-sensitive function which is better at 37 °C than at 42 °C. Extensive biophysical and biochemical characterizations revealed that the apo-form of L75F TrpR exhibits an apparent increase in α-helicity as measured by CD, and has a slightly higher urea denaturation mid-point. Fluorescence spectra indicated a more buried environment for one or both tryptophan residues (Trp19 and Trp99) of the mutant protein (*35*). This data was corroborated via NMR by detection of slower proton-deuterium exchange rates for the spectrally resolved indole ring protons of the

two tryptophan residues in L75F compared to wild-type aporepressor (*35*). Preliminary 1D and 2D-^{1}H NMR spectra indicated that L75F has a 3D structural fold that is very similar to that of WT- TrpR. It was shown that L75F binds L-trp about ten times weaker than wild type TrpR, and the resulting mutant complex binds DNA only about two to five times weaker. Taken together, these data suggested that the leucine to phenylalanine mutation at position 75 generates non-local effects on the dynamics of the protein, with minor consequences on function (*35*).

The molecular mechanism by which the point mutation of a single surface solvent-exposed loop position can lead to global changes in the TrpR protein is still unclear at present. In order to better quantify these non-local effects and their relationship to the structure and/or amide backbone dynamics of the mutant protein, an intensive NMR based study of the mutant TrpR protein L75F has been performed. This work reports the result of a three-dimensional solution structure determination of apo-L75F TrpR derived through NMR analyses. Given the importance of flexibility within the TrpR protein, and the possible long-range effects that the L75F mutation confers on dynamics, the backbone motions of the mutant TrpR protein were also investigated. The backbone dynamics of apo-L75F were derived from ^{15}N relaxation measurements using similar methodology that was originally used with holo-TrpR by Zheng et al (*12*). To quantify dynamical changes of backbone motions of the mutant, this work also investigated the backbone motions of apo-TrpR by ^{15}N relaxation analysis. This was due to the fact that dynamical analysis by ^{15}N relaxation has not been reported on the wild-type apo-TrpR protein and was needed for comparison with apo-L75F. The results

from the structural and backbone dynamics analyses of apo-L75F are presented and interpreted in terms of the known TrpR paradigm. These results are also used to speculate about how modifications within the mutant protein may affect properties which could explain the temperature phenotype.

Due to the chemical-shift overlap of proton resonance signals observed in 1D and 2D ^{1}H NMR spectra for a protein the size of TrpR (25kDa), it was necessary to employ heteronuclear NMR spectroscopy to facilitate resonance assignment. Heteronuclear NMR spectroscopy can aide in resonance assignment of highly overlap proton resonances provided the protein can be labeled with the non-radio active isotopes ^{15}N and ^{13}C. The spectral resolution of highly overlapped ^{1}H signals is improved by increasing the dimensionality of the NMR spectrum so that these problem areas are separated in 2D, 3D, and 4D spectra according to the better resolved heteronuclear resonance (i.e ^{15}N and ^{13}C) (*37*). The apo-L75F protein was labeled with $^{15}N/^{13}C$ isotopes and the structure was solved using structural restraints derived from conventional heteronuclear (^{1}H, ^{15}N, ^{13}C), multidimensional (2D, 3D, and 4D) solution NMR methods. Structural calculations were performed using the two programs Crystallography & NMR Systems (CNS) (*38*) and X-PLOR version 3.1 (*39*). Determination of the 3D structure of the L75F dimer was based on a total of 1538 ^{1}H nOe-based distance restraints (i.e. 769 unique nOe restraints/monomer), 68 dihedral angle restraints, and 62 hydrogen bond restraints, and resulted in an ensemble of 20 low energy conformers with an average root-mean-square deviation (rmsd) of 1.0 Å for

backbone atoms in the core helices A, B, C, and F, and an average rmsd value of 2.6 Å for helices D and E.

In the course of this work it was discovered that significant ^{1}H-^{15}N chemical shift changes had occurred for backbone amides in L75F when compared to the corresponding chemical shifts reported for wild-type apo-TrpR. It was hypothesized that ring-current effects introduced by the mutant residue phenylalanine may influence nearby amide groups and cause the chemical shift differences. The merit of this hypothesis was addressed by considering the physical nature of the ring-current effect (*40*) within the context of twenty calculated solution structures of apo-L75F. The data analyses suggest that such chemical shift changes cannot be accounted solely on the basis of ring current shifts originating from the leucine to phenylalanine substitution at position 75. Thus, structural and dynamical differences between apo-L75F and apo-WT-TrpR have been investigated in order to uncover a possible explanation for these non-local effects observed in the mutant protein.

Backbone ^{15}N relaxation measurements have been obtained for 54 residues of apo-WT TrpR, and 75 residues of apo-L75F. The difference in number of residues is due to significant resonance overlap observed in both proteins as well as incomplete resonance assignment available for apo-WT TrpR. Using the structures of apo-L75F and wild type apo-TrpR (*5*), along with the ^{15}N relaxation data, the motional anisotropy was determined from their respective diffusion tensor. The diffusion tensors for both wild type apo-TrpR, and apo-L75F were independently modeled as axially symmetric prolate ellipsoids when fitted to the ^{15}N relaxation data collected in this study. The anisotropy

was calculated from the principal components of the diffusion tensor ($D_{xx}=D_{yy}=D_{\perp}$, $D_{zz}=D_{\parallel}$) from the ratio $D_{\parallel}/ D_{\perp}$. This resulted in a value of 1.20 ± 0.04 for apo-L75F and a value of 1.15 ± 0.04 for the apo-WT TrpR. The structural regions of both proteins display similar relaxation signatures, and there are no significant differences regarding the diffusion tensor values $D_{\parallel}/ D_{\perp}$, which reflects the motional anisotropy. Once the diffusion tensors were established for both wild-type and mutant proteins, motional dynamics of backbone NH groups were derived and compared. Models of backbone motions within the context of an axially symmetric diffusion tensor were fit to ^{15}N relaxation data using the program NORMAdyn. The results from this analysis describes motions of NH bond vectors in terms of an order parameter and time scale of motion, similar to the study of Zheng et al (*12*). Due to the complexity of ^{15}N relaxation analysis, a detailed description of the theory and methodology of these types of experiments will be presented in Chapter 2 (Material and Methods) of this thesis. However results from these analyses indicate very similar ^{15}N relaxation profiles for both proteins and do not point to any major dynamical differences within the backbone motions. It should be noted that this work does not rule out the possibility that other dynamic differences may exist between apo-L75F and apo-WT-TrpR. Side chain dynamics obtained by ^{13}C relaxation studies or probing the slower millisecond timescale may lead to insightful contrasts between the two proteins that would help explain the effects of the L75F mutation.

The NMR study presented herein supports the biochemical and biophysical findings of Jin et al (*35*), that the leucine to phenylalanine mutation at position 75

indeed propagates long-range effects throughout the protein. This work quantifies structural and dynamical differences at the atomic level of apo-L75F by comparison with apo-WT TrpR under identical solution conditions. It is shown that hydrophobic core of apo-L75F has undergone a small perturbation. This is reflected in the distances between helices C/C', helices A/C', and helices C/F relative to corresponding values obtained from the published structures of apo-WT TrpR *(5)*. Chemical shift differences, together with inspection of the apo-L75F TrpR structures, also point to a reordering of the L-Trp binding pocket in the mutant protein. Overall the ^{15}N relaxation data probing the NH backbone dynamics do not seem to indicate major differences between the apo-forms of wild-type and mutant proteins. The only exception is that simpler models of backbone motions can be used to fit NH groups within the DNA binding domain of apo-L75F and may suggest a decrease in motional complexity of this region relative to the wild-type apo-protein. This analysis suggests that if major dynamical differences exist between the two proteins, they may manifest on a slower microsecond to millisecond time scale, or may be reflected in dynamical differences of sidechains.

Chapter 2

MATERIAL AND METHODS

Sample preparation

The *E.coli* strains CY15071 and CY15075, and the plasmid pJPR2.L75F were provided by Professor Jannette Carey (Princeton University, Princeton, NJ). Uniformly ^{15}N or $^{15}N/^{13}C$ enriched L75F protein was isolated from CY15071 or CY15075, transformed with the overproducing plasmid pJPR2·L75F. The strains were grown in M9 minimal medium enriched with $[^{15}N]NH_4Cl$ (99% ^{15}N, Cambridge isotopes) or $[^{15}N]NH_4Cl$ /[^{13}C]D-Glucose (99% ^{13}C, Cambridge isotopes) as the sole nitrogen and carbon sources respectively. Protein purification procedures were carried out as described by Jin et al (*35*), and are similar to the protein isolation and purification protocols reported for WT-TrpR. A detailed description of the protein purification procedure is presented in the next section of this work. Protein samples were concentrated to approximately 1 mM protein dimer, in the NMR buffer (500mM NaCl, 50mM NaH_2PO_4, 90% H_20 /10% D_20) at a pH=5.7. The CY15071 cell cultures were supplemented with 20 mL per liter of a 0.2 M unlabeled threonine stock solution because this strain of *E. coli* cannot produce this amino acid *de novo*. Protein samples made from CY15071 bacterial growth lacked ^{15}N or $^{15}N/^{13}C$ labeled threonine residues, and as a result were unobservable in heteronuclear NMR experiments. Uniformly labeled protein, containing ^{15}N or $^{15}N/^{13}C$ labeled threonines, was produced by

overexpressing L75F in a different bacterial strain, CY15075, grown in M9 minimal media supplemented with ^{15}N-ammonium chloride and ^{13}C-labeled glucose.^{15}N labeled wild-type aporepressor protein used for initial comparison was kindly provided by Dr. Eva Hyde and Mrs. Rosemary Parslow (University of Birmingham, Birmingham, England). Subsequent wild-type protein was expressed and purified from the pJPR2 plasmid donated by Professor Jannette Carey. Wild-type protein was concentrated to approximately 1mM protein dimer, under identical solution conditions previously described.

Protein Purification

Solutions of complete M9 minimal medium were prepared by weighing out 6g Na_2HPO_4, 3g KH_2PO4, 0.5g NaCl, 1g $^{15}NH_4Cl$ and were brought to a volume of 1.0 liter. This solution was then placed into a 2 L culture flask, autoclaved for 30 minutes and allowed to cool overnight. Typical preparations required two liters of growth medium. A small 10ml culture, containing Luria-Bertani (LB) broth, supplemented with ampicillin (10ug/ml), containing freshly transformed cells (CY10571/pJPR2.L75F or CY10575/pJPR2.L75F) was allowed to grow overnight in an incubator shaker at 37 ^{0}C and 200 rpm. The next morning, the following supplements are added to each liter of M9 medium: 20 ml of 20% glucose, 2 ml of 1 M $MgSO_4$, 1 ml of 100mg/ml ampicillin . It should be noted that 10 ml of 20% ^{13}C-glucose is substituted for ^{13}C labeling of the protein. Also, when using the CY10571 cell strain, the addition of 20 ml of 0.2M L-threonine per liter of M9 is required. The overnight culture is then

centrifuged at 7,000 x G for 10min and resuspended in 10ml of fully supplemented M9, and 5 ml of this mixture is added to each flask. Each 2 L culture flask (containing approximately 1L supplemented M9, and 5 ml of overnight culture) is placed into an incubator shaker at 37 ^{0}C, 200 rpm and grown to an OD_{600} = 0.4 to 0.5 after which time IPTG is added to a final concentration of 1.0 mM. The cultures are then allowed to grow overnight (12 to 14 hours).

Mature cultures are placed on ice and poured into 250 ml centrifuge bottles and centrifuged at 8,500 x g for 15 min. Each pellet is resuspended in 10 ml of 0.1 M Tris·HCl, pH=7.6 and 30 ul of 100mM PMSF. This results in about 90 ml of cell suspension for a 2 L culture. The cell suspension is then broken by one cycle of French press (external pressure 1300 psi). The lysate is then spun at 8,500 x g for 25 min and the supernatant is collected. This solution is placed in a room temperature water bath and a 20% streptomycin sulfate solution is added to 1% with gentle stirring. The water bath is then slowly heated to 62 ^{0}C on a hot plate and the solution is allowed to stand at 62 ^{0}C for 5 min. The solution is then removed from the water bath and chilled on ice for 30 min. The thick white precipitate that forms is centrifuged at 8,500 x g for 15 min and the supernatant is collected. The mixture is then placed in an ice bath and ammonium sulfate is added to 45% saturation with gentle stirring. After all the salt has been added the mixture is allowed to stir at 0 ^{0}C for 30 min and then centrifuged at 12,500 x g for 15 min. The resulting supernatant is collected and ammonium sulfate is added to 70% saturation, and after equilibration, spun at 12,500 x g for 15 min. The supernatant is discarded and the pellet is resuspended in 25 ml P11 buffer (10mM

$NaPO_4$, pH 7.6, 0.1mM EDTA, 0.1M NaCl). The protein solution is dialyzed against P11 buffer (4 L) overnight with three changes of buffer.

A 1.5 x 20 cm column of Whatman P-11 cellulose phosphate, equilibrated in P11 buffer, is constructed following the manufacturers protocol. The dialyzed protein solution is loaded onto the column and washed with 20 ml of P11 buffer. The column is developed using a gradient mixer with 120 ml P11 buffer containing a total concentration of 0.15 M NaCl in the mixing chamber, and 120 ml of P11 buffer containing a total concentration of 0.75 M NaCl in the gradient chamber. The column is run with a flow rate of 0.5ml/min collecting fractions every four minutes. Fractions containing protein, as determined by 280 nm absorbance (> 0.1) are run on SDS-Page gels containing 15% polyacrylamide to determine purity. Contaminating protein bands are removed by generating a fresh P11 column and repeating the above procedure. Clean fractions containing L75F-TrpR are combined and dialyzed against NMR buffer (50 mM $NaHPO_4$, pH=5.7, 0.5 M NaCl) and concentrated by passing through Centricon YM12 membrane (Amicon), using a nitrogen pressure cell, to a final volume of 0.7 to 1.0ml. Concentration of the protein solution was calculated from the 280 nm absorbance using the extinction coefficient of 1.18 cm^2 / mg (*35*). The D_2O samples are prepared by lyophilization of protein solution with known volume and concentration. The resulting powder is brought up to the original starting volume using 99.9% D2O (Cambridge isotopes).

NMR spectroscopy

All NMR spectra were acquired at 45 ^{0}C on a four channel Bruker DRX-600 spectrometer, with a triple ^{15}N, ^{13}C, ^{1}H inverse resonance probe equipped with triple axis gradients. Quadrature detection for all multidimensional NMR experiments was achieved by recording the data in States-TPPI mode in the indirect dimensions (*41*). ^{1}H and ^{13}C dimensions were referenced to DSS, while the ^{15}N dimension was referenced directly from the ^{15}N chemical shift of the amide nitrogen of Asp108 of apo wild-type TrpR reported by Jardetzky and coworkers (*11*), which allowed a direct comparison of chemical shift values. A detailed description of all experimental NMR parameters is available in appendix A. All data were processed and analyzed using NMRPipe (*42*), PIPP (*43*), and Xwinnmr (Bruker Inc.) software packages.

Two dimensional ^{1}H-^{15}N HSQC (*44*) spectra were acquired with spectral widths of 12.0 ppm in t_2 and 30.0 ppm in t_1, with the proton carrier frequency set at 4.6ppm with respect to DSS and the nitrogen carrier set at 115.5 ppm. Data were collected with 1024 complex points in t_2 and 128 complex points in t_1, using Waltz16 (*45*) for ^{15}N decoupling during data acquisition. Apodization was performed using a sine bell squared function shifted by 0.35 π radians in t_2, and a sine bell function shifted by 0.40 π radians in t_1.

Sequential ^{1}H / ^{13}C backbone and side-chain chemical shift assignments were extracted from hetronuclear NMR experiments (CBCANH, CBCA(CO)NH, C(CO)NH, HBHA(CO)NH, HC(CO)NH) (*46-49*), acquired with spectral widths of 12.0 ppm (in t_3), 67.0 ppm (in t_2), and 30.0 ppm (in t_1) for proton, carbon, and nitrogen dimensions,

respectively. Carrier frequencies were set to the same values as described previously, with the additional carbon carrier frequency set to 46.0 ppm. Data were collected with 512, 58, and 24 complex points in t_3, t_2, and t_1, respectively, using the DIPSI scheme for ^1H decoupling (*50*) during carbon evolution, and the Waltz 16 scheme for ^{15}N decoupling (*45*) during data acquisition. Similar apodization functions were used in all spectral dimensions, using shifted sine bell functions.

Structure calculations

A large portion of the nOe-based distance restraints for the structure calculations was derived from 3D ^{15}N-NOESY-HSQC (*51;52*) experiments recorded with nOe mixing periods of 50, 90, and 120 msec. Additional nOe connectivities to aliphatic protons were identified from a 3D HCCH-NOESY experiment (*53*) recorded with a nOe mixing time period of 120 msec. A total number of 1538 nOe cross peaks were assigned, with 39 representing intermolecular assignments, and served as the basis of the structure calculations. Noes were classified into four categories and restraints were given the following ranges based on qualitative analysis of cross peak intensity: strong (1.8 – 3.0 Å), medium (1.8 – 3.5 Å), weak (1.8 – 4.5Å), and very weak (1.8 – 5.0 Å). H-bonding distance restraints were identified through ^1H / ^2H amide exchange experiments and were given the boundaries 1.5 – 2.3 Å (H-O) and 2.5 – 3.3 Å (N-O). Due to the exclusively alpha-helical character of TrpR and significant overlap of spectral resonances, three bond H_N-H_α scalar couplings could not be measured reliably. The measurement of this coupling is sensitive to the Φ dihedral angle, and can be used to

restrict backbone conformation in NMR structure calculations (*54*). However, following the seminal work of D. Zhao et al (*5*), we used $^{1}H_{\alpha}$ / $^{13}C_{\alpha}$ chemical shift indexing and characteristic nOes to infer elements of alpha-helical secondary structure. This allowed us to conservatively restrict Φ angles to $-65^{\circ} \pm 45^{\circ}$ for the hydrophobic core (A, B, C, and F), and the helix-turn-helix region (D and E) to $-65^{\circ} \pm 60^{\circ}$. The ranges of these values were set large so that they alone could not force formation of alpha-helices, and better reflect the fact that these angles are based on inference rather than measure of three-bond scalar couplings.

Simulated annealing was performed on two identical extended structures spanning residues 3-108, using the program Crystallography and NMR systems (*38*). Forty structures were then calculated using the standard input file *anneal.inp* that was modified to include 4000 steps for both the high temperature and the first slow-cooling annealing stage in torsion angle space. The molecular dynamic scheme used in CNS consisted of the following stages: a). Heating in torsion angle space at 50,000 $^{\circ}$K for 60 psec with the energy constant for the van der Waals parameters scaled by 0.1; b). Cooling in torsion angle space to 2,000 $^{\circ}$K for 60 psec with ramping of the van der Waals parameters to full scale; c) Cooling in Cartesian space to 300 $^{\circ}$K for 15 psec using conventional molecular dynamics; and d), 2000 steps of conjugate-gradient Powell minimization. The weights for the NOE restraints were set to 150 kcal/mol for stages a-c, and 75 kcal/mol for stage d. The functional form of the NOE distance restraints was a flat-bottomed parabolic function with a soft asymptote. A sum averaging function was used for both NOE and H-bond restraints. The weights of the

dihedral angle restraints were set to 100 kcal/mole for stage a, 200 kcal/mole for stage b-c, and 400 kcal/mole for the final stage d.

The 40 calculated structures were further refined against NCS symmetry restraints using the program X-PLOR version 3.1 (*39*). This was done to ensure the two-fold symmetry of the L75F homodimer. NCS weighting factors were set to 25 kcal mol^{-1} $Å^{-2}$, for all backbone atoms, and 5 kcal mol^{-1} $Å^{-2}$ for all other non-hydrogen atoms. The 20 lowest energy structures were then selected and analyzed using the programs Quanta (Molecular Simulations Inc.), Procheck NMR (*55*), and DisCal (A. Hinck, unpublished). Calculations of average and pairwise rmsds were performed in X-PLOR 3.1 (*39*). Also a similar set of calculations starting with 100 structures were performed to ensure that the final structures had converged to their lowest conformational energy.

Relaxation Analysis

In the course of an NMR experiment, radio frequency pulses are applied to a spin system which brings it into a nonequilibrium state. Relaxation is the process which brings the spin system back into its equilibrium state. Relaxation analysis, as described in the context of this work, will deal with the modeling of protein backbone motions via ^{15}N NMR relaxation properties. These properties include: ^{15}N longitudinal relaxation time constant (T_1), ^{15}N transverse relaxation time constant (T_2) and heteronuclear steady state nOe (^{15}N-{^{1}H} nOe). For the remainder of this section the heteronuclear steady state nOe will simply be referred to as the nOe. The longitudinal relaxation rate R_1 is equal to $1/T_1$, and represents the rate at which non-equilibrim magnetization is returned

to its equilibrium state denoted as M^{o}_{z}. The transverse relaxation rate R_2 is equal to $1/T_2$, and represents the rate at which non-equilibrium magnetization loses its phase coherence in a direction perpendicular to the applied static magnetic field. The nOe is dependent on cross-relaxation, which is a consequence of the dipolar interaction between the ^{15}N nucleus and its attached proton. The cross-relaxation is expressed in terms of two relaxation rates, denoted as W_0 and W_2, which represent conduits that also allow nuclear spin states to return to their equilibrium populations (*56*). The measured nOe is equal to $1+(W_0-W_2)/R_1$, in which R_1 refers to the longitudinal relaxation rate of the ^{15}N nucleus (*57*). It should be noted that this above equation is specific for a heteronuclear nOe in which the gyromagnetic ratios of the two nuclei involved have opposite signs (i.e.$\gamma(^1H) = 2.67 \times 10^8$ rad/T·s, $\gamma(^{15}N) = -2.71 \times 10^7$ rad/T·s). From this equation one can see that it is possible to observe both positive and negative nOes. In a general sense this can be understood by considering the two relaxation rates W_2 and W_0. Most NH bond vectors in the protein undergo slow molecular reorientation with respect to the static magnetic field, which results in NH bond vectors being dominated by the W_0 pathway (*56*), such that W_0 is greater than W_2 and the measured nOe is positive. However when regions of the protein are flexible these NH bond vectors experience rapid reorientation such that the relaxation is dominated by the W_2 relaxation pathway (*56*), and thus leads to a negative nOe value. When measuring the nOe of a ^{15}N labeled protein, one sees both positive and negative values which convey local flexibility of NH bond vectors within the structure. The lower the nOe value, the more flexible the NH bond vector.

The spin relaxation of backbone amide ^{15}N nuclei is strongly influenced by the dipolar interaction between the ^{15}N nucleus and the attached proton, and the chemical shift anisotropy. It has been shown that ^{15}N relaxation rates and steady state nOes are dependent on five unique frequencies (0, ω_H, ω_N, ω_{H+N}, ω_{H-N}), defined within a spectral density function denoted as $J(\omega)$. The ^{15}N longitudinal (T_1) and transverse (T_2) relaxation times and heteronuclear nOe are given the following relationships (*58*):

$$1/T_1 = \{d^2/4\}[J(\omega_H-\omega_N) + 3J(\omega_N) + 6J(\omega_H+\omega_N)] + c^2(J\omega_N) \quad \text{(equation 1)}$$

$$1/T_2 = \{d^2/8\}[4J(0) + J(\omega_H-\omega_N) + 3J(\omega_N) + 6J(\omega_H) + 6J(\omega_H+\omega_N)] + \{c^2/6\}[3J(\omega_N) + 4J(0)] + R_{ex} \quad \text{(equation 2)}$$

$$nOe = 1 + \{\gamma_H/\gamma_N\}d^2[6J(\omega_H+\omega_N) - J(\omega_H-\omega_N)]T_1 \quad \text{(equation 3)}$$

with the constants d^2 and c^2 defined as

$$d^2 = \{1/10\}\,\gamma^2_H\gamma^2_N\{h/2\pi\}^2\{1/r^6\}$$

$$c^2 = \{2/15\}\,\omega^2_N\{\sigma_\parallel - \sigma_\perp\}^2$$

in which h is Planck's constant, γ_H and γ_N are the gyromagnetic ratios of the ^1H and ^{15}N nuclei, ω_H and ω_N are the Larmor frequencies of the ^1H and ^{15}N, r is the ^1H to ^{15}N internuclear distance of an amide bond (r = 1.04 Å), and $\sigma_\parallel$ and $\sigma_\perp$ are the parallel and perpendicular components of the ^{15}N chemical shift tensor and are taken to be $(\sigma_\parallel - \sigma_\perp)$ = -160 ppm (*59*).

The spectral density function, $J(\omega)$, depends on the overall molecular reorientation of the protein, as well as the internal motions of individual NH bond vectors. Direct measurement of the three relaxation parameters, T_1, T_2, nOe, does not provide sufficient information to uniquely determine the spectral density at the five frequencies expressed in equations 1-3. However, to gain insight into internal motions, this is in fact not necessary. The spectral density function can be approximated by a minimum number of parameters that correlate to internal NH bond vector motion. In this work, relaxation analysis by spectral density approximation was achieved by using the formalism of Lipari and Szabo (*13;14*). This approximation expresses the spectral density function in terms of three parameters, the values of which are derived from mathematical fittings to the experimentally obtained ^{15}N relaxation data. The exact details of this fitting procedure and a description of the parameters in terms of internal motion will be presented later. What follows directly is a review of how the molecular shapes of proteins are accounted for by the spectral density function and their effect on the ^{15}N relaxation values T_1 and T_2. It will then be shown how the parameters describing internal backbone motions are derived from NMR relaxation data using the formalism of Lipari and Szabo.

For a protein assumed to have a spherical shape (i.e isotropic), the spectral density function is expressed in terms of the overall correlation time (τ_c) for the entire molecule. Specifically, τ_c is defined as the average time taken for the molecule to reorient through one radian (*56*). Hence, the overall correlation time represents the time scale on which protein reorientation takes place in solution. Typical correlation times for proteins are

on the order of nanoseconds, and generally the lower a protein's molecular weight, the shorter its correlation time in solution. For instance, human ubiquitin with a molecular weight of 8 kDa has a reorientational correlation time of 4.6 ns (*19*), while staphyloccocal nuclease with a molecular weight of 16.8 kDa, exhibits a correlation time of 9.1 ns (*15*). The spectral density for the isotropic case is a single Lorentzian function of the form:

$$J(\omega)= 2\tau_c/1+\omega^2\tau_c^2 \qquad \text{(equation 4)}$$

with τ_c representing the overall correlation time for the protein's global reorientation in solution. The spectral density function $J(\omega)$, expressed in equation 4, tells us the power available from the surroundings (i.e from molecular motions) to bring about nuclear spin relaxation, as a function of molecular tumbling (τ_c).

In the case of TrpR, as discussed above, the protein displays a substantial deviation from spherical shape, and this anisotropy must be taken into account when considering the effects of molecular tumbling. This is achieved by expressing the spectral density as a sum of Lorenzian functions which are related to the rotational diffusion coefficients D_{xx}, D_{yy}, and D_{zz} . It has been shown that the rotational diffusion tensor of TrpR is best described by an axially symmetric model with only two unique rotational diffusion coefficients parallel ($D_{\parallel}$) and perpendicular ($D_{\perp}$) (*12*). For this condition the expression for calculating the spectral densities is given by (*60*):

$$J(\omega) = C_1 \{\tau_1/(1+\omega^2\tau_1^2)\} + C_2 \{\tau_2/(1+\omega^2\tau_2^2)\} + C_3 \{\tau_3/(1+\omega^2\tau_3^2)\} \qquad \text{(equation 5)}$$

in which,

$C_1 = \frac{3}{4} \sin^4\theta$ $C_2 = 3 \sin^2\theta \cos^2\theta$ $C_3 = \frac{1}{4} (3 \cos^2\theta - 1)^2$

and θ is the angle between the NH bond vector and the unique axis ($D_\parallel$) of the diffusion tensor. The correlation times τ_1, τ_2, and τ_3, displayed in equation 5, now depend upon the components of the diffusion tensor and are expressed as:

$\tau_1 = 1/\{4D_\parallel + 2D_\perp\}$ $\tau_2 = 1/\{D_\parallel + 5D_\perp\}$ $\tau_3 = 1/6D_\perp$

The overall correlation time τ_c for a protein experiencing axially symmetric diffusion can be calculated from the expression:

$\tau_c = (2D_\parallel + 4D_\perp)^{-1}$ and is also on the order of nanoseconds.

It is apparent from equation 5 that the spectral density function of a protein experiencing anisotropic diffusion will not only depend on the components of the diffusion tensor, but also on the orientation of the NH bond vector with respect to the $D_\parallel$ component. As a result, calculated T_1 and T_2 values derived from equations 1 and 2 will also display these dependencies when the protein experiences this type of diffusion. The effects of anisotropy ($D_\parallel/D_\perp$) and NH bond vector orientation on calculated ^{15}N-T_1 and ^{15}N-T_2 values are shown in Figure 2 for a prolate ellipsoid (reproduced from Pawley et al (*61*)). In this figure, α is the angle between the NH bond vector and the unique axis of the diffusion tensor. It should be noted that an α angle of zero degree corresponds to the NH bond vector lying coincident with the positive D_{zz} direction (also referred to as $D_\parallel$), and an angle of 90° is when the vector lies in the plane defined by

D_{xx} and D_{yy} (both also referred to as $D\perp$) (Figure 2c). The allowed range for α is between 0^o and 90^o, based on the assumption that rotational diffusion in this theoretical description will have only one sense of rotation about the D_{zz} axis, such that any angle greater than 90^o will result in a negative D_{zz} value and change the sense of rotational direction (*60*).

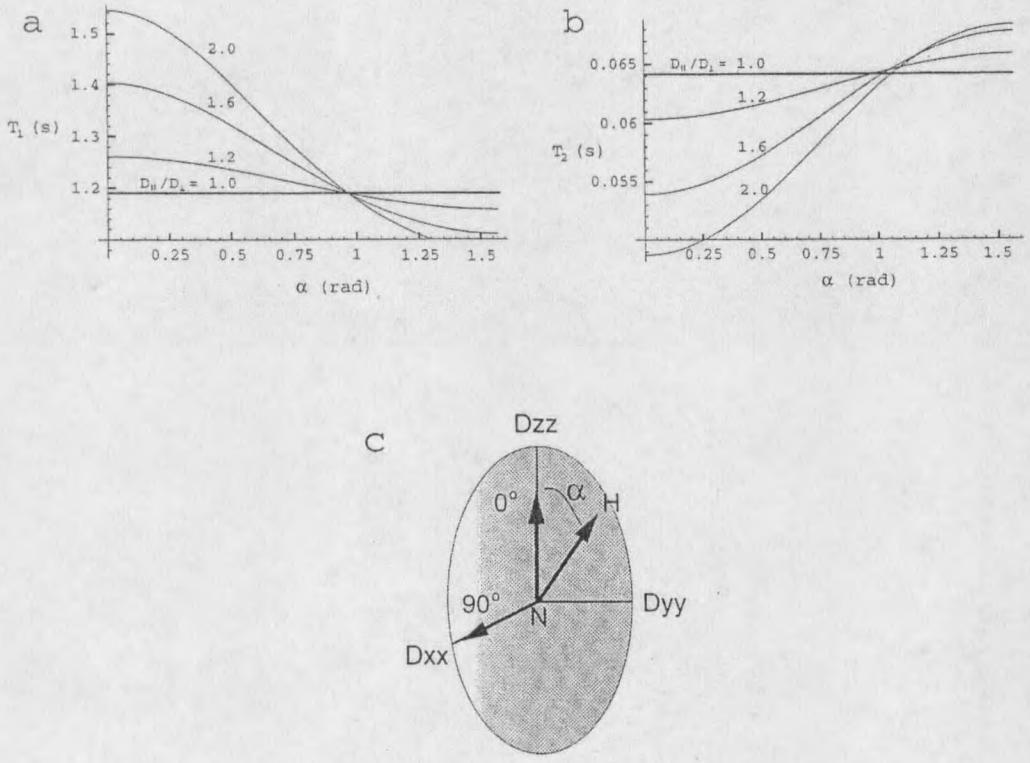

Figure 2: Effect of anisotropy on ^{15}N-T_1 and ^{15}N-T_2 for a prolate ellipsoid, reproduced from Paweley et al (60). (a) ^{15}N-T_1 as a function of four values of $D\parallel/D\perp$. (b) ^{15}N-T_2 as a function of four values of $D\parallel/D\perp$. (c) Ellipsoid corresponding to a prolate diffusion tensor displaying possible orientations (α) of an NH bond vector relative to the diffusion axis. In above diagrams (a) and (b) 1α (rad) = 57.4^o

Figure 2 demonstrates that when alpha is less then 54.7° (0.95 radians) the effects of anisotropy ($D_{\parallel}/D_{\perp}$) on the ^{15}N nucleus, shown in figures 2a and 2b, will manifest as large T_1 and small T_2 values. When calculating T_1/T_2 ratios, it is clear that as the anisotropy increases, the value of the T_1/T_2 ratio will also increase when alpha is below 54.7°. For values of alpha greater then 54.7°, the opposite trend is observed, i.e. T_1/T_2 ratio will decrease as the anisotropy increases. Using these known trends, it is possible to determine the diffusion tensor from a PDB file of the protein structure and experimentally obtained ^{15}N-T_1 and ^{15}N-T_2 values by minimizing the following equation:

$$\chi_D = \Sigma_i [\{T_{1i}/T_{2i}\}_{exp}-\{T_{1i}/T_{2i}\}_{calc}]^2/ \sigma_i^2 \qquad \text{(equation 6)}$$

where the summation extends over all assigned residues of the protein, and σ_i^2 represents the square of the propagation of error in experimentally measured T_1/T_2 values (*62*). When using equation 6, the "calc" terms refer to calculated T_1/T_2 values based on equations 1 and 2. From the PDB structure file of the protein, an initial estimate of the diffusion tensor is made, and used to calculate T_1/T_2 ratios for each amide bond vector. Using this initial estimate, and the aforementioned trends, the components of the diffusion tensor are searched for values that best agree with T_1/T_2 ratios based on experimental measurements, which consequently minimize equation 6.

By comparing the mathematical expressions for the spectral density function $J(\omega)$ described in equations 4 and 5, it can be understood how molecular shape is taken into

account in ^{15}N relaxation studies. However, local motions of individual NH bond vectors will also alter J(ω) and cause deviations from theoretical T_1, T_2, and nOe values based on equations 1-3. To take internal motions into account, we have used the formalism proposed by Lipari and Szabo (*13;14*). This treatment employs additional terms to the spectral density function which account for internal NH bond motions. In the case of axially symmetric rotation with internal motions, the spectral density function takes the form *(13;14)*:

$$J(\omega) = S^2 [C_1 \{\tau_1/(1+\omega^2\tau_1^2)\} + C_2 \{\tau_2/(1+\omega^2\tau_2^2)\} + C_3 \{\tau_3/(1+\omega^2\tau_3^2)\}] + (1-S^2) [\tau'/(1+\omega^2\tau'^2)] \quad \text{(equation 7)}$$

with $C_{1,2,3}$ and $\tau_{1,2,3}$ having the same definitions previously described in equation 5. The new term S^2, referred to as the order parameter, represents the restrictedness of NH bond vector motion, and ranges in value between 0 and 1. A value of 0 represents completely unrestricted motion of the bond vector, while a value of 1 represents a completely static NH bond vector. Relaxation studies of proteins that have employed the Lipari-Szabo formalism have shown that areas of secondary structure generally correlate to S^2 values greater than 0.7, with disordered areas (i.e loop regions, N and C termini) commonly having values below 0.7 (*16-18*). The term τ' represents a new time constant which is dependent on both the overall correlation time of the protein (τ_c) as well as the internal correlation time of the NH bond vector (τ_e), such that:

$1/\tau' = 1/\tau_c + 1/\tau_e$

τ_e represents the timescale of NH bond vector reorientation, with typical values for backbone amide groups on the order of picoseconds (*16-18*). It should be noted that the motion ascribed to an individual NH bond vector (S^2, τ_e) is taking place within the overall reorientation of the protein characterized by τ_c.

Once the diffusion tensor has been established, the order parameters and the internal correlation times can be extracted by minimization of the following equation χ^2, such that:

$$\chi^2 = \{(T_1^{exp} - T_1^{calc})^2 / \sigma_{T1}^2\} + \{(T_2^{exp} - T_2^{calc}) / \sigma_{T2}^2\} + \{(nOe^{exp} - nOe^{calc}) / \sigma_{nOe}^2\}$$

(equation 8)

where "exp" and "calc" denote the experimental and calculated values of T_1, T_2 and nOe, respectively. The term σ^2 denotes the square of the experimental uncertainty associated with the corresponding relaxation parameter, and is based on Monte Carlo analysis of independently acquired data sets (*62*). The calculated values of equation 8 are determined by holding τ_c constant, while varying S^2 and τ_e until a minimum is reached.

The theoretical descriptions given above serve as the foundation for protein backbone dynamics via ^{15}N relaxation measurements. The methodology for using ^{15}N relaxation data for backbone analysis in the presence of anisotropic molecular reorientation can be summarized as follows: 1) Acquisition of molecular coordinates of the protein's 3D structure. 2) Measurement of ^{15}N-T_1, ^{15}N-T_2, and nOe values for

backbone amide bond vectors. 3) Fitting of the diffusion tensor components based on T_1/T_2 ratios (equation 6) and the molecular coordinates of the protein. 4) Determination of internal motional parameters of NH bond vectors based on the Lipari-Szabo formalism. Each of these points as they pertain to the ^{15}N relaxation study of apo-L75F and apo-WT-TrpR will be presented.

The molecular coordinates of apo-L75F were acquired through the NMR based structural study presented in this work. Using the twenty generated structures, the minimized average structure of apo-L75F was calculated and served as the framework for the backbone dynamical analysis of the apo mutant protein. The fifteen structures of apo-WT-TrpR were obtained from the protein data bank (*63*), based on the work of Zhao et al (*5*). These structures were used to calculate the minimized average structure of apo-WT-TrpR, and provided the framework for backbone dynamical analysis of the apo wild-type protein.

Backbone amide ^{15}N T_1, T_2, and ^1H-^{15}N nOe values were measured for both apo-L75F and apo-WT-TrpR, using previously published pulse sequences (*15;16;64;65*). The T_1 relaxation profile was sampled at eight different time points (40, 96, 200, 400, 600, 800, 1000, 1200 ms). The T_2 relaxation profile was sampled at eight different time points (8, 16, 32, 40, 64, 80, 104, 152 ms), with the delay between ^{15}N 180° pulses in the CPMG sequence set to 0.5 ms. The CPMG sequence is employed to eliminate cross-correlation between the dipolar and CSA tensors (*64*) that can greatly affect T_2 relaxation measurements. Both T_1 and T_2 measurements were collected with 1024 complex data points in t_2 and 256 complex data points in t_1 using the Waltz 16 (*45*) for

^{15}N decoupling. Apodization was performed using a sine bell squared function shifted by 0.35 π radians in t_2, and a sine bell function shifted by 0.40 π radians in t_1. Spectra were recorded with 24 scans per t_1 increment using a recycle delay of 1.0 s. The ^{15}N-$\{^1H\}$-nOes were measured as the ratio of peak intensities (I/I_o), acquired with (I) and without (I_o) solvent presaturation. Spectra were collected with 1024 complex data points in t_2 and 256 complex data points in t_1, with 48 scans per t_1 increment. To avoid systematic errors in measured nOe values introduced by solvent saturation effects (*65*), nOe experiments were run with a recycle delay of 4.25 s. The T_2 and ^{15}N-$\{^1H\}$ nOe experiments were run in an interleaved manner, with T_1 experiments run consecutively using the Bruker multizg awk program (Bruker Inc.) using shuffled relaxation delays. The shuffled relaxation delays are employed to reduce systematic error of T_1 values associated with magnetic field drift of the spectrometer.

Determination of backbone amide ^{15}N T_1 and T_2 relaxation times for both mutant and wild-type proteins were determined by fitting peak volumes as a function of relaxation delay to a single exponential decay equation using conjugate gradient minimization (*62*). Peak volumes were determined by nonlinear least squares analysis of peak lineshape using the program nlinLS (Frank Delaglio, NIH\NIDDK). Error associated with T_1 and T_2 measurements was estimated by Monte Carlo simulation (*62*). Error of peak intensity associated with nOe measurements was determined from baseline noise estimates of processed spectra using the program NMRdraw (Frank Delaglio, NIH\NIDDK), with error in nOe value obtained by propagation of errors (*61*).

The relaxation analysis of both apo-L75F and apo-WT-TrpR was carried out using the program NORMAdyn (*61*). This program utilizes a stepwise approach in using ^{15}N relaxation values to determine the rotational diffusion tensor of the proteins. Before the diffusion tensor is fitted to experimental relaxation data (T_1/T_2), the program removes residues that contain nOe values (I/I_o) below 0.65, which indicate flexible NH bond vectors (*19*). Next the program removes residues with low T_2 values ($T_2 \leq T_{2\,ave} - \sigma_{T2}$), unless their T_1 values are high ($T_1 \geq T_{1\,ave} - \sigma_{T1}$). This is to ensure that relaxation data from residues with substantial internal motions are not used in the modeling of the diffusion tensor, while retaining data that contain important information regarding anisotropic tumbling effects (see figure 2). In this way, errors associated with the diffusion tensor resulting from internal motions (low nOe values) and fast chemical exchange (low T_2 values) are greatly reduced (*61*). The subset of relaxation data that survives the filtering process is then used as the experimental reference in equation 6 when determining the diffusion tensor. The NORMAdyn software assumes three different models for protein diffusion: completely isotropic, axially symmetric anisotropic (i.e. prolate ellipsoid and oblate ellipsoid), and fully anisotropic (*61*). The program uses each model and performs separate conjugate gradient minimization of equation 6 as it attempts to find the diffusion model which best represents the experimental T_1/T_2 values. Model and components of the diffusion tensor for apo-L75F and apo-WT TrpR were identified by lowest minima found by equation 6. Both the apo-L75F and apo-WT-TrpR produce experimental T_1/T_2 relaxation values that are consistent with an axially symmetric prolate model of diffusion.

Once the global tumbling parameters are established, the program uses the Lipari-Szabo formalism expressed in equation 7 to determine S^2, τ_e, and possible R_{ex} values for all amides. The NORMAdyn program attempts to fit motional parameters of individual NH bond vectors using four simpler dynamical representations derived from equation 7 and a fifth model based on the extended Lipari-Szabo formalism (*66*). The five different dynamical models are fit to experimental data for each NH bond vector while holding τ_c fixed at the value obtained from the T_1/T_2 ratio (equation 6). Each model contains the overall correlation time (τ_c), and a maximum of three internal motional parameters. Model 1 is obtained by assuming that internal motions are very fast ($\tau_e < 20$ ps) and only fits for the S^2 order parameter. Model 2 is obtained by making no assumption about the time scale of internal motion and fits for both S^2 and τ_e. Models 3 and 4 are derived from models 1 and 2 respectively, by including a non-zero chemical exchange term (R_{ex}). Model 5 is based on an extended version of the Lipari-Szabo formalism which has the form (*66*):

$$J(\omega) = 2/5[\, S^2\tau_c/\{1+(\omega\tau_c)^2\} + (1-S^2_f)\tau'_f/\{1+(\omega\tau'_f)^2\} + (S^2_f-S^2)\tau'_s/\{1+(\omega\tau'_s)^2]$$

(equation 9)

where $\tau'_f = \tau_f\,\tau_c/(\tau_f+\tau_c)$, $\tau'_s = \tau_s\,\tau_c/(\tau_s+\tau_c)$, and τ_c is the overall correlation time of the molecule. The formalism expressed in equation 9 separates the motion of the NH bond vector into a fast and slow component. The term τ_f represents the correlation time for the fast component of internal motion on a timescale (τ_f < 100 to 200 ps), and τ_s

represents the correlation time for the slow component of internal motion on a time scale ($\tau_f < \tau_s < \tau_c$). The order parameter S^2 now represents the product of two separate order parameters, such that $S^2=S^2_fS^2_s$. The terms S^2_f and S^2_s represents the restrictedness of the fast and slow components of internal motion respectively. Model 5 is obtained by assuming that τ_f is very fast ($\tau_f <$ ps) and fits for the order parameters S^2_f, S^2_s and the timescale of the slow component τ_s. The five models thus consist of the following parameters which describe NH bond vector motion (*61;67*): model (1) S^2 ; model (2) S^2 and τ_e ; model (3) S^2 and R_{ex} ; model (4) S^2, τ_e, and R_{ex}; model (5) S^2_f, S^2_s, and τ_s.

The program selects the model (1 through 5) by using a statistical protocol that has been elaborately described in great detail by Mandel et al (*67*) and Pawely et al (*61*). However important aspects of this protocol will be presented as they pertain to the analysis of results presented in this work. The relaxation analyses of apo-L75F and apo-WT-TrpR are based on the measurements of three experimental parameters T_1, T_2, and nOe obtained from NMR measurements. Each model contains a number of free parameters that are being fitted to the experimental data, with model 1 containing only one free parameter, models 2 and 3 containing two free parameters, and models 4 and 5 containing three free parameters (*67*). One expects that as the number of free parameters in the model increases so should the quality of the fit, as measured by a low χ^2 value (equation 8). This is a result of the fact that more free parameters in the model will produce a greater variability in the calculated values in equation 8, which greatly increases the likelihood of a lower χ^2 value. If the NORMAdyn software only used the

χ^2 criteria for model selection, it would only chose models 4 or 5 when performing the final relaxation analysis. This is clearly not the case. The program measures the statistical significance of reduction in χ^2 (equation 8) obtained by the incorporation of additional parameters when a simpler model, with fewer free parameters, can also describe the data. This is accomplished by using the F-test, which has the form (*67*):

$$F = p_2(\chi^2_1-\chi^2_2) / (p_1-p_2)\chi^2_2 \qquad \text{(equation 10)}$$

This equation represents the statistical analysis of model selection for a particular NH bond vector. The terms χ^2_1 and χ^2_2 represent the results of minimization of equation 8 based on two different models with p_1 and p_2 representing the degrees of freedom of each model respectively (*67*). It should be noted in equation 10, that χ^2_1 will always represent the model with the fewest free parameters in the comparison. The degree of freedom for a model is calculated by subtracting the number of free parameters contained within the model from the number of experimental parameters used in the fitting (*67*). In the case of the ^{15}N-relaxation study presented herein, the number of experimental parameters is 3 (T_1, T_2, and nOe). As a result, model 1 will have two degrees of freedom, models 2 and 3 will have one degree of freedom, and models 4 and 5 will have zero degrees of freedom. The F-test is used to discriminate between models 1 and 2, or between models 1 and 3. The model with more free parameters is selected as valid when F has a value greater than 2.0. Any value greater than 2.0 represents an 80% confidence that the reduction observed in χ^2 upon going to the more complex

model is more significant than random chance (*67*). Models 4 and 5 are not amenable to F-test statistics because both models have zero degrees of freedom (p=0 which always results in F=0). An NH bond vector is fit to one of these models (4 or 5) only if all χ^2 values obtained for models 1,2, and 3 during the selection process are above 20.0 and the χ^2 value for either model 4 or model 5 is zero (*67*). Because the statistical legitimacy of these three parameter models cannot be determined by F-test, residues that are assigned to models 4 or 5 will only be considered in a qualitative sense (i.e. representing complex motion, not adequately described by simple Lipari-Szabo analysis) in the relaxation analysis of apo-L75F and apo-WT TrpR.

Chapter 3

RESULTS

Structure Calculations

Resonance assignments for apo-L75F TrpR were carried out using standard methods applied previously to WT TrpR, and several backbone amide assignments for apo-WT TrpR were also confirmed independently in the present work. The 2D ^{1}H-^{15}N-HSQC correlation spectra of the two proteins recorded under identical temperature, pH, and buffer conditions are shown in Figure 3. This comparison indicates that, as reported previously (*35*), the two proteins have very similar overall structures, although slight differences in cross-peak number and resonance frequency are evident in the spectra of Figure 3. A summary of all backbone chemical shift differences observed from ^{1}H-^{15}N-HSQC spectra are shown in Table 1.

Using a combination of 2D and 3D heteronuclear NMR experiments, the backbone and sidechain resonances of apo-L75F TrpR were assigned. Of the 107 peptide groups, and excluding the four prolines of each L75F-TrpR monomer, 102 ^{15}N/ ^{N}H resonances and 105 $^{13}C_{\alpha}$, could be assigned unambiguously. A complete listing of all chemical shift assignments is included as supplementary material in appendix A.

Regions of secondary structure within apo-L75F TrpR were evaluated using a combination of the chemical shift index (CSI) (*68*) (*21;69*)for both $^{1}H_{\alpha}$ and $^{13}C_{\alpha}$, nOe-

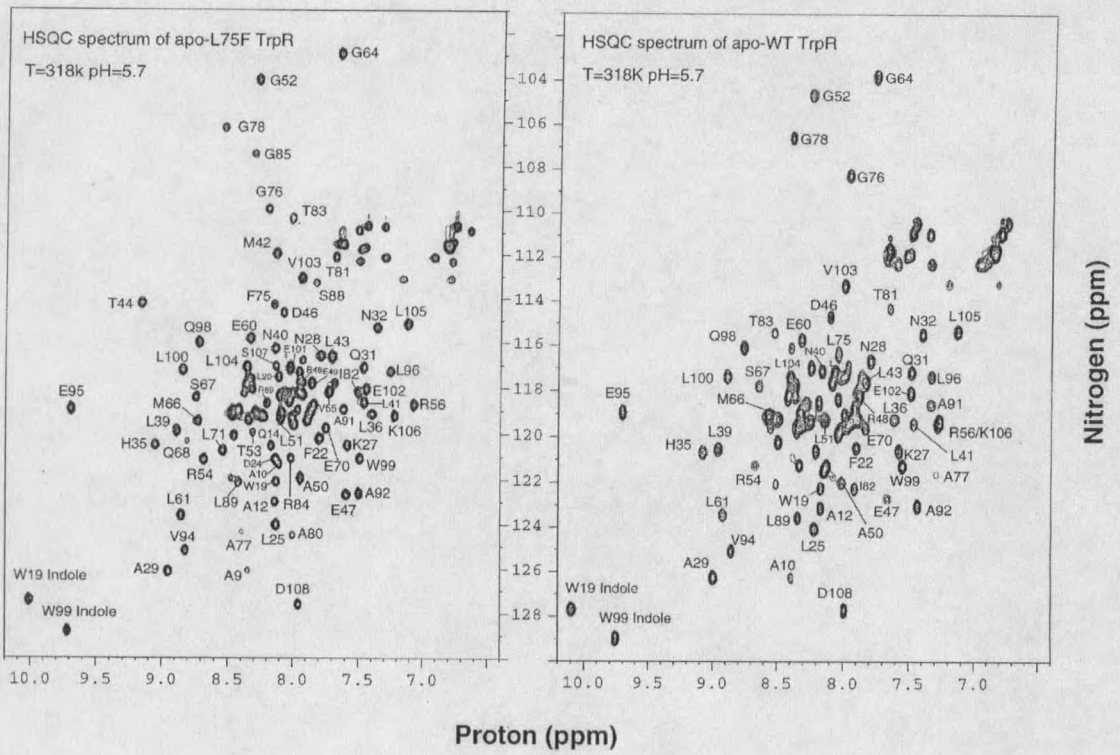

Figure 3: 2D ^{1}H-^{15}N HSQC spectra. Spectra of uniformly ^{15}N-labeled apo-L75F TrpR (left) and apo-WT TrpR (right) were recorded at 45 °C in 500mM NaCl, 50mM Na_2HPO_4, and 90% H_2O / 10% D_2O at pH=5.7. Some residues are omitted for clarity.

based short- and medium-distance estimates, and $^{1}H/^{2}H$ exchange information. The results are summarized in Figure 4. As expected for an all-helical protein and as found previously for WT-TrpR (*4-6*), the patterns shown reflect the presence of well-defined helices encompassing chain segments corresponding to helices A, B, C, and F. Chain segments corresponding to helices D and E exhibit some, though less strong or complete, indications of helical character. However, compared to previously published nOe assignments of apo-WT TrpR (see Figure 1 of reference 5), chain segment 67 to 92 of apo-L75F TrpR exhibits more pronounced helical chemical shift indices, and the D-E

residue	Δ^1H_N (ppm)	$\Delta^{15}N$ (ppm)	residue	Δ^1H_N (ppm)	$\Delta^{15}N$ (ppm)	residue	Δ^1H_N (ppm)	$\Delta^{15}N$ (ppm)
Met 1	na	na	Pro 37	----	---	Asn 73	0.13	-1.32
Ala 2	na	na	Leu 38	-0.15	-0.26	Glu 74	-0.49	-0.91
Gln 3	na	na	Leu 39	-0.03	-0.62	Phe 75	---	---
Gln 4	na	na	Asn 40	-0.08	-0.69	Gly 76	0.32	1.75
Ser 5	na	na	Leu 41	-0.08	-0.68	Ala 77	1.01	1.44
Pro 6	na	na	Met 42	0.02	-1.17	Gly 78	0.23	-0.17
Tyr 7	na	na	Leu 43	-0.15	-1.03	Ile 79	na	na
Ser 8	na	na	Thr 44	0.05	-1.21	Ala 80	na	na
Ala 9	na	na	Pro 45	---	---	Thr 81	0.10	-2.03
Ala 10	na	na	Asp 46	0.02	0.10	Ile 82	-0.36	-3.90
Met 11	na	na	Glu 47	-0.02	0.26	Thr 83	-0.47	-4.42
Ala 12	na	na	Arg 48	0.10	-0.46	Arg 84	na	na
Glu 13	na	na	Glu 49	0.06	0.15	Gly 85	na	na
Gln 14	na	na	Ala 50	-0.01	0.10	Ser 86	na	na
Arg 15	na	na	Leu 51	0.00	-0.22	Asn 87	0.57	na
His 16	0.03	0.21	Gly 52	0.05	-0.49	Ser 88	na	na
Gln 17	0.00	-0.09	Thr 53	0.07	na	Leu 89	0.11	-1.30
Glu 18	0.01	-0.07	Arg 54	0.04	-0.49	Lys 90	0.13	0.00
Trp 19	0.03	-0.95	Val 55	-0.15	-0.69	Ala 91	0.31	0.36
Leu 20	0.07	-0.15	Arg 56	-0.18	-0.68	Ala 92	0.16	-0.28
Arg 21	na	na	Ile 57	-0.25	1.14	Pro 93	---	---
Phe 22	-0.04	-0.21	Val 58	-0.01	na	Val 94	0.01	0.14
Val 23	0.07	-1.67	Glu 59	0.00	-0.04	Glu 95	0.03	-0.01
Asp 24	0.06	-0.36	Glu 60	0.05	0.08	Leu 96	-0.01	-0.05
Leu 25	0.03	0.11	Leu 61	0.01	0.24	Arg 97	0.09	-0.12
Leu 26	0.00	-1.56	Leu 62	-0.02	-0.42	Gln 98	0.00	0.01
Lys 27	0.07	0.04	Arg 63	0.15	na	Trp 99	0.00	-0.18
Asn 28	0.05	-0.08	Gly 64	-0.08	-0.78	Leu100	-0.01	-0.13
Ala 29	0.03	0.00	Glu 65	0.04	na	Glu 101	0.03	-0.17
Tyr 30	0.03	-1.92	Met 66	0.22	0.38	Glu 102	0.01	-0.03
Gln 31	0.03	-0.03	Ser 67	0.03	0.95	Val 103	-0.01	-0.29
Asn 32	0.01	-0.26	Gln 68	1.03	0.86	Leu104	-0.01	-0.25
Asp 33	0.05	-0.06	Arg 69	-0.02	0.22	Leu105	-0.04	-0.23
Leu 34	0.03	0.10	Glu 70	-0.22	-0.08	Lys 106	0.01	-0.05
His 35	0.00	-0.16	Leu 71	-0.34	na	Ser 107	na	na
Leu 36	-0.04	-0.25	Lys 72	na	na	Asp108	0.03	0.00

Table 1: Chemical shift differences are defined as Δ(ppm) = (apo-L75F TrpR) – (apo-WT TrpR). Chemical shift values are taken from references 9 and 11, corrected when necessary for differences in chemical shift referencing. na means that the chemical shift values for apo-WT TrpR are not available for comparison with apo-L75F TrpR.

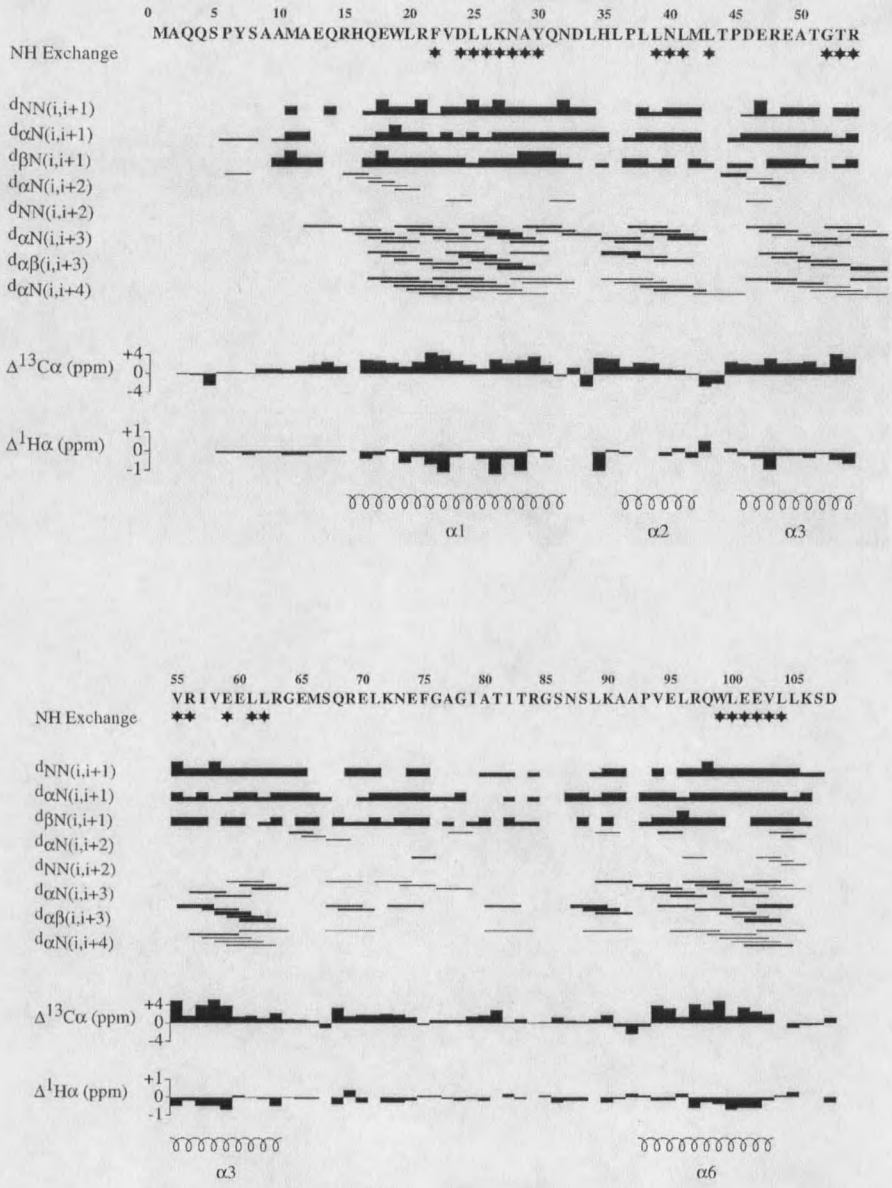

Figure 4: Summary of amide exchange data, patterns of sequential and short-range nOes, and secondary shifts for apo-L75F. The protein sequence is included in the top row, using one-letter amino acid code. Filled stars denote residues for which the amide proton exchange constant is > 20 min. nOe connectivities are diagrammed on the next eight rows. The height of the box reflects intensity of the cross-peak classified as strong (tallest) medium, weak, and very weak (shortest): sequential nOes are depicted from the first residue involved to the appropriate downstream residue. Differences in parts per million in $^{1}H\alpha$ and $^{13}C\alpha$ chemical shifts relative to random coil values are shown in the rows labeled $\Delta H\alpha$ and $\Delta C\alpha$. Regions identified as α-helical are shown in last row.

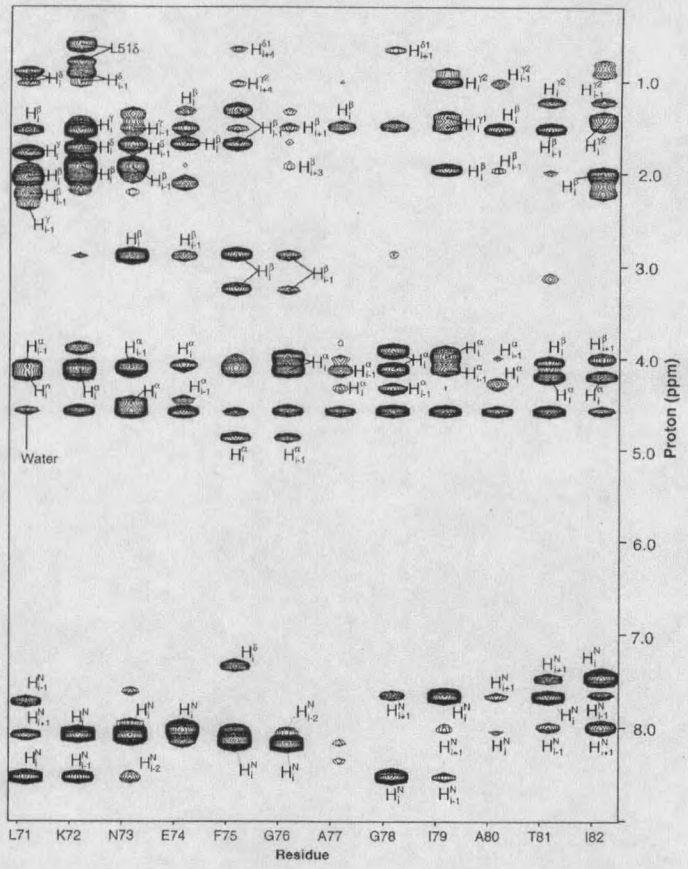

Figure 5: Sequential strips extracted from 3D ^{15}N-edited ^{1}H-^{1}H NOESY spectrum of apo-L75F TrpR. nOe cross-peaks originating from the amides of residues 71-82 are displayed. The plot is reconstructed using the plot_sequence program (D. Garrett, NIH) of ^{15}N planes extracted from the ^{15}N-edited ^{1}H-^{1}H NOESY spectrum of apo-L75F TrpR recorded at 45° C with a nOe mixing period of 120 ms. Cross-peak partners for each amide peak and the water signal at 4.58 ppm are marked.

helix region displays a larger number of nOe connectivities, although it still lacks many of the longer-range nOes characteristic of well-formed helices, such as the $d_{N\alpha}(i, i+3)$ nOes. Figure 5 displays a portion of the ^{15}N-edited ^{1}H-^{1}H NOESY spectrum of apo-L75F-TrpR reconstructed to present sequential backbone amide nOe strips for residues 71 to 82. The data include a number of strong well-developed sequential and intra-

residue crosspeaks for residues in this chain segment. Many of the nOe crosspeaks are unique to the L75F mutant due to the Phe75 side-chain. However, a direct comparison with the ^{15}N-edited spectral region of apo-WT-TrpR is impractical due to severe resonance overlaps of corresponding residues in the 3D-^{15}N-edited ^{1}H-^{1}H NOESY spectrum of apo-WT-TrpR recorded under identical solution conditions (data not shown).

A total of 769 uniquely identified nOe restraints, amounting to 1538 nOe restraints for the symmetric protein dimer, were used to calculate the three-dimensional structure of apo-L75F TrpR in solution. Potential inter-monomer contacts were identified with the aid of previously published WT TrpR NMR structures (*4;5*), and the corresponding nOes in our data were evaluated first in preliminary calculated structures of apo-L75F TrpR and then iteratively in progressively refined structures. Twenty-five of the 39 inter-monomer nOes used in the structure calculations were derived from very well-resolved regions of the spectrum, for example, crosspeaks with aromatic or upfield-shifted methyl protons. Figure 6 portrays portions of a ^{13}C edited NOESY spectrum acquired on apo-L75F. A nOe cross-peak was assigned as an inter-monomer connectivity only after all other possible identifications had been dismissed.

An ensemble of 40 structures was calculated using the program CNS (*38*), and further refined against NCS restraints with X-PLOR, version 3.1(*39*). Twenty structures of lowest conformational energy were selected from this ensemble for use in the structural analysis. Table 2 summarizes the experimental restraints used in the 3D structure calculations and the statistics for the final set of 20 structures.

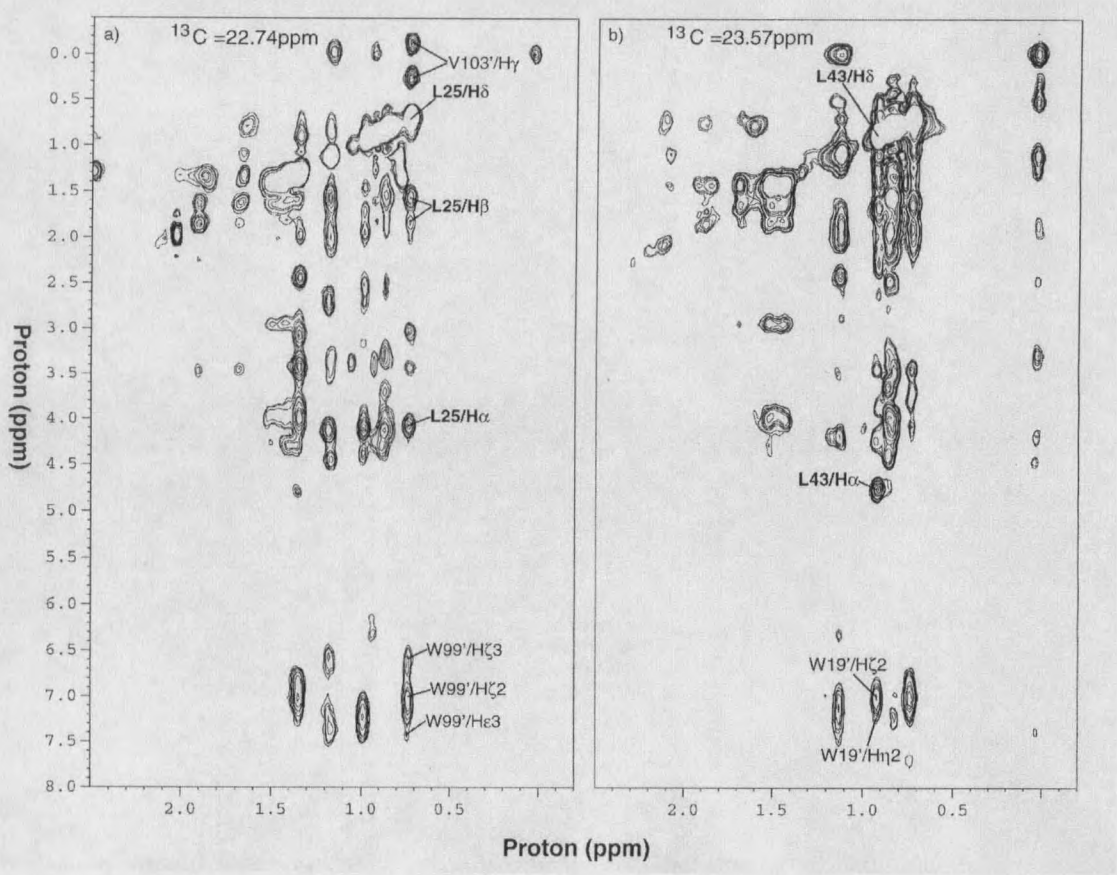

Figure 6: This figure presents two carbon slices in the methyl region of a 3D HCCH-NOESY spectrum at ^{13}C chemical shifts of 22.74 ppm and 23.57 ppm. From the spectrum on the right, the Leu 25 methyl protons at 0.77 ppm in ^{1}H possess strong inter-monomer nOes to the upfield shifted protons of Val 103' located at 0.36 ppm and -0.09 ppm and to the downfield shifted aromatic protons of Trp 99' located between 6.5 and 7.5ppm. The spectrum on the left displays the crowded region around the methyl protons of Leu 43 at 1.08 ppm in the ^{1}H dimension, with a clear inter-monomer nOe to the downfield shifted aromatic protons of Trp 19' around 7.0ppm.

Table 2. Structural statistics for the final simulated annealing structures of apo L75F

(A) Experimental restraints per monomer	
Total NOE restraints	769
Sequential ($\|i-j\| = 1$)	356
Short Range ($1 < \|i-j\| < 4$)	350
Long Range ($\|i-j\| > 4$)	24
Inter-subunit	39
Hydrogen bond restraints	31
Experimental dihedral angles φ restraints	68
Restraint violations	
distances	
number > 0.3 Å	0
dihedral	
number > 3°	0
(B) Statistics for the calculated structures	{SA}[c]
Deviation from idealized geometry	
Bonds (Å)	0.0023 ± 0.0001
Angles (deg.)	0.54 ± 0.01
Improper (deg.)	0.42 ± 0.01
Final Energies (kcal/mol)	
Distance restraints	69.35 ± 6.37
Dihedral angles	0.030 ± 0.06
Nonbonded (REPEL)	15.4 ± 4.21
Root-mean-square deviations	
Average atomic rmsd Å	
Backbone atoms	
Dimer core (helices A, B, C, A', B', C')	1.07 Å
DNA-binding domain (helices D, E, D', E')	2.80 Å
Average atomic rmsd Å	
Backbone atoms	
Monomer core (helices A, B,C)	0.82 Å
DNA-binding domain (helices D, E)	1.75 Å

The backbone overlay of the 20 structures is shown in Figure 7A. The average root-mean-square deviation (rmsd) for backbone atoms in this set of 20 apo-L75F TrpR dimer structures is 1.8 Å.

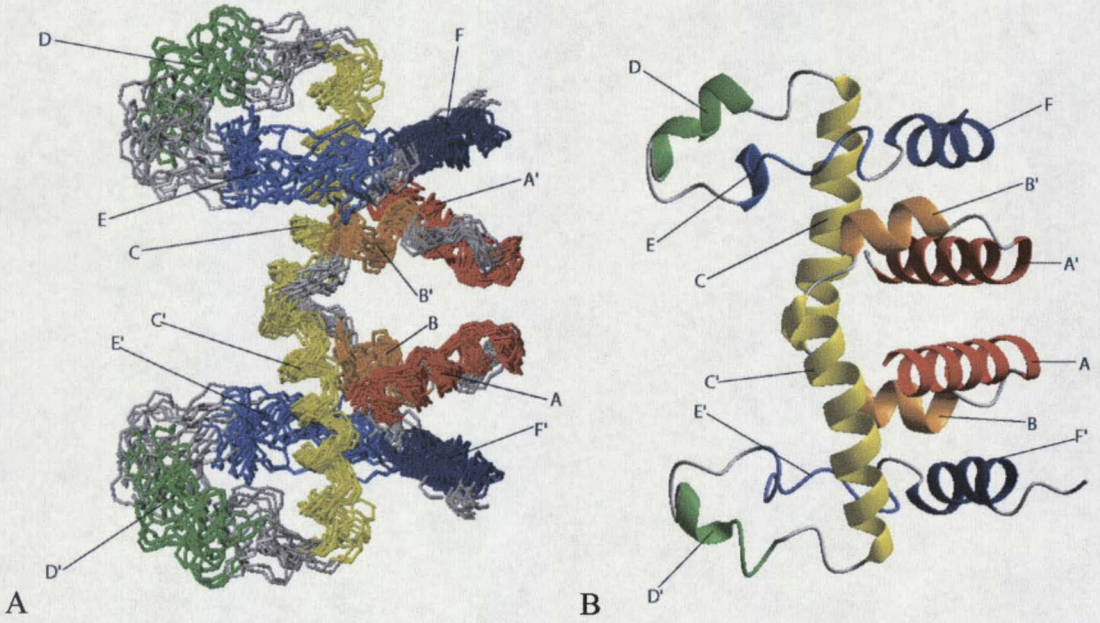

Figure 7A and B: (A) Family of accepted apo-L75F TrpR structures. This figure depicts the overlay of backbone heavy atoms (N, Cα, CO) of residues 3-108 for 20 lowest-energy structures relative to the hydrophobic core (helices A-C,F of both subunits). Residues in helix A (16-32) are color coded red, those in helix B (37-42) orange, those in helix C (45-63) yellow, those in helix D (68-74) green, those in helix E (81-90), and those in helix F (93-103) indigo. The N and C termini have been omitted for clarity. (B) Ribbon diagram of the minimized average structure of apo-L75F TrpR generated from the 20 lowest energy NMR structures.

Helical regions in the final 20 structures of apo-L75F TrpR were delineated with the aid of the Procheck NMR analysis software (*55*), and include residues 16-32 (helix A), residues 37-42 (helix B), residues 46-63 (helix C) and residues 93-103 (helix F). Helical trends were observed for some residues in the D and E regions of the protein, as

assessed by CSI and the limited set of nOe patterns, although these segments cannot be defined as helices by Procheck due to the incompleteness of characteristic nOe patterns and lack of slowing exchanging amides in these regions. Helical regions are shown in Figure 7B as solid-ribbon diagrams and as they appear on the energy minimized average structure of apo-L75F generated from the 20 structures shown in Figure 7A. Helical areas are represented as ribbons, with the colored regions of the hydrophobic core (A-C,F/A'-C',F') corresponding to the helical boundaries delineated by Procheck NMR. Areas involved in DNA binding denoted as regions D/D' and E/E' in Figure 7B have been shown for completeness. The ribbon segments displayed in regions D, D' as well as region E are considered artifacts of the minimization procedure and are not considered to be representative of well-defined helical structure.

Because of this distribution of more versus less well-defined helices in apo-L75F, backbone-atom rmsds were computed separately for chain segment 67 to 92, helices D and E of each monomer, and for helices comprising the hydrophopic core of the apo-L75F TrpR dimer (helices A-C and F from each monomer). The average rmsd for backbone atoms was found to be 1.0 Å in the ABCF dimer core, while in the DNA-binding regions (residues 68-74 + 81-90) the average rmsd is 2.8 Å (Table 2). This indicates that the backbone within helices D and E is much less defined relative to the ABCF dimer core, a trend that is also seen in the NMR structures of WT-apo-TrpR (5).

The overall dimensions of the final structures were compared to those of apo-TrpR NMR structures previously reported by Jardetzky and coworkers (5). The distance between the Leu 62 C_α atom and the Leu 62' C_α atom, which provides a measure of the

size of the dimer core perpendicular to the dimer axis, is 44.2Å ± 3.0Å in apo-L75F TrpR compared to the value of 40.5Å ± 1.5 Å for apo-WT-TrpR (5). The distance between the D 46 C_α atom and the S 86' C_α atom, which provides an indication of the size of the L-Trp binding pocket, was measured to be 16.9Å ± 1.1Å for apo-L75F-TrpR and within experimental error of the 15.3Å ± 2.8Å value reported for apo-WT-TrpR (5). The packing of helices A, B and F around the central C/C' core of the protein was investigated by measuring additional C_α to C_α distances within each of these helical regions. The distance between the H 16 C_α atom to the H 16' C_α atom was measured, and provided an estimate of the spacing between helices A and A' in a direction perpendicular to the helix C/C' core of the protein. This distance was measured to be 32.5 ± 1.6Å for apo-L75F and 32.8 ± 0.7Å for apo-WT-TrpR. The distances of three Cα atoms, located in residues which correspond to the N-terminal, center, and C-terminal of each helix (A, B, and F) to C_α atoms in helix C were estimated from the twenty calculated structures of apo-L75F. These measurements were used to approximate the packing distance between helices A /C', B /C', and C/F of apo-L75F, and were compared to measurements taken from inspection of 15 wild-type structures reported in the protein databank. A summary of the selected atoms and results are presented in Table 3. Because all residues in these proteins have symmetric counterparts in the additional subunit, measurements reported in Table 3 for particular C_α to C'_α distances represent averaging with the symmetry related sites.

Table 3: Average C_α to C_α distance for selected sites of apo-L75F and apo-WT-TrpR reported in Angstroms (Å). Distances reported are between the C_α atoms of paired residues listed in column 1. Residues are listed by three letter amino acid abbreviations. Highlighted with * indicate significant differences between the wild-type (WT) and mutant protein.

Residues	apo-L75F (Å)	apo-WT-TrpR (Å)
Leu62/Leu62'	*44.2 ± 1.5	40.5 ± 1.5
Asp46/Ser86'	16.9 ± 1.1	15.4 ± 2.8
His16/His16'	32.5 ± 1.6	32.8 ± 0.7
His16/Glu49'	*9.6 ± 0.5	12.6 ± 1.3
Asp24/Glu49'	16.5 ± 0.6	17.4 ± 0.4
Asn32/Glu49'	25.8 ± 0.7	26.9 ± 1.0
Pro37/Arg54'	15.2 ± 0.9	13.9 ± 1.0
Asn40/Arg54'	*15.2 ± 0.9	11.7 ± 1.4
Met42/Arg54'	*10.6 ± 1.0	7.3 ± 1.0
Pro93/Leu62	12.2 ± 1.3	13.3 ± 1.6
Gln98/Leu62	12.5 ± 1.1	12.9 ± 1.2
Val103/Leu62	*3.6 ± 0.8	10.6 ± 0.6

As can be seen from Table 3, the overall dimensions of apo-L75F are similar to those measured for apo-WT-TrpR. While the size of the L-trp binding pocket, and the distance between the N-terminal regions of helices A and A' are identical within experimental error, there are some small differences in the position of the helices relative to each other within the hydrophobic core of the two proteins. The C/C' core of the mutant protein, as reported by the Leu 62 Cα to Leu 62' Cα distance, is slightly longer than the wild-type protein. Also, the N-terminal of helix A represented by the H

16 Cα to Glu 49' Cα distance is approximately 2 Å closer to helix C' in the mutant protein relative to the wild-type protein. Residues M 42 and V 103 located in helices B and F respectively appear to be shifted away from the C/C' core by approximately 3 Å in the mutant protein indicating that subtle changes in the orientation of helices in the hydrophobic core of apo-L75F have occurred.

It is surprising that the number of chemical shift differences observed in ^{15}N-HSQC spectra when comparing apo-L75F to apo-WT-TrpR (Figure 3 and Table 1), and the unique set of nOes observed in 3D ^{15}N-edited ^{1}H-^{1}H NOESY spectra (Figure 5) would result from a single point mutation. Inspection of Table 1 shows that many of the more dramatic changes in NH chemical shifts have occurred in the vicinity of the phenylalanine mutation site, suggesting that residues in this area may be experiencing a common perturbation source. Given the aromatic nature of the newly introduced phenylalanine, it is hypothesized that a ring current generated from the mutant residue is affecting local environments, and may be the source of many chemical shift variations detected within the apo-L75F protein. It has been reported that the ring current effect has a $1/r^3$ distance dependence, and becomes negligible at distances greater than 5.5Å (*40*). As a result a ring current generated by phenylalanine 75 should only influence residues within a close spatial proximity to the mutation site.

In order to assess the influence of the ring current effect caused by the Leu-to-Phe substitution on backbone NH chemical shifts, the distances between the Cα of Phe 75 and the Cα of affected sites were estimated by examination of the twenty accepted structures shown in Figure 7A. Taking into account the uncertainty in side chain

position and the ring flipping of Phe 75, a conservative estimate of 10.0 Å was used to assess ring current effects. Residues with Cα distances greater than 10.0 Å from the Phe 75 Cα atom are expected to experience negligible perturbations due to the ring current effect created by the introduction of the aromatic ring at position 75.

Residue	Region	Δ ^{1}H ppm	Δ ^{15}N ppm	Distance Å
Trp 19'	Helix A	0.03	-0.95	26.8 ± 1.9
Val 23'	Helix A	0.07	-1.67	29.7 ± 2.0
Leu 26'	Helix A	0.00	-1.56	29.5 ± 2.2
Tyr 30'	Helix A	0.03	-1.92	34.7 ± 2.3
Leu 39'	Helix B	-0.03	-0.62	26.8 ± 2.3
Asn 40'	Helix B	-0.08	-0.69	25.7 ± 2.4
Leu 41'	Helix B	-0.08	-0.68	22.4 ± 2.4
Met 42'	Helix B	0.02	-1.17	21.9 ± 2.2
Leu 43'	B-turn-C	-0.15	-1.03	24.1 ± 2.3
Thr 44'	B-turn-C	0.05	-1.21	22.8 ± 2.3
Gly 52	Helix C	0.05	-0.49	20.0 ± 2.6
Arg 54	Helix C	0.04	-0.49	17.6 ± 1.9
Val 55	Helix C	-0.15	-0.69	20.4 ± 1.7
Ile 57	Helix C	-0.25	1.14	15.4 ± 1.8
Gly 64	C-turn-D	-0.08	-0.78	17.8 ± 2.6
Ser 67	C-turn-D	0.03	0.95	12.1 ± 1.6
Gln 68	Helix D	1.03	0.86	10.6 ± 1.7
Asn 73	Helix D	0.13	-1.32	5.5 ± 0.1
Glu 74	Helix D	-0.49	-0.91	3.8 ± 0.0
Gly 76	D-turn-E	0.32	1.75	3.8 ± 0.0
Ala 77	D-turn-E	1.01	1.44	5.6 ± 0.6
Thr 81	Helix E	0.10	-2.03	11.2 ± 1.4
Ile 82	Helix E	-0.36	-3.90	10.2 ± 1.5
Thr 83	Helix E	-0.47	-4.42	10.9 ± 1.9
Asn 87	Helix E	0.57	na	22.2 ± 2.2
Leu 89	Helix E	0.11	-1.30	27.3 ± 2.5

Table 4: Tabulation of residues and locations in apo-L75F TrpR for amide chemical shift differences > 0.5 ppm reported in Table 1. Distances are from the Phe 75 Cα atom to affected residue Cα measured in Å and derived by considering all twenty structures. Shown in distance column is the average value ± one standard deviation.

Residues that exhibit substantial chemical shift perturbation and lie beyond the 10.0 Å cutoff are considered to experience protein-mediated electronic perturbations independent of the ring current generated by the aromatic ring of Phe 75. From the 74 residues of apo-L75F for which complete $^{1}H/^{15}N$ chemical shift comparisons could be made with apo-WT-TrpR, 26 residues display chemical shift differences greater than 0.5 ppm in either the proton and/or nitrogen dimensions. A listing of these 26 residues along with the measured C_α distances and locations within L75F secondary structure are summarized in Table 4. As can be seen in Table 4, changes in chemical shift values observed for residues located close to the mutation site in the helix D-turn-helix E region are likely the result of the ring current generated by Phe75. However numerous residues located in helices A, B, and C are well outside the 10.0 Å threshold of ring current influence, and suggest that possible long-range conformational disturbances caused by the Phe75 mutation may affect the chemical shifts of these residues.

^{15}N Relaxation Analysis

Amide backbone dynamics of apo-WT TrpR and apo-L75F TrpR have been compared using ^{15}N relaxation data measured by 2D ^{1}H-^{15}N NMR spectroscopy. Each ^{15}N-T_1, ^{15}N-T_2, and ^{15}N-{^{1}H} nOe value was measured in duplicate for both wild-type apo-TrpR and apo-L75F-TrpR mutant to assess data reproducibility. Relaxation parameters of 75 residues were established for apo-L75F, while only 55 residues of apo-WT could be fully categorized. The limited set of apo-WT TrpR amides originated from incomplete NMR assignments available for WT-TrpR (*9*), and/or due to severe

resonance overlaps in the 2D ^{1}H-^{15}N HSQC spectrum precluding accurate determination of integrated peak intensities.

^{15}N-Relaxation Results: apo-L75F TrpR

The results from relaxation measurements for apo-L75F are shown in Figures 8 through 10. A complete listing of all relaxation parameters (T_1, T_2, and nOe) measured for apo-L75F are listed in appendix B. Figures 8 through 10 portray the average relaxation values (^{15}N-T_1, ^{15}N-T_2, and ^{15}N-{^{1}H} nOe, respectively) for all measurable residues, with the error bars representing ± one standard deviation between the duplicate sets of measurements. The average ^{15}N-T_1 and ^{15}N-T_2 time constants for residues found in the hydrophobic core (helices A-C, F) of apo-L75F were 812 ± 41 ms , and 76 ± 10 ms for T_1 and T_2 respectively. Residues located within the H-T-H binding domain (helices D and E) resulted in average relaxation times of 790 ± 46 ms and 82 ± 17 ms for T_1 and T_2 respectively. It has been reported (*12*) that residues in the N and C terminal parts of holo-WT TrpR possess large T_1 and T_2 values. This is also observed for residues occupying similar regions in the apo-L75F protein. Specifically, Tyr 7 and Asp 108 exhibit ^{15}N-T_2 and ^{15}N-{^{1}H} nOe values that are about two standard deviations larger than for residues found in the core of the protein, with ^{15}N-T_2 values of 283 ms and 684 ms, and ^{15}N-{^{1}H} nOe values of -0.17 and -1.1, respectively. The average nOe value for residues in the hydrophobic core of apo-L75F is 0.75 ± 0.04, with residues occupying the H-T-H domain displaying average nOe values of 0.62 ± 0.05. Four

residues (Ala 9, Ala 10, Ser 107, and Asp 108) exhibit negative nOe values and are all located on the N and C terminal arms of the protein.

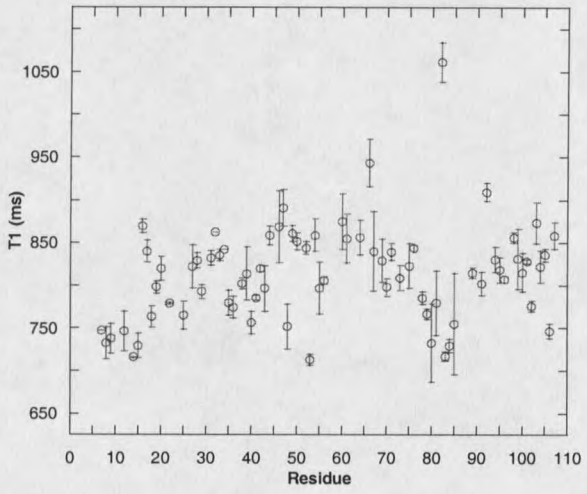

Figure 8: Plot of ^{15}N-T_1 relaxation values (msec) for apo-L75F as a function of residue number. Error bars represent ± 1 standard deviation between two duplicate measurements.

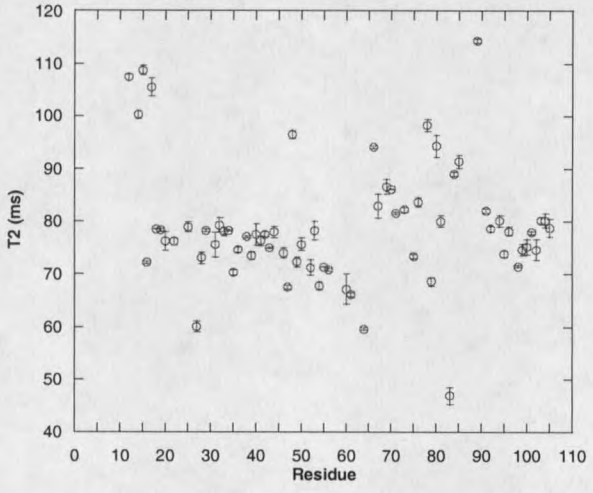

Figure 9: Plot of average ^{15}N-T_2 values (msec) for apo-L75F-TrpR as a function of residue number. Error bars represent ±1 standard deviation between duplicate measurements.

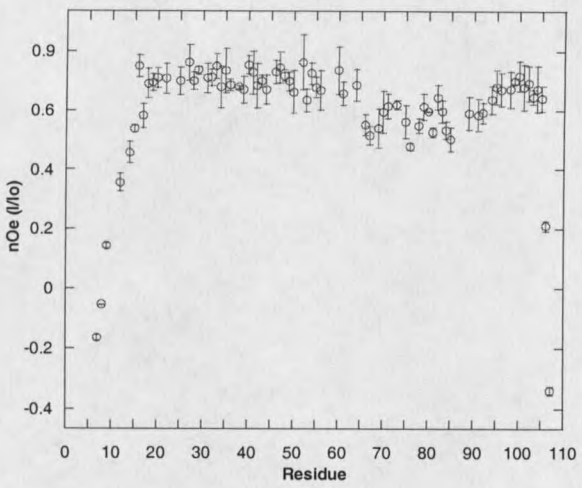

Figure 10: Plot of average ^{15}N-{^{1}H} nOes measured as the ratio (I/I_o) for apo-L75F TrpR as a function of residue number. Error bars represent ±1 stadard deviation between two duplicate measurements.

^{15}N-Relaxation Results: apo-WT-TrpR

The results from ^{15}N relaxation measurements for apo-WT TrpR are shown in Figures 11 through 13. Complete listings of all relaxation parameters for apo-WT TrpR are tabulated in appendix C. Figures 11 through 13 are graphs of average relaxation values (^{15}N-T_1, ^{15}N-T_2, and ^{15}N-{^{1}H} nOe, respectively) for each resolvable residue of apo-WT TrpR, with the error bar representing ± one standard deviation between duplicate measurements. The average ^{15}N-T_1 and ^{15}N-T_2 relaxation time constants for residues in the hydrophobic core of the wild-type protein (helices A-C,F) were measured to be 838 ± 34 ms for T_1 and 70 ± 6 ms for T_2. For residues in the H-T-H

domain of the protein, average T_1 and T_2 values were 762 ± 31 ms and 76 ± 13 ms, respectively.

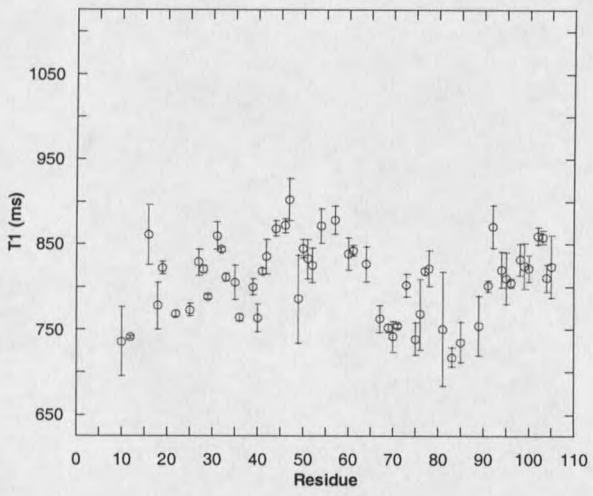

Figure 11: Plot of ^{15}N-T_1 relaxation values (msec) for apo-WT TrpR as a function of residue number. Error bars represent ±1 standard deviation between two duplicate measurements.

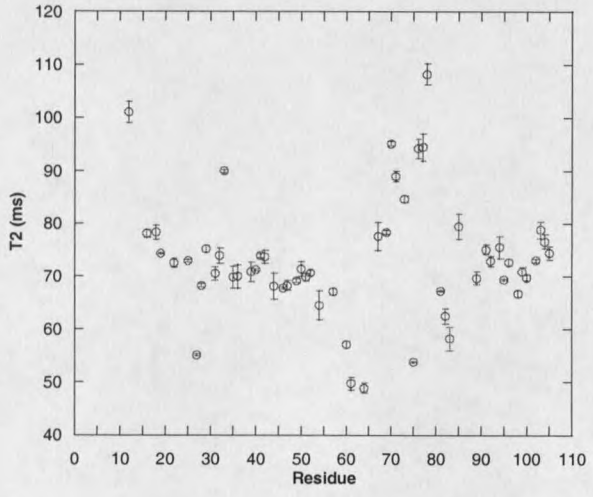

Figure 12: Plot of average ^{15}N-T_2 values (ms) for apo-WT-TrpR as a function of residue number. Error bars represent ± 1 standard deviation between two duplicate measurements.

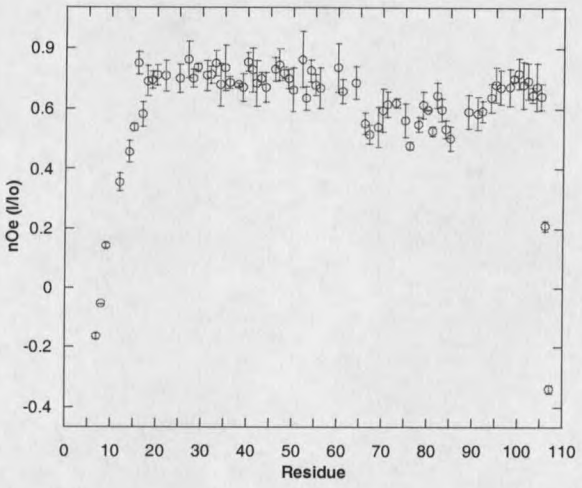

Figure 13: Plot of average ^{15}N-{^{1}H} nOes measured as the ratio (I/I_o) for apo-WT TrpR as a function of residue number. Error bars represent ± 1 standard devations between two duplicate measurements.

Table 5: Summary of ^{15}N relaxation values

	apo-L75F TrpR			*apo-WT TrpR*		
Helix	^{15}N-T_1 (ms)	^{15}N-T_2 (ms)	nOe	^{15}N-T_1 (ms)	^{15}N-T_2 (ms)	nOe
A,B,C,F	812 ± 41	76 ± 8	0.75 ± 0.04	838 ± 34	70 ±6	0.79 ± 0.04
D,E	790 ± 46	82 ± 17	0.62 ± 0.05	764 ± 31	76 ± 13	0.64 ± 0.08

The T_1 and T_2 values measured for apo-WT-TrpR are within experimental error of the values obtained for apo-L75F. The average nOe value for residues in the hydrophopic core of apo-WT TrpR was found to be 0.79 ± 0.04, with residues within the H-T-H region displaying values of 0.64 ± 0.08, which are also comparable to values obtained

for apo-L75F. The results of ^{15}N relaxation measurements conducted on both apo-L75F and apo-WT-TrpR are summarized in Table 5.

^{15}N Backbone Dynamics

Relaxation data collected on both apo-L75F and apo-WT TrpR were analyzed in terms of motional anisotropy and NH backbone dynamics using the Lipari-Szabo formalism. This type of analysis was greatly facilitated by using a suite of programs collectively referred to as NORMAdyn (*61*). Using this software and NMR based PDB structure files representing both apo-L75F and apo-WT-TrpR, the inertial tensor for each protein was calculated. The eigenvectors of each inertial tensor provided the orientation relative to the molecular frame of the respective protein and initial estimates of the global tumbling parameters used in the modeling of the diffusion tensor for apo-L75F and apo-WT-TrpR. This technique has been described in the Materials and Methods section of this work and is based on the minimization of equation 6 presented therein. It was determined that the model of rotational diffusion that best describes the ^{15}N relaxation data collected on both apo-WT TrpR and apo-L75F TrpR is an anisotropic axially symmetric diffusion tensor. The final values for the principal components of the diffusion tensor were $D_{\parallel} = 1.83 \pm 0.03 \times 10^7\ s^{-1}$ and $D_{\perp} = 1.53 \pm 0.02 \times 10^7\ s^{-1}$ for apo-L75F. The principal components of apo-WT TrpR were given as $D_{\parallel} = 1.74 \pm 0.04 \times 10^7\ s^{-1}$ and $D_{\perp} = 1.51 \pm 0.02 \times 10^7\ s^{-1}$. The overall correlation time was then calculated from the principal components of the diffusion tensor using equation 8 and yielded values of 10.2 ± 0.2 ns and 10.5 ± 0.2 ns for apo-L75F and WT-

trpR, respectively. Considering the corresponding fold and size of the two proteins, the similarity of the correlation times is of no surprise and the difference observed is not regarded as significant.

In the last section, the rotational diffusion of both apo-proteins were best modeled as axially symmetric tensors with the degree of anisotropy given by the ratio of $D_{\parallel}/D_{\perp}$. This ratio for apo-L75F has a value of 1.20 ± 0.04 which is within experimental error of the value 1.15 ± 0.04 obtained for apo-WT-TrpR. It has been discussed that considerable degrees of anisotropy can affect ^{15}N-T_1 and ^{15}N-T_2 values when NH bond vectors are closely aligned to the parallel component of an axially symmetric diffusion tensor (see Figure 2). The ^{15}N relaxation study reported on holo-WT-TrpR by Zheng et al (*12*), revealed that backbone amide groups in helix C have pronounced increases in T_1/T_2 ratios relative to amide groups in other locations of the protein. Furthermore, it was shown that these increases in ^{15}N T_1/T_2 ratios for residues within helix C correlate to NH bond vectors that are closely aligned to the parallel component of the diffusion tensor. To determine if these same trends could be observed in the relaxation data collected in this study on both the apo-L75F and apo-WT-TrpR proteins, plots of T_1/T_2 ratios were constructed and compared to NH bond vector orientations relative to $D_{\parallel}$. Errors in T_1/T_2 ratios were calculated by propagating error in each T_1 and T_2 measurement using the partial derivative method (*70*). Figure 14 displays the calculated ^{15}N T_1/T_2 ratios as a function of residue number for apo-L75F, and compares these values to the backbone NH bond vector orientation relative the principal component ($D_{\parallel}$) of the diffusion tensor. It is interesting to note that in the helix C region, residues

45-63 display a significant increase in T_1/T_2 ratios, and a decrease in bond vector orientation relative to $D_{\|}$.

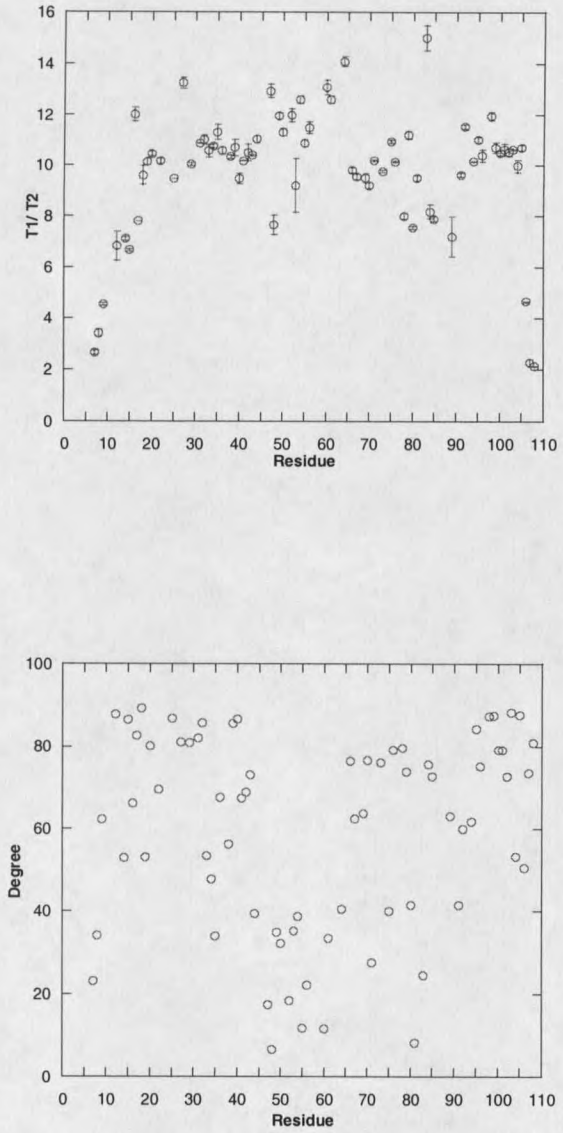

Figure 14: ^{15}N T_1/T_2 ratios for apo-L75F TrpR as a function of residue number (top), and backbone NH bond vector orientation relative to $D_{\|}$ of diffusion tensor (bottom). Amides in helix C (residues 45-63) have high T_1/T_2 ratios and are aligned closely along $D_{\|}$.

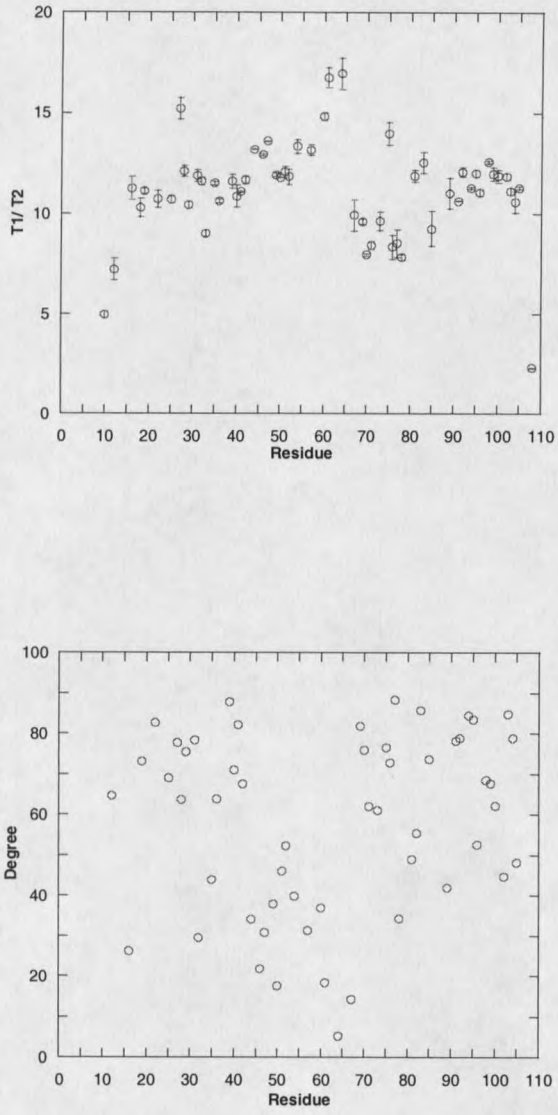

Figure 15: ^{15}N T_1/T_2 ratios for apo-WT TrpR as a function of residue number (top), and backbone NH bond vector orientation relative to $D_{\|}$ of diffusion tensor (bottom). As for apo-L75F, amides in helix C (residues 45-63) have high T_1/T_2 ratios and are aligned closely along $D_{\|}$.

This is expected for residues that have NH bond vectors oriented closely parallel to the principal axis of the diffusion tensor (i.e. $\alpha < 54.7^{o}$). This same effect is also observed in the helix C region of apo-WT TrpR shown in figure 15. In both proteins, it is clear that anisotropic reorientation manifests itself in the ^{15}N relaxation data. These data indicate that the principal components of the respective diffusion tensors are aligned closely along the helix C regions of both apo-L75F and apo-WT-TrpR proteins, and are consistent with similar measurements reported on holo-WT-TrpR by Zheng et al. It should be noted that discrepancies between certain T_1/T_2 ratios and corresponding NH bond vector orientations (i.e. residue A 50, and G 52 in apo-L75F) which are inconsistent from expected theoretical trends (see figure 2) are here considered to be the result of the error associated with measured T_1/T_2 values and the fact that theoretical trends presented in Figure 2 are derived with the assumption of a completely rigid protein backbone.

Once the model of diffusion had been established for both proteins, Lipari-Szabo model selection and the corresponding dynamical parameters were determined for all residues in which T_1, T_2 , and ^{15}N-{^{1}H} measurements were possible. A summary of model selection results for both apo-L75F and apo-WT-TrpR are presented in Table 6. As can be seen in Table 6, both proteins display a similar trend with the majority of analyzed residues best described by models 1 or 2. Complete listings of results from Lipari-Szabo analysis are presented for both apo-L75F and apo-WT in appendix D. The Lipari-Szabo models tabulated in appendix D are listed 1 through 5 and include the

corresponding parameters: model (1) S^2; model (2) S^2 and τ_e; model (3) S^2 and R_{ex} ; model (4) S^2, τe, and R_{ex}; and model (5) S^2, S^2_f, τ_e.

Table 6 Model selection results for apo-L75F and apo-WT-TrpR

Model†	apo-L75F number‡	apo-WT number‡
1	17	16
2	34	20
3	9	10
4	1	2
5	11	5

† Dynamical models as described in the text.

‡ Number of backbone NH groups fit to a given dynamical model.

Graphical representations of order parameters color-coded onto the backbone of the minimized average structure of apo-L75F and apo-WT-TrpR are presented in Figures 16 and 17, respectively. It is clear from these figures that the majority of the analyzed residues in both proteins exhibit restricted NH bond vector motions. The average order parameter value for the residues of apo-L75F is 0.82 ± 0.13, with a corresponding value of 0.85 ± 0.10 for apo-WT-TrpR amides. Also, both mutant and wild-type apo-proteins display large amplitude motions for residues located in the proteins' C-terminal regions. Large amplitude motions are also observed in the N-terminal region of apo-L75F.

Similar motions in the N-Terminal of apo-WT-TrpR are not observed due to incomplete relaxation data recorded for this region of the protein. However slight differences in model selection and the value of order parameters are evident in the helix D-turn-helix E region when comparing the two proteins. The significance of these results is discussed in the following chapter.

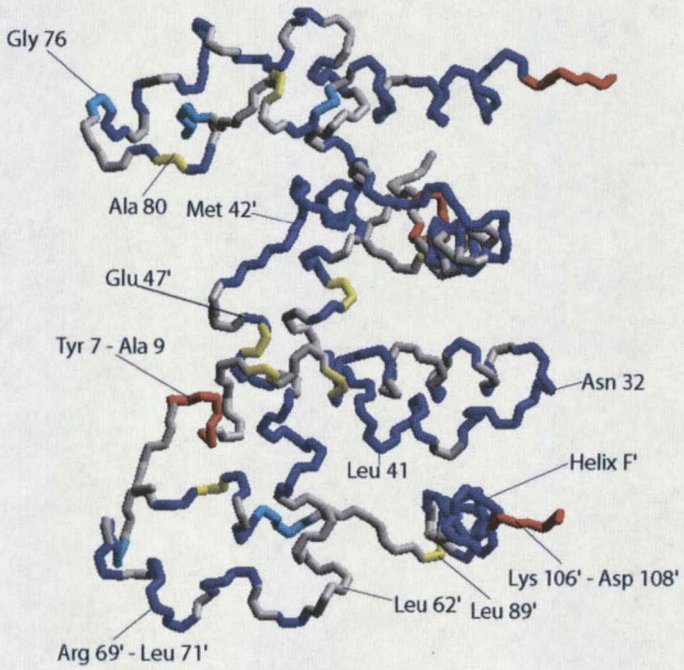

Figure 16: Backbone trace of apo-L75F TrpR color-coded by the value of the generalized order parameter (S^2). The color scheme is: $S^2 \geq 0.85$ blue; $0.84 \geq S^2 \geq 0.75$ cyan; $0.74 \geq S^2 \geq 0.6$ yellow; $S^2 \leq 0.59$ red. Residues for which order parameters were not determined are colored grey.

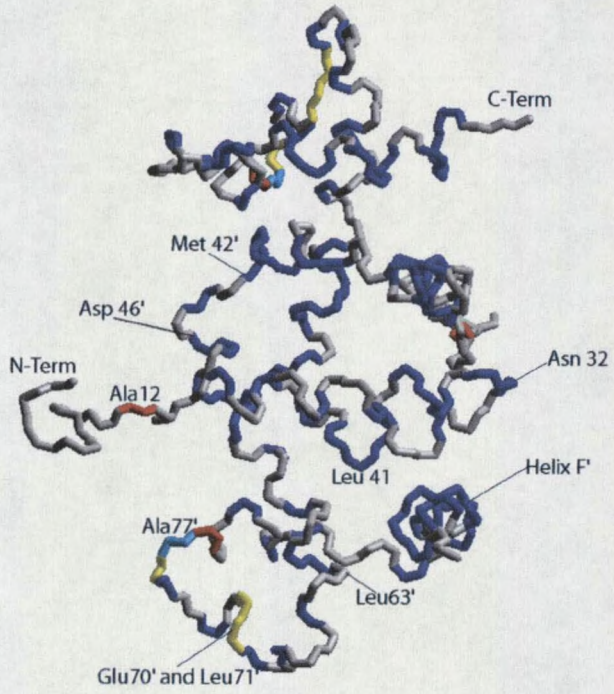

Figure 17: Backbone trace of apo-WT TrpR color-coded by the value of the generalized order parameter (S^2). The color scheme is: $S^2 \geq 0.85$ blue; $0.84 \geq S^2 \geq 0.75$ cyan; $0.74 \geq S^2 \geq 0.6$ yellow; $S^2 \leq 0.59$ red. Residues for which order parameters were not determined are colored grey.

Chapter 4

DISCUSSION

The structure of apo-L75F was determined using structural restraints based on NMR analysis. Comparisons of the NMR solution structures of apo-L75F to the published NMR structures of apo-WT TrpR have revealed that the two proteins exhibit very similar global folds. Helical regions in the hydrophobic core of apo-L75F were delineated based on the NMR data tabulated in Figure 4 and analysis with Procheck NMR software (*55*). These results are in excellent agreement with previous data reported for WT-apo TrpR. The size of the L-Trp binding pocket as well as the distance between the H16 Cα and H16' Cα atoms are within experimental error of the values determined for apo-WT TrpR.

In order to distinguish between local chemical shift perturbations caused by the ring current of the newly introduced phenylalanine ring and long-range origins of NH chemical shift differences that were observed in the two-dimensional ^{1}H-^{15}N correlation NMR spectrum of apo-L75F-TrpR, C_{α} distances between Phe75 and the affected sites were estimated from inspection of the NMR solution structures of apo-L75F. It has been discussed that the ring current effect is negligible beyond 5.5 Å and is expected to influence residues that lie within a relatively short distance to the mutation. A conservative estimate of 10 Å from the Cα atom of Phe75 was used in our analysis to probe possible ring current effects due to the mutation, taking into account ring flipping

and uncertainty in side chain positions. From Table 4, it is evident that many residues located in close proximity to the mutation site and residing in helix D and the D-turn- E region (e.g. Asn73, Glu74, Gly76, and Ala77) exhibit large chemical shift perturbations which can be rationalized by the ring current effect created by introduction of Phe75. This assessment is supported by the observation of weak nOes between the amide and aliphatic protons of Glu74, Gly76, and Ile79 and aromatic protons of Phe75, thus demonstrating that these residues experience the influence of the Phe75 phenylalanine ring. In contrast, several residues listed in Table 4 display Phe75 Cα to Cα distances that are well beyond the distance limit of ring current effect estimated in this analysis. For instance, residues Trp19', Val23', Leu26', and Tyr30' of helix A are approximately 30 Å away from Phe75, suggesting that these residues experience indirect long-range perturbations introduced by the mutation. Similar results are noted for residues in helix B and through the B-turn-C region of the protein. Residues 39-42 are approximately 25 Å from the closest site of the mutation, yet display noticeable differences in amide backbone chemical shift values when compared to apo-WT TrpR. Ala91 exhibits a moderate change in NH chemical shift values and is located 26.3 ± 2.4 Å from the mutation site. This residue is positioned within the E-turn-F region of the protein. Examination of the family of 20 structures of apo-L75F revealed that Met42', Leu43', Thr44' and Ala91 are all clustered within a spherical boundary of approximately 10 Å in diameter, with the center of this sphere set at approximately 26.0 Å from the closest Phe75 Cα atom. This suggests that there may be a common perturbation source affecting the chemical shifts of these residues which is independent of the ring current

introduced by Phe75. Given the significant changes in chemical shifts observed for residues Ser67, Gln68, Thr81, Ile82, and Thr83, and the intermediate distances they reveal from the Phe75 Cα position, it was concluded that these changes may result from a mixture of local (i.e. ring current) as well as long-range contributing factors.

Analysis of the helical orientations within the hydrophobic core revealed the presence of subtle structural changes when comparing mutant and wild-type proteins. From inspection of table 3 and figure 18, one can see that the apo-L75F mutant structure has undergone a slight expansion in the C/C' helical regions reflected in a longer Leu62 Cα to Leu62' Cα distance. Figure 18 and Table 3 also indicate that the relative orientation of helix A in the mutant protein has changed as well. This is reflected in identical values (within experimental errors) of the Asn32/Glu49' Cα-to-Cα distances for both mutant and wild-type proteins, and a significantly shorter His16/Glu49' distance in apo-L75F. Such distance measurements suggest that the orientation of helix A in the mutant protein has changed and has pivoted around its C-terminal residue Asn32 bringing His16 about 2 Å closer to residue Glu49' located in the central region of helix C'.

The orientations of helices B and F relative to helix C or C' have also changed noticeably when compared to the solution structures of apo-WT TrpR. The three residues Pro37, Asn40, and Met42 are located in the N-terminal, central, and C-terminal regions of helix B, respectively. The average distance between the Cα atoms of these residues and the Cα atom of Arg54' was measured for both apo-L75F and apo-WT TrpR. Arg54' is also located in the central region of helix C', and any change in the

relative orientation of helix B should be reflected in the Cα distances of Pro37, Asn40, and Met42. As can be seen in Table 3 and in Figure 18, both Asn40 and Met42 are approximately 3 Å further away from Arg54'in apo-L75F-TrpR.

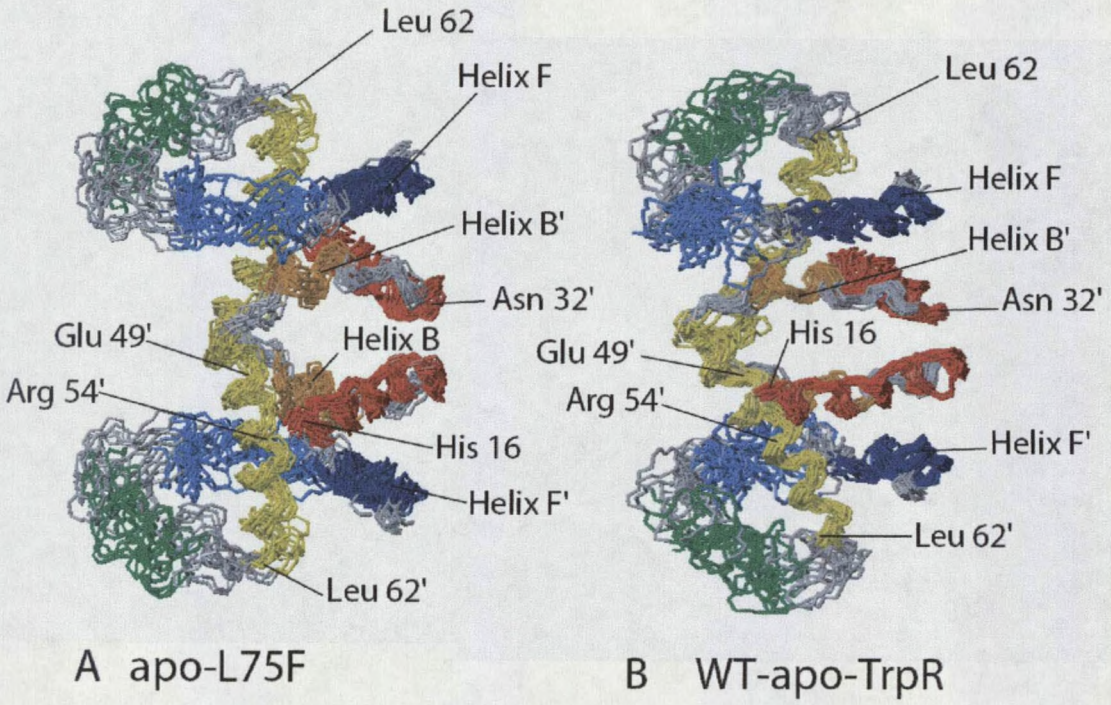

Figure 18: Comparison of backbone overlays of the accepted structures for (A) apo-L75F and (B) apo-WT TrpR taken from Zhao et al. Regions of the backbone color for both proteins are color coded as follows: Red residues 16-32, Orange residues 37-42, Yellow residues 45-62, Green residues 68-74, blue, Indigo residues 93-103. Approximate locations of residues have been pointed out for clarity.

This also suggests that the orientation of helix B in the mutant protein has been altered and has pivoted about the N-terminal residue Pro37. A similar observation can be made about the orientation of helix F in the L75F mutant. For example, the residues Pro93, Gln98, and Val103 are located in the N-terminal, central, and C-terminal regions of

helix F, respectively. Distance measurements between the Cα atoms of these residues and the Cα atom of Leu62 should give an indication of the orientation of helix F around the C-terminal region of helix C. Any change in the relative position of helix F in apo-L75F should also be reflected in longer Cα-to-Cα distances. As reported in Table 3, only one of the residues, Val103 of helix F, possesses a significant longer Cα to Cα distance. This indicates that the orientation of helix F in apo-L75F has also changed albeit slightly, and pivots about its N-terminal residue Pro93 relocating Val103 about 3 Å away from the C-terminal part of helix C. These data indicate that while mutant and wild-type proteins share similar global folds in solution, the Leu-to-Phe mutation confers long-range effects on the relative orientations of helices that make up the hydrophobic core of the mutant dimer. It is interesting to note that many residues which display substantial amide chemical shift changes and are well removed from the mutation site are located in regions of the protein where changes in helical orientations have been observed. Residues within helices A, B, and F all exhibit non-local chemical shift effects that may result from perturbation of electronic environments due to slight changes in the orientation of the helices making up the hydrophobic core the protein.

A unique ^{1}H-^{1}H NOESY cross-peak that was first observed by Jin et al. (*35*) in the unassigned spectrum of apo-L75F was tentatively described as an interaction between two slowly exchanging amide protons. In this work, this nOe cross-peak has been unambiguously identified and found to result from dipolar interactions between the amide protons of residues Met42 and Leu43. It has also been shown that these two residues display pronounced chemical shift differences when compared to apo-WT

TrpR (Table 1), and both are located beyond the influence of the ring current generated by Phe75 (Table 4). This unique interaction observed in apo-L75F between Met42 and Leu43 amide protons points toward the presence of structural changes that may have taken place in this region of the protein due to the leu to phe substitution at residue position 75

The chemical shift perturbation observed in apo-L75F for the backbone amide of Leu43 may be due to possible differences in packing of aromatic sidechains such the indole ring of tryptophan 19 around the C-terminal region of helix B. When examining the minimized average structure of apo-L75F and apo-WT TrpR, it is observed that the amide proton of Leu43 is less than 10.0Å away from the indole protons of Trp19'. Any alteration in the position of the ring current field generated by Trp19' could conceivably influence the chemical shifts of nearby residues. While this is only speculation, it is interesting to note that residues Trp19, Val23, Leu26, and Tyr30, all of which exhibit pronounced amide chemical shift changes, are all located on the same side of helix A. The chemical shift differences noted for these residues may stem from an alteration of the orientation of helix A relative to the positions of the other alpha helices making up the protein hydrophobic core. It is also interesting to consider that in the published report of Jin et al.(22), it was noted that fluorescence spectra indicated a more buried environment (blue-shifted) for one or both tryptophan residues of the mutant protein. From the chemical shift observations, it is most likely that Trp19 is the one tryptophan that has been perturbed by the mutation.

The structural alterations in the B-turn-C region reflected in nOe and chemical shift data could possibly affect the apo-L75F mutant in its ability to interact with its cofactor, as this region of the protein forms part of the binding pocket for L-Trp. In apo-WT TrpR, the carbonyl oxygens of Asn40, Leu41, and Leu43 participate in hydrogen bond formation with the guanidino group of Arg84 (*2;3*). In holo-WT TrpR, the α-amino group of L-Trp displaces the guanidino group of Arg84. We postulate that changes detected in the B-turn-C region of apo-L75F-TrpR may compromise important hydrogen bonding contacts and thus be related to the altered L-Trp binding properties of the mutant protein.

The observation of small but significant structural changes so far from the mutation site have directly confirmed the long-range nature of the effects of the L75F mutation within the framework of a very similar three-dimensional solution structure to that of the wild-type TrpR protein. The present case is especially intriguing considering the conservative nature of the amino acid substitution and the solvent-exposed location of residue 75.

Another highly characterized TrpR mutant which also contains a single point mutation in the protein DNA binding domain is A77V. There are some striking similarities between L75F and A77V. Both apo-mutants exhibit increased α-helicity as measured by CD and reveal more buried environments for tryptophan residues. NMR investigations have also shown that A77V has a three-dimensional structural fold that is very similar to that of wild-type TrpR (*30*). The fundamental difference between the A77V and L75F proteins resides in their ability to interact with DNA operator

sequences at low L-Trp concentrations. A77V has been classified as a super repressor because it can repress transcription of specific operons *in vivo* at lower L-Trp concentrations than wild-type repressor (*23*). The L75F mutant is not viewed as a super repressor yet from a biophysical point of view, the structural features (i.e. both TrpR mutants exhibit blue shifted tryptophan fluorescence spectra and increased helical content as measured by circular dichroism) seem closely related to those of the A77V TrpR protein.

Through structural and dynamic investigations of A77V and other TrpR mutants, it has been established that the intrinsic flexibility of the protein DNA binding domain is critical for operator recognition as well as for ligand binding (*31*). This link stresses the point that modest changes in sequence brought about by single point mutations can have profound consequences on protein function. The studies of the L75F-TrpR protein have demonstrated that mutational effects are not necessarily confined to the local mutation site but can manifest themselves throughout the protein architecture. TrpR represents an interesting case in that the protein structure and dynamics are dependent on both L-Trp cofactor and DNA binding events. Given the relationship between TrpR structure, dynamics, and function, the effect of the L75F mutation is also expected to manifest itself at the level of motional dynamics. In order to provide further insight into the effects of the Leu-to-Phe mutation, internal motions of backbone amides were thus probed by ^{15}N NMR relaxation methods.

The published ^{15}N relaxation data of holo-WT-TrpR point to a uniform distribution of relaxation parameters throughout the entire protein backbone, with no significant

differences in relaxation parameters for amides located within the TrpR DNA binding region. Elevated ^{15}N-T_1 and ^{15}N-T_2 values and depressed ^{15}N-{^1H} nOe values are usually indicative of fast internal motions on the subnanosecond timescale (*71*). Typically, backbone regions are considered to be undergoing fast internal motions when differences in relaxation parameters are two or more standard deviations from their measured average values (*12;15;16*). With this criterion, Jardetzky and coworkers concluded that only residues Met11, Lys106, and Asp108 located in the N and C termini of holo-WT-TrpR have ^{15}N amide relaxation values indicative of fast subnanosecond internal motions (*12*). The uniformity of the ^{15}N- T_1, T_2, and nOe values reported for holo-WT-TrpR within the hydrophobic core and the protein DNA binding domain was thus taken as evidence for the lack of fast subnanosecond backbone internal motions. And it was thus concluded that the entire backbone chain of holo-WT-TrpR does not exhibit substantially large amplitude NH bond vector motions, but is in contrast very rigid on the nanosecond timescale except for amides dynamics in the N- and C-termini of the protein.

In this work, ^{15}N relaxation experiments were performed on both apo-L75F and apo-WT TrpR under identical solution conditions, as reported in the material and methods section of this thesis. The ^{15}N NMR relaxation data presented herein indicate that the two apo-proteins exhibit similar ^{15}N NMR relaxation profiles in solution. Within experimental errors, both apo-proteins appear to display very comparable relaxation behavior for backbone amide groups residing in the hydrophobic core and in the DNA binding region. The common trends observed in both proteins (Table 5) are

slightly elevated ^{15}N-T_2, and lowered ^{15}N-T_1 and ^{15}N-{^1H} nOe values for amides located in the protein DNA binding region relative to relaxation values measured for residues in the hydrophobic core. However, the differences in relaxation rate constants for residues within the DNA binding domain of apo-WT TrpR are not considered to be significant because the differences are less than one standard deviation from average ^{15}N-T_1, ^{15}N-T_2, and ^{15}N-{^1H}nOe values computed for the entire protein. These results thus suggest that as a whole, the DNA binding domain in apo-WT TrpR is not experiencing fast internal backbone amide motions. This same conclusion is reached when analyzing the relaxation parameters for amides in the DNA-binding region of apo-L75F. However, this analysis does not rule out the possibility that individual differences between NH bond vector motions for specific residues of apo-WT and apo-L75F exist. Rather, these observations suggest that both apo-proteins have very similar ^{15}N NMR relaxation characteristics. Furthermore, the ^{15}N relaxation parameters for both apo-proteins while distinct from values measured for holo-WT-TrpR do not represent sufficiently large differences to suggest that major dynamical changes take place within the DNA binding region when the apo-protein is converted to its holo-form, at least for backbone amide motions on the subnanosecond timescale.

In this work, rotational diffusion tensors for global reorientation of the apo-proteins in solution were extracted from ^{15}N-T_1 and ^{15}N-T_2 relaxation measurements. These calculations are consistent with an axially symmetric model of rotational diffusion for both wild-type and mutant proteins, and yield within experimental errors identical overall correlation times of approximately 10 ns. The anisotropy for the

rotational diffusion of the two proteins in solution was determined from respective $D_{\parallel}/D_{\perp}$ ratios which were determined to be very similar when considering the propagation of errors derived from the uncertainty associated with the $D_{\parallel}$ and $D_{\perp}$ components. The anisotropy extracted from this study yielded $D_{\parallel}/D_{\perp}$ values of 1.20 ± 0.04 and 1.15 ± 0.04 for apo-L75F and apo-WT TrpR, respectively. However, the anisotropies calculated for both apo-L75F and apo-WT TrpR while in agreement are substantially lower than the $D_{\parallel}/D_{\perp}$ value of 1.28 reported for holo-WT TrpR (12). Similarly, the overall correlation times calculated for both apo-proteins (again while in agreement) with τ_c equals to 10.2 ± 0.2 ns and 10.5 ±0.2 ns for apo-L75F and apo-WT TrpR respectively, are slightly shorter then the τ_c value reported for holo-WT TrpR of 13 ns (*12*). The origin of these discrepancies is not clear at present but may reflect the structural reorganization that occurs upon L-Trp cofactor binding. It has been discussed that the overall shape of a protein influences its relaxation properties and the anisotropy of its global reorientation in solution. In the case of TrpR, the binding of the L-Trp cofactor results in the observations of additional nOes for residues located within helix E, of backbone atoms within this helix shifting away from the dyad axis by as much as two to four angstroms on average (5). Any structural alteration associated with ligand binding will thus influence the rotational characteristics of TrpR in solution and may be at the origin of these differences in calculated rotational anisotropies for the apo and holo forms of the protein. In support of this reasoning, it is well-known that the anisotropy of rotational diffusion of a protein in solution can be altered by allosteric and/or ligand binding processes (*57*).

The results from the Lipari-Szabo analysis presented in Figure 16 and appendix D demonstrate that a majority of the protein backbone amides in apo-L75F TrpR exhibit restricted subnanosecond NH bond vector motions, as shown by order parameter (S^2) values ranging from 0.8 to 0.96. For the hydrophobic core of apo-L75F, an average S^2 is determined to be 0.91 ± 0.05, while an average S^2 of 0.84 ± 0.04 is calculated for amides located within helices D and E. Such data thus suggest that on the nanosecond motional timescale the protein backbone is quite rigid. From our limited ^{15}N relaxation measurements of apo-WT TrpR, average S^2 values of 0.92 ± 0.03 and 0.89 ± 0.05 have been computed for backbone NH bond vectors located in the hydrophobic core and DNA binding region of the protein, respectively. A graphical depiction of these results is presented in Figure 17. These results are comparable to S^2 values determined in apo-L75F. From these measurements, it thus appears that the L75F mutation has had no significant effect on the picosecond to nanosecond internal motions of backbone amides, with both apo-L75F and apo-WT TrpR indicating that the NH bond vector motions are just as restricted in the DNA binding domain as they are in the hydrophobic core of the proteins. This result is consistent with the observations of Zheng et al. for holo-WT-TrpR (12). For the holo-protein, the authors reported an average S^2 value of 0.81 ± 0.10 over the entire protein backbone with values for residues in the DNA binding domain displaying no substantial deviations from the ones in the protein hydrophobic core. Considering the results presented in this thesis and observations made by Zheng et al,, we conclude that the binding of L-Trp to the apo-repressor does not influence subnanosecond backbone motions of amides located within the DNA

binding domain. Furthermore by comparing the dynamical parameters extracted for apo-L75F and apo-WT TrpR, we conclude that the Leu-to-Phe substitution at position 75 does not cause significant changes in S^2 values that would have indicated the presence of subnanosecond motional differences for amides located in the core versus the D-E helical region of apo-L75F-TrpR.

The S^2 values of apo-L75F and apo-WT TrpR were also compared on a residue by residue basis in an attempt to assess if specific differences could be observed and whether these may correlate with residues exhibiting perturbed NH backbone chemical shifts. It is expected that events affecting ^{15}N NMR relaxation parameters which are sensitive to the nanosecond timescale would have very little or no influence on chemical shift parameters since the later are commonly influenced by motional events on the slower millisecond timescale. However, it was reasoned that if a backbone amide group displayed a substantial decrease in S^2 value as a result of mutation, the NH bond vector may experience a different local magnetic environment (i.e. the amide group would have a larger range of motions) that could potentially cause a change in chemical shift. Residues Gly52, Arg54, Val55, and Ile57 of helix C display moderate chemical shift perturbations, yet S^2 values for Gly52 and Arg54 are almost identical in both apo-proteins. As expected, this observation demonstrates that the chemical shift differences observed in apo-L75F for these residues do not correlate with changes in amplitude of NH bond vector motions. This further implies that the expansion of helices C and C' reflected in the longer Leu62 Cα-to-Leu62' Cα distance in the mutant protein seems to have little or no effect on subnanosecond backbone amide motions in

this area. This is not too surprising given that helices C and C' are buried within the hydrophobic core. A similar conclusion is drawn when considering residues located within the L-Trp binding site. Residues Leu41 and Met 42 also exhibit significant chemical shift variations when compared to apo-WT TrpR NH chemical shifts (Table 1) but give rise to identical model selection and S^2 NMR dynamical parameters for both apo-proteins. These results also support the conclusion that structural perturbations detected within the L-Trp binding site have no major effect on subnanosecond NH backbone dynamics.

Even though little change is observed in average S^2 values when evaluating apo-L75F and apo-WT TrpR, an interesting contrast is seen with regards to model selection results. The majority of backbone NH groups of both apo-proteins are well-described by simpler models of motion, i.e. models 1 or 2. This indicates that the preponderance of backbone motions can be depicted as simple librations of NH bond vectors without the need to introduce a chemical exchange term or a more complex motional model that includes fast and slow internal motion components (*67*). Yet, there is an interesting difference in the model selection results for amides located within the DNA binding domain and surrounding the mutation site. Residues in the apo-L75F protein located adjacent or very close to the substitution site at position 75 (i.e. Glu70, Leu71, Phe75, and Gly76) are characterized by model 2 with S^2 values greater than 0.84. These same residues in apo-WT TrpR have surprisingly different model selection with lower S^2 values. For apo-WT-TrpR, residues Glu70, Leu71, and Gly76 are all described by model 5 with S^2 values lower than 0.72. The native Leu75 amide in wild-type apo-

TrpR is described by model 4. While it has been stated that models 4 and 5 can only be treated in a qualitative sense due to overparametrization, these results suggest that complex backbone motions that may be taking place within the DNA binding domain of and that require the extended Lipari-Szabo formalism for meaningful descriptions of the dynamics in apo-WT TrpR become simplified by the Leu-to-Phe substitution at position 75 in the mutant protein. Specifically, motions that are represented by a chemical exchange term for Leu75 of apo-WT TrpR appear to be absent in apo-L75F at the corresponding Phe75 position. Furthermore, model 5 assumes that the NH bond vector samples two distinct motions taking place on two different timescales described by two internal correlation times τ_s and τ_f. The lack of this complex motion and motion associated with chemical exchange in apo-L75F-TrpR may reflect a reduction of backbone movement or stiffening around the mutation site due to the introduction of a bulky hydrophobic phenylalanine side chain a residue position 75.

Given this possibility as to the nature of backbone amide dynamic changes taking place within apo-L75F, it is interesting to note that a similar phenomenon has been proposed to explain the reduction of amide exchange rates observed in the A77V TrpR mutant protein (*30*). Jardetzky and coworkers speculated that the decrease in amide exchange rates observed for amides located in the vicinity of the A77V mutation site may have originated from a "damping mechanism" (*30*) of backbone motions in this area, and that this event could possibly increase local amide hydrogen bonding interactions resulting in protection against $^1H/^2H$ exchange. This is not meant to imply that events taking place on the timescale of amide exchange (millisecond or longer) are

correlated to ^{15}N amide backbone dynamics taking place on the faster subnanosecond timescale. Furthermore, the lack of a careful quantification of amide backbone exchange rates for the L75F protein prevents at this time a conclusive determination as to whether or not increases in local hydrogen bonding interactions are taking place around the Phe75 location. Rather, this reasoning is only meant to suggest that the introduction of the phenylalanine side chain at position 75 may cause an analogous reduction of the backbone amide motions around the mutation site as was observed for the A77V TrpR mutant. In effect, the phenylalanine may act as an anchor on the backbone of the protein which results in higher S^2 values and less complicated NH bond vector motions for some amides located within the DNA binding domain.

It has been mentioned in the introduction that in the presence of 5-MT, the L75F TrpR protein displays a temperature-sensitive phenotype which is different at 37 °C than at 42 °C (*22*). Therefore, there must be some event taking place within the bacterial cells expressing the L75F-TrpR protein which is temperature dependent and which could provide a molecular basis for the observed temperature-sensitive phenotype. One possible way to gain insight into the temperature-sensitivity of the L75F mutation may be to examine ^{15}N-edited and ^{13}C-edited ^{1}H-^{1}H NOESY spectra as a function of temperature and to assess whether spectral differences are evidences of possible side chain conformational transitions. These signs might include an increase or decrease in intensity of particular nOe cross-peaks in the spectra, which may reflect changes in intra/inter-helical nOe patterns of residues within the cofactor binding pocket as well as other functionally relevant regions of the protein. These results could

then serve to probe possible structural factors that may help explain the temperature-sensitive phenotype observed for mutant cell strains containing L75F TrpR.

Another way one might gain insight into the origins of the temperature-sensitivity of the L75F mutation is by considering possible motional differences for protein residues at the two temperatures. By conducting ^{15}N relaxation experiments at 37 °C and 45°C, one may be able to detect differences in dynamical parameters. For examples, these differences may manifest themselves in different model selection results and/or changes in dynamic parameters (e.g. S^2,τ_e, R_{ex}) for certain backbone amides. Any significant change could point toward relevant internal motions within the L75F backbone that may be related to the temperature-sensitive phenotype. A similar approach utilizing ^{13}C NMR relaxation experiments could also be employed to probe possible differences in side chain dynamics as a function of temperature within the L75F protein.

Although the present ^{15}N dynamic analysis has not revealed major differences between apo-L75F and apo-WT TrpR, there are some indications that a reduction of backbone motions is taking place around the Phe75 mutation site compared to the corresponding location in apo-WT TrpR. However in order to unambiguously resolve this issue, additional ^{15}N-T_1, ^{15}N-T_2 and ^{15}N-{^1H} nOe data will need to be collected at a different magnetic field strengths (e.g. 500 MHz) for both apo-L75F and apo-WT TrpR. By analyzing the static magnetic field dependence of the relaxation, these experiments would permit the measurements of additional NMR relaxation parameters increasing the number of experimental variables to 6, and would result in 3 degrees of

freedom for the fitting of models 4 and 5. Such experiments would permit us to assess the legitimacy of the model selection results reported for helix D in apo-WT TrpR by F-test statistics, and to better verify that the reduction of the complexity of NH bond vector motions as suggested by model selection 2 in apo-L75F-TrpR is indeed real.

It is also quite possible that subnanosecond amide backbone motions are not sensitive to slower motional effects that may be caused by the Leu-to-Phe substitution at position 75. The dynamic results and similarities reported for both apo-L75F and apo-WT TrpR presented in this work support such a conclusion. This possibility is further strengthened by a recent report that fast timescale dynamic motions within the backbone of a mutant of the nitrogen regulatory protein C (NtrC) are comparable to the motions observed within the native protein (*72*).

Nevertheless even if backbone amide motions are unchanged, this does not exclude the possibility that the subnanosecond motions of side chain atoms in TrpR are sensitive to the L75F mutation. This expectation is not unreasonable as there are many reports in the literature of changes in subnanosecond side chain dynamics while backbone motions may or may not be altered. For example in Staphylococcal Nuclease, methyl groups dynamics are significantly influenced by the binding of Ca^{+2} and reflect a reduction of CH bond vector side chain motions in regions near the binding site (*62*). NMR studies of calmodulin have also reported a reduction of subnanonecond side chain (methyl) dynamics in areas involved in peptide binding (*73*). These studies suggest that for many protein systems side chain dynamics are more sensitive to ligand binding processes, and that investigations of internal motions of side chains by ^{13}C NMR

relaxation measurements may be more effective probes of changes caused by amino acid substitutions in proteins. This ^{13}C NMR relaxation methodology will be employed in future experiments to further investigate potential differences in internal dynamics between apo-WT and apo-L75F-TrpR proteins. Direct comparisons of these results may thus lead to better insights as to the nature of dynamical differences that are suspected to take place in L75F-TrpR due to the Phe75 mutation. Any difference in side chain motions between wild-type and mutant proteins may provide important clues about the conformational entropy of TrpR which is expected to be an important thermodynamic factor when considering differences in ligand binding affinity between L75F and wild-type TrpR proteins (*73*). Given the abundance of leucine resides in both wild-type (19 leucine residues) and L75F (18 leucine residues) and their distribution throughout the protein structures with at least one residing in each of the six α-helices, the study of methyl group dynamics in TrpR could be greatly simplified by selective ^{13}C labeling of leucine residues.

The TrpR protein is one of the better characterized allosteric systems, with its repressor function being dependent on conformational (*5;6*) and dynamical changes (*8;9*) that are associated with L-Trp cofactor and DNA binding. Many of the relevant changes are known to be located far away from the ligand binding sites indicating that long-range communication (i.e. allosteric transitions) within this system is critical for function. Much of the work on the TrpR system has been devoted to a careful characterization of allosteric changes taking place within the protein and how these conformational conversions relate to function. Structural studies of TrpR have revealed

important conformational transitions that take place within the DNA binding domain upon ligand binding. Given the vast amount of knowledge collected on this regulatory protein, it is surprising that the exact mechanisms by which ligand binding affinity and specifity are modulated through protein structural and dynamic changes is still poorly understood. Mutational studies have been very useful by revealing that molecular perturbations influencing the dynamics of residues within the DNA binding domain of TrpR alter significantly the protein's ability to function. From these extensive studies, it is now well-established that molecular flexibility within the TrpR DNA binding domain is critical for operator recognition. Any change in structure and/or dynamics associated with mutations, particularly within the DNA binding domain, will conceivably have dramatic affect on the protein and its functional properties. Our results that the Leu-to-Phe substitution within the DNA binding domain of apo-L75F TrpR produces long-range effects are consistent with such thinking and emphasize the crucial importance of the D-E helical region for TrpR repressor function as well as the unique interplay between the protein structure and dynamics that modulates the ligand binding properties of TrpR.

The original work of Jin et al. and the study presented herein have thus unequivocally demonstrated that many long-range effects are transmitted throughout the protein as a consequence of the L75F mutation. Nevertheless, the structural and dynamic data presented in this thesis have also shown that challenges remain in order to fully understand this protein and to be able to specifically attribute changes in protein amino acid sequence to variations in biophysical and functional properties. As mentioned

previously, it is surprising that given the vast amounts of biophysical, structural, and dynamic data available about the tryptophan repressor protein, as well as results from numerous mutational studies, our knowledge of the exact mechanism(s) by which a single point mutation can propagate non-local change throughout the TrpR protein is still very limited. In light of the fact that dynamical changes for residues within the DNA binding domain of TrpR affect the protein's ability to discriminate between closely resembling operator DNA sequences, it is clear that the protein function is closely connected to the internal motions of its atoms. The work presented here suggests that dynamic changes may also have profound effects on the global structural characteristics of TrpR as well.

Chapter 5

CONCLUSION

The NMR structural study reported in this thesis about the temperature sensitive apo-L75F TrpR protein has revealed that the overall three dimensional structure is very similar to that of apo-WT TrpR. The family of twenty structures that were generated resulted in a 1.0 Å average rmsd for backbone atoms located in the hydrophobic core of the protein and 2.8 Å average rmsd for backbone atoms residing in the DNA binding domain. Measurement of the dimension of the hydrophobic core perpendicular to the dyad axis as reflected by the Leu62 C_α –to-Leu62'C_α distance revealed an increase of approximately 4.0 Å in the apo-L75F protein compared to wild-type. Additional distance measurements that probed the orientations of helices within the hydrophobic core also highlighted slight structural differences relative to apo-WT TrpR. Comparisons of chemical shift values for backbone amides of apo-L75F versus apo-WT TrpR indicated substantial differences for twenty-six residues located throughout the proteins tertiary structure. These distances estimates thus demonstrated that the newly introduced phenylalanine at position 75 is very likely influencing chemical shifts of residues in close proximity to the mutation site (i.e. less then 10.0 Å) via ring-current effects. Areas involved in the binding of the L-Trp cofactor in the B-turn-C region of the protein are too distant from the mutation site (greater than 10.0 Å) to be influenced by the ring current of Phe75. These results suggest that structural changes in this part of the protein may be responsible for the chemical shift differences observed for amides in

the B-turn-C region, and might reflect the decrease in L-Trp cofactor binding affinity originally reported in L75F-TrpR by Carey and co-workers (*35*). The NMR-based structural data have thus provided substantial evidence that the mutation propagates long-range effects throughout the protein structure as was initially proposed by Jin et al. (*35*).

^{15}N relaxation analyses performed on both apo-L75F and apo-WT TrpR have shown that the two proteins have very similar backbone amide dynamical behavior on the nanosecond timescale, as is reflected in comparable ^{15}N-T1, T2 relaxation and ^{15}N-{^{1}H} nOe values and fitted order parameters. Model selection results have also shown that the majority of the amide motions for both proteins can be characterized by motional models 1 or 2. However differences in model selections have been observed for certain residues in helix D suggesting that the L75F mutation may have reduced the complexity of NH bond vector movement and the extent of NH bond vector motions for residues near to the mutation site. Even though additional relaxation measurements will be required to fully resolve this issue, the current results suggest that possible changes in the dynamics within the protein DNA binding domain due to the introduction of the phenylalanine at position 75 exhibit themselves as local restrictions in amplitude of amide backbone movements. The global structural changes reflected in differential helical orientations within the hydrophobic core may also be a contributing factor to explain the lower biochemical activity of the L75F TrpR mutant.

Future Directions

It has been mentioned that additional ^{15}N relaxation measurements at 500 MHz would permit more reliable model selection results and may help confirm the existence of differences in dynamical motions within helix D of apo-L75F. The ^{15}N relaxation results presented here report solely on events taking place on the picosecond to nanosecond timescale. However as a result of the leu to phe75 substitution, motional events taking place on slower timescales such as millisecond chemical exchange processes may also be important and significant. Plans are to characterize these slower timescale motions by measuring transverse rotating frame time constants $^{15}N\text{-}T_{1\rho}$. Such measurements are analogous to measuring transverse relaxation rates in the laboratory frame, i.e. $^{15}N\text{-}T_2$, except that instead of employing a CPMG pulse train during the transverse relaxation delay in the NMR pulse sequence, a continuous spin lock is used (*74*). In the absence of chemical exchange (R_{ex}), the two experiments yield identical results, i.e. $^{15}N\text{-}T_{1\rho}$ equals $^{15}N\text{-}T_2$ (*74*). When substantial chemical exchange processes are present, measured transverse relaxation rates are no longer equal, with $^{15}N\text{-}T_{1\rho}$ values being greater than corresponding $^{15}N\text{-}T_2$ values. This phenomenon is due to the presence of delays between the 180° refocusing pulses that are used in the $^{15}N\text{-}T_2$ CMPG pulse train to improve the reproducibility of the experiments and are typically set to 1ms (*75*). However chemical exchange events taking place on the millisecond timescale will not be properly refocused in these ^{15}N- transverse relaxation experiments and will result in systematically lower $^{15}N\text{-}T_2$ values (*74*). The continuous spin lock utilized in $^{15}N\text{-}T_{1\rho}$ experiments eliminates the decrease in signal intensity caused by

chemical exchange in the ^{15}N-T_2 CPMG experiment and results in measurements of higher ^{15}N-$T_{1\rho}$ values relative to ^{15}N-T_2 values when R_{ex} is nonzero (*74;76*). Future plans are to conduct ^{15}N-$T_{1\rho}$ experiments of this type on apo-L75F and apo-WT TrpR and to compare the resulting ^{15}N-$T_{1\rho}$ values to corresponding ^{15}N-T_2 parameters. Such studies will enable us to determine if slower timescale amide motions are indeed present in apo-L75F-TrpR. These results will then be cross-checked against the model selection results produced by NORMAdyn that had introduced a R_{ex} term when fitting the three standard ^{15}N-T_1, T_2, and ^{15}N-{^1H}-nOe parameters measured in the present work.. This analysis will not only enable us to determine if slower timescale motions are present but will also permit us to assess whether a correlation exists between these motions and the local and non-local perturbations that have been observed in apo-L75F and reported in this thesis.

Future experiments will also involve dynamical investigations of the holo-forms of both L75F and WT-TrpR in order to gain better insights into the motional influence of L-Trp binding on the internal dynamics of backbone and side-chain atoms, and to assess whether the anisotropy of the protein's overall rotational diffusion tensor changes upon cofactor binding. The anisotropy for the rotational diffusion tensor of both holo-L75F and holo-WT-TrpR will be calculated in a manner analogous to what was done in this thesis for the apo-proteins using the NORMAdyn software, and will be compared to the published results of Jardetzky and coworkers on the holo-WT-TrpR. By investigating the motional dynamics of holo-proteins under identical experimental conditions, such experiments will permit us to assess whether the differences in $D_{\parallel}/D_{\perp}$

ratios that have appeared here between apo-L75F and apo-WT TrpR and those reported for holo-WT-TrpR by Zheng et al (12) are truly real or whether the discrepancies are a reflection of differences in experimental conditions because the studies have been conducted many years apart in two different laboratories.

REFERENCES

References

1. Joachimiak, A., Kelley, R. L., Gunsalus, R. P., Yanofsky, C., and Sigler, P. B. (1983) *Proc. Natl. Acad. Sci. U. S. A 80*, 668-672.

2. Schevitz, R. W., Otwinowski, Z., Joachimiak, A., Lawson, C. L., and Sigler, P. B. (1985) *Nature 317*, 782-786.

3. Zhang, R. G., Joachimiak, A., Lawson, C. L., Schevitz, R. W., Otwinowski, Z., and Sigler, P. B. (1987) *Nature 327*, 591-597.

4. Arrowsmith, C., Pachter, R., Altman, R., and Jardetzky, O. (1991) *Eur. J. Biochem. 202*, 53-66.

5. Zhao, D., Arrowsmith, C. H., Jia, X., and Jardetzky, O. (1993) *J. Mol. Biol. 229*, 735-746.

6. Zhang, H., Zhao, D., Revington, M., Lee, W., Jia, X., Arrowsmith, C., and Jardetzky, O. (1994) *J. Mol. Biol. 238*, 592-614.

7. Otwinowski, Z., Schevitz, R. W., Zhang, R. G., Lawson, C. L., Joachimiak, A., Marmorstein, R. Q., Luisi, B. F., and Sigler, P. B. (1988) *Nature 335*, 321-329.

8. Arrowsmith, C., Czaplicki, J., Iyer, S., and Jardetzky, O. (1991) *Journal of the American Chemical Society 113*, 4020-4022.

9. Czaplicki, J., Arrowsmith, C., and Jardetzky, O. (1991) *J. Biomol. NMR 1*, 349-361.

10. Gryk, M. R., Finucane, M. D., Zheng, Z., and Jardetzky, O. (1995) *J. Mol. Biol. 246*, 618-627.

11. Finucane, M. D. and Jardetzky, O. (1995) *J. Mol. Biol. 253*, 576-589.

12. Zheng, Z., Czaplicki, J., and Jardetzky, O. (1995) *Biochemistry 34*, 5212-5223.

13. Lipari, G. and Szabo, A. (1982) *Journal of the American Chemical Society 104*, 4546-4559.

14. Lipari, G. and Szabo, A. (1982) *Journal of the American Chemical Society 104*, 4559-4570.

15. Kay, L. E., Torchia, D. A., and Bax, A. (1989) *Biochemistry 28*, 8972-8979.

16. Barbato, G., Ikura, M., Kay, L. E., Pastor, R. W., and Bax, A. (1992) *Biochemistry 31*, 5269-5278.

17. Stone, J., Fairbrother, W., Palmer, A. G., Reizer, J., Saier, M. H., and Wright, P. E. (1992) *Biochemistry 31*, 4394-4406.

18. Clore, G. M., Driscoll, P. C., Wingfield, P. T., and Gronenborn, A. M. (1992) *Biochemistry 29*, 7387-7401.

19. Tjandra, N., Feller, S. E., Pastor, R. W., and Bax, A. (1995) *Journal of the American Chemical Society 117*, 12562-12566.

20. Farrar, T. C. and Becker, E. D. (1971) *Pulse and Fourier Transform NMR* Academic Press, New York, NY.

21. Wishart, D. S. and Nip, A. M. (1998) *Biochem. Cell Biol. 76*, 153-163.

22. Jin, L., Yang, J., and Carey, J. (1993) *Biochemistry 32*, 7302-7309.

23. Kelley, R. L. and Yanofsky, C. (1985) *Proc. Natl. Acad. Sci. U. S. A 82*, 483-487.

24. Hurlburt, B. K. and Yanofsky, C. (1990) *J. Biol. Chem. 265*, 7853-7858.

25. Reedstrom, R. J. and Royer, C. A. (1995) *J. Mol. Biol. 253*, 266-276.

26. Fernando, T. and Royer, C. (1992) *Biochemistry 31*, 3429-3441.

27. Ladbury, J. E., Wright, J. G., Sturtevant, J. M., and Sigler, P. B. (1994) *J. Mol. Biol. 238*, 669-681.

28. Reedstrom, R. J., Martin, K. S., Vangala, S., Mahoney, S., Wilker, E. W., and Royer, C. A. (1996) *J. Mol. Biol. 264*, 32-45.

29. Lawson, C. L., Zhang, R. G., Schevitz, R. W., Otwinowski, Z., Joachimiak, A., and Sigler, P. B. (1988) *Proteins:Struct. Funct. Genet. 3*, 18-31.

30. Gryk, M. R. and Jardetzky, O. (1996) *J. Mol. Biol. 255*, 204-214.

31. Gryk, M. R., Jardetzky, O., Klig, L. S., and Yanofsky, C. (1996) *Protein Sci. 5*, 1195-1197.

32. Marmorstein, R. Q., Joachimiak, A., Sprinzl, M., and Sigler, P. B. (1987) *J. Biol. Chem. 262*, 4922-4927.

33. Marmorstein, R. Q. and Sigler, P. B. (1989) *J. Biol. Chem. 264*, 9149-9154.

34. Lawson, C. L. (1996) in *Biological Structure and Dynamics* (Sarma, R. H. and Sarma, M. H., Eds.) Adenine Press, Albany,New York.

35. Jin, L., Fukayama, J. W., Pelczer, I., and Carey, J. (1999) *J. Mol. Biol. 285*, 361-378.

36. Bennett, G. N. and Yanofsky, C. (1978) *J. Mol. Biol. 121*, 179-192.

37. Cavanagh, J., Fairbrother, W., Palmer, A. G., and Skelton, N. (1996) in *Protein NMR spectroscopy* pp 410-531, Academic Press, San Diego.

38. Brunger, A. T., Adams, P. D., Clore, G. M., DeLano, W. L., Gros, P., Grosse-Kunstleve, R. W., Jiang, J. S., Kuszewski, J., Nilges, M., Pannu, N. S., Read, R. J., Rice, L. M., Simonson, T., and Warren, G. L. (1998) *Acta Crystallogr. D. Biol. Crystallogr. 54 (Pt 5)*, 905-921.

39. Brunger, A. T. (1992) *X-PLOR version 3.1, A systemfor X-ray Crystallography and NMR* Yale University Press, New Haven, CT..

40. Case, D. A. (1995) *J. Biomol. NMR 6*, 341-346.

41. Marion, D., Ikura, M., Tschudin, R., and Bax, A. (1989) *Journal of Magnetic Resonance 85*, 393-399.

42. Delaglio, F., Grzesiek, S., Vuister, G. W., Zhu, G., Pfeifer, J., and Bax, A. (1995) *Journal of Biomolecular Nmr 6*, 277-293.

43. Garrett, D. S., Powers, R., Gronenborn, A. M., and Clore, G. M. (1991) *Journal of Magnetic Resonance 95*, 214-220.

44. Bodenhausen, G. and and Ruben, D. J. (1980) *Chem. Phys. Lett. 69* 185-189.

45. Shaka, A. J., Keeler, J., and Freeman, R. (1983) *Journal of Magnetic Resonance 53*, 313-340.

46. Grzesiek, S. and Bax, A. (1992) *Journal of the American Chemical Society 114*, 6291-6293.

47. Grzesiek, S. and Bax, A. (1992) *Journal of Magnetic Resonance 99*, 201-207.

48. Grzesiek, S. and Bax, A. (1993) *Journal of Biomolecular Nmr 3*, 185-204.

49. Grzesiek, S., Anglister, J., and Bax, A. (1993) *Journal of Magnetic Resonance Series B 101*, 114-119.

50. Shaka, A. J., Lee, C. J., and Pines, A. (1988) *Journal of Magnetic Resonance 77*, 274-293.

51. Marion, D., Kay, L. E., Sparks, S. W., Torchia, D. A., and Bax, A. (1989) *Journal of the American Chemical Society 111*, 1515-1517.

52. Kay, L. E., Marion, D., and Bax, A. (1989) *Journal of Magnetic Resonance 84*, 72-84.

53. Bax, A., Clore, G. M., Driscoll, P. C., Gronenborn, A. M., Ikura, M., and Kay, L. E. (1990) *Journal of Magnetic Resonance 87*, 620-627.

54. Pardi, A., Billeter, M., and Wuthrich, K. (1984) *J. Mol. Biol. 180*, 741-751.

55. Laskowski, R. A., Rullmannn, J. A., MacArthur, M. W., Kaptein, R., and Thornton, J. M. (1996) *J. Biomol. NMR 8*, 477-486.

56. Derome, A. E. (1993) in *Modern NMR Techniques for Chemistry Research* pp 97-127.

57. Palmer, A. G., Williams, J., and McDermott, A. (1996) *Journal of Physical Chemistry 100*, 13293-13310.

58. Abragam, A. (1962) *Principles of Nuclear Magnetism* Oxford University Press (Clarendon), London.

59. Hiyama, Y., Niu, C. H., Silverton, J. V., Bavoso, A., and Torchia, D. A. (1988) *Journal of the American Chemical Society 110*, 2378-2383.

60. Woessner, D. E. (1962) *J. Chem. Phys. 36*, 1-4.

61. Pawley, N. H., Wang, C., Koide, S., and Nicholson, L. K. (2001) *J. Biomol. NMR 20*, 149-165.

62. Nicholson, L. K., Kay, L. E., Baldisseri, D. M., Arango, J., Young, P. E., Bax, A., and Torchia, D. A. (1992) *Biochemistry 31*, 5253-5263.

63. Berman, H. M., Westbrook, J., Feng, Z., Gilliland, G., Bhat, T. N., Weissig, H., Schindyalov, I. N., and Bourn, P. E. (2000) *Nucleic Acid Research 28*, 235-242.

64. Kay, L. E., Nicholson, L. K., Delaglio, F., Bax, A., and Torchia, D. A. (1992) *Journal of Magnetic Resonance 97*, 359-375.

65. Grzesiek, S. and Bax, A. (1993) *Journal of the American Chemical Society 115*, 12593-12594.

66. Clore, G. M., Szabo, A., Bax, A., Kay, L. E., Driscoll, P. C., and Gronenborn, A. M. (1990) *Journal of the American Chemical Society 112*, 4989-4991.

67. Mandel, A. M., Akke, M., and Palmer, A. G., III (1995) *J. Mol. Biol. 246*, 144-163.

68. Wishart, D. S., Bigam, C. G., Yao, J., Abildgaard, F., Dyson, H. J., Oldfield, E., Markley, J. L., and Sykes, B. D. (1995) *J. Biomol. NMR 6*, 135-140.

69. Wishart, D. S. and Sykes, B. D. (1994) *J. Biomol. NMR 4*, 171-180.

70. Bevington, B. R. and Robinson, D. K. (1992) *Data Reduction and Error Analysis for the Physical Sciences* McGraw-Hill, New York,NY.

71. Copie, V., Tomita, Y., Akiyama, S. K., Aota, S., Yamada, K. M., Venable, R. M., Pastor, R. W., Krueger, S., and Torchia, D. A. (1998) *J. Mol. Biol. 277*, 663-682.

72. Volkman, B. F., Lipson, D., Wemmer, D. E., and Kern, D. (2001) *Science 291*, 2429-2433.

73. Lee, A. L., Kinnear, S. A., Wand, A. J., and . (2000) *Nat. Struct. Biol. 7*, 72-77.

74. Szyperski, T., Luginbuhl, P., Otting, G., Guntert, P., and Wuthrich, K. (1993) *J. Biomol. NMR 3*, 151-164.

75. Peng, J. W., Thanabal, V., and Wangner, G. (1991) *Journal of Magnetic Resonance 95*, 421-427.

76. Ishima, R. and Torchia, D. A. (1999) *J. Biomol. NMR 14*, 369-372.

APPENDICES

APPENDIX A

EXPERIMENTAL PARAMETERS AND CHEMICAL SHIFT ASSIGNMENT

APPENDIX A

NMR Experiments and Parameters used to acquire Chemical Shift Assignments and Structural Restraints

And complete chemical shift assignments for apo-L75F TrpR

Experiment	Solvent	Sweep Width/Carrier (ppm)			Acquired Data (complex Points)			Mixing Time	Number
		F1	F2	F3	F1	F2	F3	(ms)	of Scans
^{1}H-^{15}N HSQC	H_2O	30.0/115.5	12.5/4.72		128	1024			64
HNCA	H_2O	29.9/118.0	24.0/56.0	15.0/4.72	28	64	512		32
HNCACB	H_2O	30.0/115.5	67.2/46.0	12.5/4.72	32	58	512		32
CBCA(CO)NH	H_2O	30.0/115.5	67.2/46.0	12.0/4.72	24	58	512		32
C(CO)NH	H_2O	30.0/115.5	67.0/46.0	12.0/4.72	24	58	512		32
HBHA(CO)NH	H_2O	30.0/115.5	9.0/4.72	11.0/4.72	32	64	512		32
HC(CO)NH	H_2O	30.0/115.5	9.0/4.72	12.0/4.72	32	68	512		32
^{15}N-NOESY-HSQC	H_2O	12.5/4.72	30.0/115.5	12.5/4.72	80	48	512	50, 90, 120	16
3D-HCCH-TOCSY	$^{2}H_2O$	6.67/2.50	30.0/39.0	6.67/2.50	58	64	512	22.8	16
3D-HCCH-NOESY	$^{2}H_2O$	12.5/4.72	53.0/39.0	12.5/4.72	80	64	512	120	8
^{1}H-^{13}C-CT-HSQC (T=12ms)	$^{2}H_2O$	40.0/46.0	12.5/4.72		156	512			100

Chemical Shift Assignments for apo-L75F TrpR

Residue	H^N	^{15}N	C_α	H^α	C_β	H^β	C_γ	H^γ	C_δ	H^δ	C_ε	H^ε
Met 1												
Ala 2												
Gln 3	8.27	121.06	53.92	4.40	27.28	2.08	31.81	2.45				
Gln 4	8.46	122.03	53.60	4.42	27.80	2.11	31.79	2.43				
Ser 5	8.05	116.67	53.81		62.02							
Pro 6			61.68	4.43	29.74	2.25/1.76	25.06	2.00	48.78	3.75/3.88		
Tyr 7	7.96	119.10	55.97	4.59	36.60	2.96/3.13						
Ser 8	7.92	116.92	56.49	4.38	61.84	3.94						
Ala 9	8.34	126.17	51.71	4.28	16.55	1.50						
Ala 10	8.10	121.37	51.68	4.31	16.54	1.48						
Met 11	8.00	118.25	54.78	4.39	30.65	2.11/2.54						
Ala 12	8.12	123.04	52.37	4.20	16.42	1.52						
Glu 13	8.19	119.35	56.54	4.30	27.57	2.16		2.44				
Gln 14	8.17	120.61	56.65	4.30	26.55	1.40						
Arg 15	8.31	118.71	56.51	4.32	28.16	2.00		1.83	41.56	3.28		
His 16	8.32	119.78		4.75		3.42/3.54						
Gln 17	8.34	118.03	57.00	4.03	26.17	2.30/2.37	31.92	2.62				
Glu 18	8.44	120.16	57.53	4.16	26.89	2.42/2.11	34.69	2.64/2.40				
Trp 19	8.12	122.12	57.01	4.86	27.07	3.52/3.71						
Leu 20	8.06	117.54	55.56	3.61	37.85	1.88/1.43	24.52	1.66	19.83	0.88		
Arg 21	7.97	119.64	57.62	4.17	27.77	2.10/1.93		1.62	41.93	3.30		
Phe 22	7.77	120.28	60.68	4.04	35.35	3.17/3.46						
Val 23	7.85	119.25	64.71	2.96	29.20	1.92	20.30/20.41	1.08/0.10				
Asp 24	8.11	121.14	55.32	4.52	39.31	2.67/2.74						
Leu 25	8.13	124.06	55.99	4.17	40.32	1.92/1.65		1.35	22.75/24.16	0.77/0.90		

Residue	H^N	^{15}N	C_α	H^α	C_β	H^β	C_γ	H^γ	C_δ	H^δ	C_ε	H^ε
Leu 26	8.22	119.26	55.08	3.83	38.15	1.84/1.75	24.75	1.25	24.60/21.30	0.78/0.81		
Lys 27	7.56	120.57	58.00	2.73	30.18	2.03/1.72	21.98	0.97	27.31	1.64	39.94	2.93
Asn 28	7.76	116.63	53.87	4.45	36.87	3.11						
Ala 29	8.92	126.20	53.72	3.40	15.52	1.15						
Tyr 30	8.43	119.10	59.64	4.72	35.98	2.70						
Gln 31	7.43	117.17	56.05	4.10	26.27	2.23						
Asn 32	7.33	115.38	51.07	4.77	38.18	2.60/1.97						
Asp 33	7.93	117.34	53.94	4.82	37.76	2.56/3.1						
Leu 34	8.31	117.69	51.35	4.27	41.30	1.36	23.35	1.19	20.40/23.93	0.58/0.07		
His 35	9.02	120.56	57.37	3.60	26.57	1.93/1.80						
Leu 36	7.38	119.20	57.34	4.28	35.59	1.68/1.44	24.99	1.30	23.11/21.71	0.99/0.97		
Pro 37			63.27	4.42	28.69	2.22/1.77	25.37	2.03	47.44	3.48/3.35		
Leu 38	7.82	118.90	56.54	4.20	39.63	1.55/1.80	25.03	1.66	22.44/24.83	1.22/0.95		
Leu 39	8.86	119.91	56.39	4.22	39.69	2.49/1.92		2.10	23.74/20.22	1.14/1.27		
Asn 40	8.10	116.32	52.62	4.62	36.10	2.78/2.84						
Leu 41	7.43	118.67	54.94	4.40	41.06	2.22/1.89	25.05	1.58	22.12	0.92		
Met 42	8.11	111.98	54.27	4.30	31.19	2.20/2.09		2.71/2.84				
Leu 43	7.67	116.66	51.30	4.83	42.76	1.48	26.04	1.73	23.52/25.68	0.95/1.08		
Thr 44	9.15	114.20	58.21	3.96	65.68	4.83						
Pro 45			64.30	4.71	29.30	2.11/2.41		1.93/1.71	47.90	3.51		
Asp 46	8.06	114.76	54.82	4.37	38.15	2.69/2.53						
Glu 47	7.57	122.74	56.78	3.96	27.67	1.73		2.28				
Arg 48	7.92	117.82	58.55	3.54	28.17	1.46		1.24	41.34	2.67/1.73		
Glu 49	7.83	117.84	57.12	4.14	27.21	2.11/2.16	34.53	2.25/2.46				
Ala 50	7.92	122.00	53.23	4.17	15.47	1.52						
Leu 51	8.10	119.13	56.78	3.89	38.70	1.99		1.75	23.54/21.00	0.80/0.61		

Residue	H^N	^{15}N	C_α	H^α	C_β	H^β	C_γ	H^γ	C_δ	H^δ	C_ε	H^ε
Gly 52	8.25	104.20	45.31	4.18								
Thr 53	8.33	119.28	64.74	4.06	66.54	4.42	20.34	1.43				
Arg 54	8.67	121.21	58.37	3.85	28.31	2.13	25.48	1.97	42.40	3.34/2.91		
Val 55	7.70	118.27	65.49	3.55	29.27	2.50	22.91/20.20	1.37/1.03				
Arg 56	7.04	118.77	56.65	4.21	27.01	2.17		1.78	34.87	3.05		
Ile 57	7.91	118.34	63.48	3.80	35.49	1.78	15.38($C_{\gamma 2}$)	1.40/0.66($H^{\gamma 2}$)				
Val 58	8.04	118.71	65.80	3.47	29.21	2.23	21.94/19.82	1.09/0.87				
Glu 59	8.45	119.02	58.55	3.66	27.64	2.12/2.40	34.07	2.25/2.09				
Glu 60	8.30	115.81	56.11	4.43	26.85	2.03/2.22	33.27	2.60/2.79				
Leu 61	8.83	123.70	55.66	4.21	39.78	2.01/1.87		1.39	24.50/22.83	0.73/0.87		
Leu 62	8.26	119.13	55.03	4.09	40.28	1.99/1.89	25.00	1.40		0.75/0.88		
Arg 63	8.39	119.06	57.08	3.98	26.68	2.02/1.96		1.67	41.27	3.34		
Gly 64	7.62	102.91	44.51	4.01								
Glu 65	7.86	119.34	55.40	4.33	29.09	1.92/2.13	34.31	2.26				
Met 66	8.71	119.54	54.43	4.48	32.54	2.10/1.95	31.00	2.64/2.58				
Ser 67	8.73	118.54	55.34	4.40	63.04	4.13/4.09						
Gln 68	8.81	120.41	57.43	4.07	26.22	2.17/2.21	31.73	2.46/2.50				
Arg 69	8.19	118.73	56.57	4.11	28.11	1.88/1.94	24.98	1.68	41.39	3.28		
Glu 70	7.71	119.82	56.55	4.09	28.01	2.12	35.13	2.34/2.25				
Leu 71	8.52	120.76	55.78	4.22	40.61	2.03/1.58		1.73	22.52	1.00/0.94		
Lys 72	8.07	119.36	56.88	4.10	30.19	1.91/1.95	23.06	1.48/1.52	27.35	1.72	40.16	3.03
Asn 73	8.08	118.37	53.34	4.52	36.52	2.89						
Glu 74	8.05	118.21	55.91	4.11	27.87	1.68/1.33	32.72	2.55/2.61				
Phe 75	8.13	114.23	55.67	4.85	38.42	3.23/2.91						
Gly 76	8.19	110.04	44.35	4.13/3.96								
Ala 77	8.37	124.41	51.34	4.31	16.82	1.50						

Residue	H^N	^{15}N	C_α	H^α	C_β	H^β	C_γ	H^γ	C_δ	H^δ	C_ε	H^ε
Gly 78	8.52	106.31	44.37	3.87/4.11								
Ile 79	7.71	117.86	61.00	3.90	35.98	1.96	15.61($C_{\gamma 2}$)	1.39/0.98($H^{\gamma 2}$)				
Ala 80	7.97	124.51	52.54	4.22	16.33	1.50						
Thr 81	7.68	112.28	63.12	4.20	66.96	4.02		1.22				
Ile 82	7.54	118.39	59.71	4.20	36.03	2.00	16.08($C_{\gamma 2}$)	1.45/0.87($H^{\gamma 2}$)				
Thr 83	8.01	110.71	61.14	4.34	67.55	3.96	20.28	1.19				
Arg 84	7.98	121.11	55.07	4.42	28.15	1.97		1.73		3.25		
Gly 85	8.28	107.51	43.79	4.13/3.88								
Ser 86	8.25	115.68	57.74	4.3	61.82	3.92						
Asn 87	8.41	119.31	51.93	4.67	36.54	2.87/2.97						
Ser 88	7.83	113.41	56.84	4.40	62.43	3.75/3.99						
Leu 89	8.41	122.16	54.78	4.20	39.83	1.63/1.82	27.15	1.61	23.12/21.54	0.91/0.87		
Lys 90	7.94	118.28	56.61	4.05	30.18	1.90	23.02	1.55	27.14	1.73	40.24	3.07
Ala 91	7.59	119.03	49.81	4.36	17.15	1.41						
Ala 92	7.47	122.69	48.13	4.58	15.63	1.47						
Pro 93			60.71	4.64	30.11	2.04	25.78	2.60/2.24	48.46	4.04/3.63		
Val 94	8.81	125.26	64.42	3.78	29.62	2.22	19.91/18.32	1.17/1.03				
Glu 95	9.65	118.95	57.97	4.15	26.36	2.04/2.15	34.47	2.40				
Leu 96	7.23	117.35	55.32	4.49	40.19	1.39	24.86	1.70	22.21/19.83	1.20/1.01		
Arg 97	7.98	119.43	59.09	3.81	28.07	1.98		1.61	41.34	3.31		
Gln 98	8.70	116.04	57.01	4.12	26.44	2.18	32.34	2.50/2.59				
Trp 99	7.48	121.13	59.57	4.35	26.48	3.37/3.48						
Leu 100	8.82	117.27	55.50	3.51	40.71	2.07		1.14	24.02/21.40	0.74/0.83		
Glu 101	8.02	117.13	58.11	3.70	27.57	2.08/2.18	35.23	2.57/2.10				
Glu 102	7.42	118.09	57.21	3.96	27.58	2.11/2.15	33.85	2.39/2.21				
Val 103	7.92	113.16	62.39	3.81	30.05	1.36	18.84/17.32	0.36/-0.09				

Residue	H^N	^{15}N	C_α	H^α	C_β	H^β	C_γ	H^γ	C_δ	H^δ	C_ε	H^ε
Leu 104	8.34	117.15	53.97	4.32	40.63	1.35/1.75		1.60	24.19/20.80	0.78		
Leu 105	7.08	115.21	52.98	4.50	39.27	2.01/1.64		1.65	23.38/20.81	0.90/0.85		
Lys 106	7.20	119.24	54.38	4.39	30.77	1.90	22.53	1.42/1.39	27.11	1.71	40.22	3.02
Ser 107	8.11	117.05	56.04	4.51	62.31	3.88						
Asp 108	7.95	127.57	53.66	4.43	40.21	2.67						

*For chemical shift referencing to DSS, -0.06 ppm and 1.77 ppm should be added respectively to the ^1H and ^{13}C chemical shift entries tabulated herein.

APPENDIX B

^{15}N RELAXATION VALUES FOR APO-L75F

APPENDIX B

^{15}N Relaxation Values for apo-L75F TrpR

Residue	^{15}N-T_1(ms)	^{15}N-T_2(ms)	^{15}N-{^{1}H} nOe (I/Io)
Met1			
Ala2			
Gln3			
Gln4			
Ser5			
Pro6			
Tyr7	747,747	281,286	-0.18,-0.17
Ser8	719,745	211,205	-0.06,-0.06
Ala9	725,750	160,159	0.16,0.18
Ala10			
Met11			
Ala12	730,763	107,107	0.40,0.46
Glu13			

Residue	^{15}N-T_1(ms)	^{15}N-T_2(ms)	^{15}N-{^1H} nOe (I/Io)
Gln14	716,715	101,100	0.52,0.56
Arg15	720,739	108,109	0.59,0.58
His16	864,875	72,72	0.83,0.77
Gln17	831,849	107,104	0.65,0.69
Glu18	755,772	79,78	0.78,0.70
Trp19	793,803	78,78	0.76,0.72
Leu20	810,829	77,75	0.79,0.80
Arg21			
Phe22	778,779	77,76	0.79,0.72
Val23			
Asp24			
Leu25	753,776	80,78	0.78,0.71
Leu26			
Lys27	804,840	61,59	0.86,0.87
Ans28			
Ala29	787,798	78,78	0.80,0.82
Tyr30			
Gln31	839,826	77,74	0.79,0.72
Asn32	862,862	78,80	0.78,0.75
Asp33	831,840	78,77	0.82,0.77
Leu34	842,842	78,78	0.78,0.79

Residue	^{15}N-T_1(ms)	^{15}N-T_2(ms)	^{15}N-{^1H} nOe (I/Io)
His35	790,769	70,70	0.84,0.80
Leu36	783,765	74,75	0.75,0.77
Pro37			
Leu38	798,807	77,77	0.73,0.72
Leu39	792,836	73,73	0.75,0.78
Asn40	747,765	78,76	0.83,0.78
Leu41	783,787	77,76	0.74,0.81
Met42	817,822	79,77	0.79,0.79
Leu43	777,815	75,75	0.76,0.77
Thr44	851,866	77,79	0.75,0.76
Pro45			
Asp46			
Glu47	875,905	68,67	0.82,0.76
Arg48	733,770	96,97	0.78,0.79
Glu49	854,867	72,73	0.77,0.72
Ala50	844,858	75,76	0.76,0.66
Leu51			
Gly52	839,849	70,72	0.88,0.81
Thr53	708,717	77,79	0.71,0.73
Arg54	845,872	67,68	0.80,0.82
Val55	776,818	71,71	0.75,0.75

Residue	^{15}N-T_1(ms)	^{15}N-T_2(ms)	^{15}N-{^1H} nOe (I/Io)
Arg56	810,802	71,71	0.76,0.76
Ile57			
Val58			
Glu59			
Glu60	852,897	65,69	0.84,0.83
Leu61	835,874	66,66	0.73,0.67
Leu62			
Arg63			
Gly64	841,870	60,59	0.67,0.72
Glu65			
Met66	923,962	94,94	0.62,0.56
Ser67	806,873	84,81	0.57,0.53
Gln68			
Arg69	812,847	86,87	0.63,0.63
Glu70	791,805	86,86	0.69,0.68
Leu71	836,846	82,81	0.69,0.62
Lys72			
Asn73	799,819	82,82	0.67,0.65
Glu74			
Phe75	804,804	74,73	0.64,0.66
Gly76	841,846	83,84	0.52,0.50

Residue	^{15}N-T_1(ms)	^{15}N-T_2(ms)	^{15}N-{^{1}H} nOe (I/Io)
Ala77			
Gly78	790,780	99,98	0.61,0.57
Ile79	762,771	68,69	0.69,0.75
Ala80	700,765	93,95	0.64,0.64
Thr81	752,806	79,81	0.57,0.55
Ile82			
Thr83	721,713	48,46	0.66,0.62
Arg84	724,734	89,89	0.59,0.51
Gly85	713,797	90,92	0.58,0.63
Ser86			
Asn87			
Ser88			
Leu89	820,810	114,114	0.67,0.69
Lys90			
Ala91	792,811	82,82	0.66,0.64
Ala92	902,916	78,79	0.66,0.74
Pro93			
Val94	821,841	81,79	0.71,0.68
Glu95	808,829	73,74	0.77,0.77
Leu96	805,810	78,79	0.76,0.77
Arg97			

Residue	^{15}N-T_1(ms)	^{15}N-T_2(ms)	^{15}N-{^1H} nOe (I/Io)
Gln98	852,861	71,72	0.77,0.74
Trp99	807,856	75,74	0.76,0.82
Leu100	799,831	76,74	0.81,0.77
Glu101	830,826	78,78	0.78,0.80
Glu102	771,780	73,76	0.79,0.67
Val103	856,890	81,80	0.71,0.76
Leu104	809,835	81,79	0.78,0.75
Leu105	830,841	78,80	0.72,0.72
Lys106	740,752	159,160	0.23,0.21
Ser107	847,869	374,388	-0.37,-0.35
Asp108	1346,1363	633,736	-1.21,-1.08

APPENDIX C

^{15}N RELAXATION VALUES FOR APO-WT TRPR

APPENDIX C

^{15}N Relaxation Values for apo-WT TrpR

Residue	^{15}N-T_1(ms)	^{15}N-T_2(ms)	^{15}N-{^1H} nOe (I/Io)
Met1			
Ala2			
Gln3			
Gln4			
Ser5			
Pro6			
Tyr7			
Ser8			
Ala9			
Ala10	764,707	154,154	
Met11			
Ala12	740,741	100,102	0.38,0.38
Glu13			
Gln14			

Residue	^{15}N-T_1(ms)	^{15}N-T_2(ms)	^{15}N-{^{1}H} nOe (I/Io)
Arg15			
His16	886,836	78,79	0.79,0.77
Gln17			
Glu18	797,758	79,77	
Trp19	827,817	74,74	0.77,0.79
Leu20			
Arg21			
Phe22	771,765	73,72	0.80,0.86
Val23			
Asp24			
Leu25	778,767	73,73	0.82,0.81
Leu26			
Lys27	840,818	54,55	0.80,0.80
Ans28	832,817	69,68	0.77,0.80
Ala29	790,786	75.76	0.83,0.78
Tyr30			
Gln31	848,870	70,71	0.80,0.77
Asn32	846,841	75,73	0.75,0.73
Asp33	814,807	90,90	
Leu34			
His35	820,791	68,71	0.84,0.85

Residue	^{15}N-T_1(ms)	^{15}N-T_2(ms)	^{15}N-{^{1}H} nOe (I/Io)
Leu36	760,767	68,71	0.77,0.79
Pro37			
Leu38			
Leu39	807,793	72,70	0.85,0.87
Asn40	775,751	71,71	0.77,0.77
Leu41	821,815	74,74	0.84,0.77
Met42	850,821	75,73	0.76,0.79
Leu43			
Thr44	874,861	70,66	0.72,0.71
Pro45			
Asp46	877,865	68,68	0.85,0.79
Glu47	919,884	69,68	0.83,0.85
Arg48			
Glu49	822,749	69,69	0.82,0.77
Ala50	852,837	70,72	0.82,0.85
Leu51	850,816	69,70	0.75,0.75
Gly52	840,811	70,71	0.76,0.79
Thr53			
Arg54	885,856	63,66	0.80,0.76
Val55			
Arg56			

Residue	^{15}N-T_1(ms)	^{15}N-T_2(ms)	^{15}N-{^1H} nOe (I/Io)
Ile57	889,886	68,68	0.79,0.78
Val58			
Glu59			
Glu60	851,825	57,57	0.73,0.77
Leu61	847,838	49,50	0.89,0.75
Leu62			
Arg63			
Gly64	841,812	48,50	0.76,0.72
Glu65			
Met66			
Ser67	751,773	79,76	0.58,0.45
Gln68			
Arg69	755,748	78,79	0.54,0.51
Glu70	754,728	95,95	0.58,0.60
Leu71	756,752	88,89	0.58,0.55
Lys72			
Asn73	811,792	85,84	0.78,0.80
Glu74			
Leu75	752,725	54,54	0.58,0.53
Gly76	797,738	93,95	0.43,0.43
Ala77	821,815	93,96	0.56,0.54

Residue	^{15}N-T_1(ms)	^{15}N-T_2(ms)	^{15}N-{^1H} nOe (I/Io)
Gly78	836,806	110,107	0.44,0.44
Ile79			
Ala80			
Thr81	798,798	67,67	0.64,0.65
Ile82			
Thr83	710,725	59,57	0.62,0.61
Arg84			
Gly85	752,718	77,81	0.63,0.61
Ser86			
Asn87			
Ser88			
Leu89	779,729	68,71	0.67,0.77
Lys90			
Ala91	806,796	74,76	0.68,0.71
Ala92	888,852	72,74	0.70,0.71
Pro93			
Val94	834,805	77,74	0.71,0.73
Glu95	831,819	69,69	0.75,0.78
Leu96	810,800	72,73	0.74,0.73
Arg97			
Gln98	845,819	66,67	0.76,0.73

Residue	^{15}N-T_1(ms)	^{15}N-T_2(ms)	^{15}N-{^1H} nOe (I/Io)
Trp99	843,805	71,70	0.79,0.82
Leu100	832,810	69,70	0.85,0.84
Glu101			
Glu102	867,852	73,73	0.74,0.76
Val103	864,852	80,78	0.72,0.73
Leu104	821,799	76,78	0.69,0.73
Leu105	850,798	74,75	0.63,0.65
Lys106			
Ser107			
Asp108	1287,1320	503,563	-1.14,-1.13

APPENDIX D

LIPARI-SZABO RESULTS

APPENDIX D

Lipari-Szabo analysis of apo-L75F and apo WT TrpR

Results from Lipari-Szabo analysis on apo-L75F TrpR

Residue	model	S^2	S^2 err	S^2_f	S^2_f err	τ_e(ns^{-1})	τ_e err	R_{ex}(s^{-1})	R_{ex} err
7	2	0.54	0.19	1	N.A.	0.58	0.24	0	N.A.
8	5	0.23	0.04	0.81	0.05	0.93	0.042	0	N.A.
9	5	0.36	0.04	0.81	0.05	0.99	0.063	0	N.A.
12	5	0.60	0.03	0.88	0.03	0.99	0.078	0	N.A.
14	5	0.63	0.02	0.89	0.02	1.19	0.079	0	N.A.
15	2	0.88	0.02	1	N.A.	0.68	0.282	0	N.A.
16	3	0.86	0.04	1	N.A.	0	N.A.	1.57	1.51
17	2	0.68	0.03	1	N.A.	0.02	0.405	0	N.A.
18	1	0.93	0.02	1	N.A.	0	N.A.	0	N.A.
19	1	0.92	0.02	1	N.A.	0	N.A.	0	N.A.
20	2	0.90	0.03	1	N.A.	0.02	0.019	0	N.A.
22	1	0.93	0.02	1	N.A.	0	N.A.	0	N.A.
25	1	0.94	0.02	1	N.A.	0	N.A.	0	N.A.
27	3	0.91	0.03	1	N.A.	0	N.A.	3.38	0.545
29	1	0.91	0.04	1	N.A.	0	N.A.	0	N.A.
31	1	0.90	0.02	1	N.A.	0	N.A.	0	N.A.
32	1	0.88	0.01	1	N.A.	0	N.A.	0	N.A.
33	1	0.89	0.03	1	N.A.	0	N.A.	0	N.A.
34	2	0.88	0.07	1	N.A.	0.02	0.532	0	N.A.
35	1	0.96	0.02	1	N.A.	0	N.A.	0	N.A.
36	2	0.93	0.02	1	N.A.	0.05	0.107	0	N.A.
38	2	0.91	6.82	1	N.A.	0.05	4.02E+09	0	N.A.
39	1	0.94	0.02	1	N.A.	0	N.A.	0	N.A.
40	1	0.97	0.02	1	N.A.	0	N.A.	0	N.A.
41	1	0.92	0.02	1	N.A.	0	N.A.	0	N.A.
42	2	0.89	0.02	1	N.A.	0.02	0.021	0	N.A.
43	2	0.94	0.02	1	N.A.	0.049	0.084	0	N.A.
44	2	0.88	0.02	1	N.A.	0.027	0.016	0	N.A.
47	3	0.89	0.03	1	N.A.	0	N.A.	1.24	0.572
48	5	0.61	0.63	0.82	0.03	4.54	394.818	0	N.A.
49	2	0.94	0.02	1	N.A.	0.045	0.041	0	N.A.
50	2	0.89	0.02	1	N.A.	0.029	0.012	0	N.A.
52	3	0.93	0.02	1	N.A.	0	N.A.	0.29	0.565
53	2	0.89	0.24	1	N.A.	1.25	7.97E+09	0	N.A.
54	3	0.90	0.03	1	N.A.	0	N.A.	1.52	0.56
55	2	0.94	0.06	1	N.A.	0.061	0.821	0	N.A.
56	2	0.94	0.01	1	N.A.	0.054	0.173	0	N.A.
60	3	0.91	0.02	1	N.A.	0	N.A.	1.49	0.623
61	3	0.92	0.02	1	N.A.	0	N.A.	1.35	0.568
64	3	0.91	0.04	1	N.A.	0	N.A.	3.4	0.707
66	2	0.75	0.01	1	N.A.	0.037	0.005	0	N.A.
67	2	0.84	0.02	1	N.A.	0.087	0.101	0	N.A.

Result for apo-L75F (cont.)

Residue	model	S^2	S^2 err	S^2_f	S^2_f err	$\tau_e(ns^{-1})$	τ_e err	$R_{ex}(s^{-1})$	R_{ex} err
69	2	0.86	0.05	1	N.A.	0.076	0.252	0	N.A.
70	2	0.85	0.02	1	N.A.	0.047	0.011	0	N.A.
71	2	0.86	0.02	1	N.A.	0.048	0.011	0	N.A.
73	2	0.85	0.06	1	N.A.	0.051	0.449	0	N.A.
75	2	0.91	0.02	1	N.A.	0.11	0.128	0	N.A.
76	2	0.82	0.02	1	N.A.	0.087	0.013	0	N.A.
78	5	0.68	0.03	0.84	0.02	1.143	0.175	0	N.A.
79	2	0.95	0.05	1	N.A.	0.25	0.548	0	N.A.
80	5	0.68	0.04	0.90	0.03	1.588	0.368	0	N.A.
81	2	0.85	0.02	1	N.A.	0.843	0.238	0	N.A.
83	4	0.89	0.27	1	N.A.	1.056	59.624	6.31	1.567
84	5	0.76	0.03	0.93	0.02	1.087	0.124	0	N.A.
85	2	0.81	0.04	1	N.A.	0.94	0.342	0	N.A.
89	5	0.54	0.04	0.73	0.03	1.924	0.513	0	N.A.
91	2	0.89	0.02	1	N.A.	0.076	0.281	0	N.A.
92	2	0.83	0.02	1	N.A.	0.046	0.008	0	N.A.
94	2	0.86	0.02	1	N.A.	0.037	0.011	0	N.A.
95	1	0.94	0.02	1	N.A.	0	N.A.	0	N.A.
96	2	0.90	0.02	1	N.A.	0.033	0.018	0	N.A.
98	3	0.86	0.02	1	N.A.	0	N.A.	1.79	0.415
99	1	0.92	0.02	1	N.A.	0	N.A.	0	N.A.
100	1	0.92	0.02	1	N.A.	0	N.A.	0	N.A.
101	1	0.90	0.03	1	N.A.	0	N.A.	0	N.A.
102	2	0.95	0.04	1	N.A.	0.041	0.547	0	N.A.
103	2	0.85	0.02	1	N.A.	0.035	0.008	0	N.A.
104	1	0.90	0.03	1	N.A.	0	N.A.	0	N.A.
105	2	0.89	0.01	1	N.A.	0.047	0.015	0	N.A.
106	5	0.36	0.03	0.79	0.03	1.088	0.038	0	N.A.
107	5	0.11	0.02	0.69	0.02	0.81	0.016	0	N.A.
108	2	0.28	0.06	1	N.A.	0.095	0.088	0	N.A.

Only residues in which Lipari-Szabo analysis could be performed are shown, with an entry of N.A corresponding to not applicable.

Results from Lipari-Szabo analysis on apo-WT TrpR

Residue	model	S^2	S^2 err	S^2_f	S^2_f err	$\tau_e(ns^{-1})$	τ_e err	$R_{ex}(s^{-1})$	R_{ex} err
12	5	0.60	0.03	0.89	0.02	0.973	0.063	0	N.A.
16	1	0.86	0.06	1	N.A.	0	N.A.	0	N.A.
19	2	0.91	0.03	1	N.A.	0.028	0.025	0	N.A.
22	1	0.96	0.02	1	N.A.	0	N.A.	0	N.A.
25	1	0.96	0.02	1	N.A.	0	N.A.	0	N.A.
27	3	0.91	0.03	1	N.A.	0	N.A.	4.54	0.769
28	1	0.96	0.02	1	N.A.	0	N.A.	0	N.A.
29	1	0.92	0.02	1	N.A.	0	N.A.	0	N.A.
31	1	0.92	0.02	1	N.A.	0	N.A.	0	N.A.
32	1	0.91	0.02	1	N.A.	0	N.A.	0	N.A.
35	1	0.93	0.02	1	N.A.	0	N.A.	0	N.A.
36	1	0.97	0.02	1	N.A.	0	N.A.	0	N.A.
39	3	0.94	0.03	1	N.A.	0	N.A.	0.4	0.631
40	2	0.96	0.55	1	N.A.	0.086	63.15	0	N.A.
41	1	0.92	0.02	1	N.A.	0	N.A.	0	N.A.
42	2	0.88	0.03	1	N.A.	0.013	0.026	0	N.A.
44	1	0.95	0.02	1	N.A.	0	N.A.	0	N.A.
46	3	0.91	0.03	1	N.A.	0	N.A.	0.49	0.679
47	3	0.87	0.03	1	N.A.	0	N.A.	1.35	0.62
49	2	0.95	0.25	1	N.A.	0.009	18.422	0	N.A.
50	1	0.92	0.02	1	N.A.	0	N.A.	0	N.A.
51	2	0.91	0.05	1	N.A.	0.039	1.981	0	N.A.
52	2	0.92	0.02	1	N.A.	0.038	0.167	0	N.A.
54	3	0.89	0.03	1	N.A.	0	N.A.	1.3	0.661
57	1	0.92	0.03	1	N.A.	0	N.A.	0	N.A.
60	3	0.92	0.04	1	N.A.	0	N.A.	3.17	0.823
61	3	0.94	0.05	1	N.A.	0	N.A.	4.63	1.759
64	3	0.95	0.04	1	N.A.	0	N.A.	5.21	0.82
67	2	0.83	0.03	1	N.A.	0.964	0.401	0	N.A.
69	2	0.88	0.03	1	N.A.	0.555	0.306	0	N.A.
70	5	0.67	0.04	0.87	0.03	1.247	0.179	0	N.A.
71	5	0.71	0.04	0.89	0.03	1.17	0.162	0	N.A.
73	1	0.85	0.08	1	N.A.	0	N.A.	0	N.A.
75	4	0.90	0.03	1	N.A.	0.511	0.839	4.26	0.971
76	5	0.66	0.04	0.87	0.03	0.86	0.113	0	N.A.
77	2	0.78	0.03	1	N.A.	0.062	0.229	0	N.A.
78	5	0.57	0.02	0.81	0.02	1.027	0.075	0	N.A.
81	2	0.94	0.02	1	N.A.	0.278	0.198	0	N.A.
83	4	0.88	0.04	1	N.A.	0.894	0.427	4.18	0.811
85	2	0.88	0.03	1	N.A.	0.822	0.403	0	N.A.
89	2	0.93	0.02	1	N.A.	0.549	0.317	0	N.A.

Result for apo-WT (cont.)

Residue	model	S^2	S^2 err	S^2_f	S^2_f err	$\tau_e(ns^{-1})$	τ_e err	$R_{ex}(s^{-1})$	R_{ex} err
91	2	0.90	0.02	1	N.A.	0.083	0.169	0	N.A.
92	2	0.88	0.02	1	N.A.	0.048	0.013	0	N.A.
94	2	0.90	0.02	1	N.A.	0.054	0.017	0	N.A.
95	2	0.94	0.02	1	N.A.	0.06	0.747	0	N.A.
96	1	0.93	0.02	1	N.A.	0	N.A.	0	N.A.
98	3	0.91	0.02	1	N.A.	0	N.A.	1.34	0.472
99	1	0.93	0.02	1	N.A.	0	N.A.	0	N.A.
100	3	0.92	0.03	1	N.A.	0	N.A.	0.49	0.545
102	2	0.89	0.02	1	N.A.	0.034	0.011	0	N.A.
103	2	0.86	0.02	1	N.A.	0.037	0.01	0	N.A.
104	2	0.89	0.05	1	N.A.	0.062	0.427	0	N.A.
105	2	0.86	0.01	1	N.A.	0.077	0.015	0	N.A.

Only residues in which Lipari-Szabo analysis could be performed are shown, with an entry of N.A corresponding to not applicable.